④

AD-A194 612

THE
OHIO
STATE
UNIVERSITY

Autoregressive Moving Average Modeling
of Radar Target Signatures

Randolph L. Moses
Rob Carrière

The Ohio State University

ElectroScience Laboratory

Department of Electrical Engineering
Columbus, Ohio   43212

Department of the Navy
Office of Naval Research
800 N. Quincy Street
Arlington, Virginia 22217-5000

DTIC
SELECTE
MAY 1 0 1988
C H

88 5 00   152

50272-101

REPORT DOCUMENTATION PAGE	1. REPORT NO.	2.	3. Recipient's Accession No.

4. Title and Subtitle

Autoregressive Moving Average Modeling or Radar Target Signatures

5. Report Date
January 1988

6.

7. Author(s)
Randolph L. Moses and Rob Carriere

8. Performing Organization Rept. No.
717220-6

9. Performing Organization Name and Address

The Ohio State University ElectroScience Laboratory
1320 Kinnear Road
Columbus, Ohio 43212

10. Project/Task/Work Unit No.

11. Contract(C) or Grant(G) No

(C) N00014-85-K-0321

(G)

12. Sponsoring Organization Name and Address

Department of the Navy
Office of Naval Research
800 N. Quincy Street
Arlington, VA 22217-5000

13. Type of Report & Period Covered

Technical

14.

15. Supplementary Notes

16. Abstract (Limit: 200 words)

A method for characterizing radar target signatures with Autoregressive Moving Average (ARMA) models is developed. A parameterization of the model that corresponds directly to the geometric properties of the target is chosen, and an efficient algorithm for estimating these parameters is presented. Procedures for minimizing the effects of unmodeled dynamics are also developed. Experiments on radar measurements obtained from a compact range are presented to test the effectiveness of the ARMA modeling procedure.

17. Document Analysis   a. Descriptors

b. Identifiers/Open-Ended Terms

c. COSATI Field/Group

18. Availability Statement	19. Security Class (This Report)	21. No. of Pages
Approved for public release; distribution is unlimited.	Unclassified	158
	20. Security Class (This Page)	22. Price
	Unclassified	

(See ANSI–Z39.18)   See Instructions on Reverse   OPTIONAL FORM 272 (4–77)
(Formerly NTIS–35)
Department of Commerce

i

Contents

iii

For
I
d
ion

n/

Availability Codes

Dist	Avail and/or Special
A-1	

QUALITY INSPECTED 4

List of Figures

1. Introduction

When first developed in World War II, radar was used to detect the presence of objects within its range. Initially, radars could report the position and possibly the velocity of detected objects (called "targets"), but it soon became evident that more information was desirable. Modern civilian air control solves the information problem by requiring each aircraft to transmit information about itself, using a transponder [1]. However, the problem of obtaining a characterization of the target when it is unable or unwilling to volunteer that information remains a topic of current research.

The response of the target to the radar signal (the radar return) contains a considerable amount of information about the target, because the target distorts the radar waves as they wash over it. The exact nature of the distortion depends on the shape and orientation of the target. It should therefore be possible to extract information about the shape and orientation of the target from the radar return. If we have a database containing shape information about all known aircraft (the catalog), we can identify the target by comparing the shape information extracted from the radar return to the various entries in the catalog. This process is known as radar target identification (RTI).

The radar target identification system typically consists of a signal processing stage followed by a feature classification stage. The signal processing step involves operating on the raw radar data to extract salient "features" of that data which can be readily used for target classification. This report addresses the signal processing part of the RTI problem.

1

Traditionally, target identification methods have used direct frequency domain data from the radar. The "features" used for classification consist of raw frequency domain data [2,3,4,5]. This method requires little or no signal processing, but has the disadvantage that one obtains no geometric characterization of the target. (Geometric information is useful because it can provide information about the target even when classification or identification is not possible.) More recently, Fourier Transform (FT) methods have been applied [6]; these methods first convert the frequency domain radar data into an estimate of the downrange impulse response of the target. Classification then proceeds based on some extracted features from this downrange impulse response (such as range of strong scattering centers, etc.). While this concept is potentially very useful for RTI applications, the use of FT methods presents some problems. First, FT methods are resolution limited, so closely spaced scattering centers may not be resolved. Second, FT methods are nonparametric; thus, there is no data reduction from the raw radar data to the downrange impulse response. Data reduction is desirable because classification algorithms are computationally burdensome if the number of features is large.

In this report we develop and test an alternate radar signal processing approach. This approach applies AutoRegressive Moving Average (ARMA) modeling techniques to radar target data. Like FT methods, the ARMA modeling technique produces an estimate of the downrange impulse response of the target. However, unlike the FT model the ARMA method is parametric; the output of the signal processing stage consists of a small number of parameters which can be directly used for classification. ARMA methods are also not resolution limited by the bandwidth of the radar data as are FT methods. Thus, these ARMA modeling methods posses

2

some potentially useful properties for radar target identification.

In this report we first derive the ARMA signal processing method. We then present an analytical comparison between the ARMA method and the FT method. We also discuss some strategies of data averaging which can be used in both methods. Finally, we apply these signal processing techniques to compact range measurements of scale models of several commercial aircraft.

2. The ARMA Modeling Method

This chapter describes the basic theory behind the ARMA modeling method as applied to the RTI problem. Note that the theory as presented here is somewhat different from standard developments [7,8], because the standard development assumes that the measured data is in the time domain, whereas the radar data is in the frequency domain. Thus, in the radar target identification application, the time and frequency domains are interchanged with respect to standard ARMA applications.

2.1 The Radar Target Data

It is assumed that measurements of the response of the targets are in the form of coherent steady-state response values (amplitude and phase) at a number of frequencies; this corresponds to frequency measurements taken with a radar that emits either a continuous wave or a relatively long pulse (with respect to the length of the target). Realistic data for this type of measurement is available from the OSU ESL Compact Range Database. Due to the construction of the Compact Range, this data can be considered noise and distortion free, and is therefore suitable for the construction of a catalog [2]. To simulate the measurements a real radar would take, the compact range data can be corrupted by noise.

The data from the Compact Range is organized as follows: for each target there are two arrays, *amp* and *phase*, such that:

$$amp_i = |y(f_i)| \tag{2.1}$$

$$phase_i = \angle y(f_i) \tag{2.2}$$

4

where $y(f_i)$ is the steady-state response of the target at frequency $f_i = f_0 + i\delta_f$. For the particular data base we have used in this study,

$$f_0 = 1\text{GHz} \tag{2.3}$$

$$\delta_f = 50\text{MHz} \tag{2.4}$$

while i ranges from 0–220, so the highest available frequency is 12 GHz.

The targets are scale models of existing commercial aircraft (Boeing 747, 727, and 707; DC10 and Concorde); scale factors vary from 130 to 200, so the compact range measurement frequencies correspond to "real-world" frequencies in the 5–92 MHz range).

2.2 The ARMA Model

ARMA modeling techniques are used in various areas: in communications, including adaptive matched filters, in transmission channels (see [9]), and in geologic surveying by means of acoustical procedures (used e.g. to find oil and gas: see [10,11,12]). Throughout this report we will refer to the frequency domain representation of the radar return as the *data*, and to the range or time domain representation as the *downrange signal*, in keeping with standard terminology. This report will be solely concerned with the application of ARMA techniques to the RTI problem, and therefore use the "reverse" domain formulation that is appropriate to that problem; so data is transformed from the frequency domain into the time domain, not the other way around.

The signal processing problem considered here is: given N coherent radar measurements $\{y(f_k)\}_{k=0}^{N-1}$, estimate the downrange impulse response of the target. The

5

general formulation of such a signal estimator entails two steps

1. Parameterize the impulse response function (choose a model).

2. Estimate the parameters of that model.

The parameterization we use is based on the ARMA model. The ARMA model assumes that the radar data can be described as:

$$y(f_k) = -\sum_{i=1}^{na} a_i y(f_{k-i}) + \sum_{j=0}^{nc} c_j \xi(f_{k-j})$$

where:

$$f_k = f_0 + k\delta_f \tag{2.5}$$

$$y(f_k) = \text{coherent radar data at frequency } f_k \tag{2.6}$$

$$\xi(f_k) = \text{a complex zero mean white noise process with variance 1} $$
$$\text{(orthonormal white noise)} \tag{2.7}$$

This model can be represented as:

$$A(q^{-1})y(f_k) = C(q^{-1})\xi(f_k) \tag{2.8}$$

where

$$A(q^{-1}) = 1 + a_1 q^{-1} + \cdots + a_{na} q^{-na} \tag{2.9}$$

$$C(q^{-1}) = c_0 + c_1 q^{-1} + \cdots + c_{nc} q^{-nc} \tag{2.10}$$

$$q^{-1} = \text{unit delay operator } (q^{-1}y(f_k) = y(f_{k-1})). \tag{2.11}$$

Note that we need to specify the orders na and nc of the polynomials A and C. We will discuss ways to do this for our given application in Chapter 4.

6

From this description of the discrete frequency domain measurements, we can find a description of the downrange response via the inverse $\mathcal{Z}$-transform:

$$Y(l) = \frac{C(e^{jl})}{A(e^{jl})} \qquad -\pi \leq l \leq \pi \tag{2.12}$$

where l is scaled time and is related to actual time by

$$t = \frac{-l + \pi}{4\pi\delta_f}$$

and where δ_f is the separation between the frequency samples. The range in meters relates to the time delay by the speed of light; thus the range relates to scaled time by:

$$r = c\frac{-l + \pi}{4\pi\delta_f} \tag{2.13}$$

From here we can also very easily find the maximum unambiguous range: this is the value of r for $l = -\pi$:

$$R = \frac{c}{2\delta_f} \tag{2.14}$$

If the target extends beyond this range, aliasing effects will occur. That is, responses in this range will be "folded over" and added to the response in the unambiguous range [13].

Combining equations (2.13) and (2.14), and substituting into equation (2.12) we get

$$Y(r) = \frac{C(e^{j\pi(1-2r/R)})}{A(e^{j\pi(1-2r/R)})} \tag{2.15}$$

as the target impulse response, where r is the range in meters, or

$$Y(t) = \frac{C(e^{j\pi(1-2t/T)})}{A(e^{j\pi(1-2t/T)})} \tag{2.16}$$

7

where t is the time in seconds, and $T = R/c$ is the maximum unambiguous time.

It should be noted from (2.15) that the estimated downrange response is a ratio of two polynomials. This type of model offers the combined advantages of parameter parsimony and good approximation performance [14]. In fact, it can be shown [14] that any function can be approximated arbitrarily closely with the model (2.15).

2.3 Pole-Residue Parameterization of the ARMA Model

While the ARMA parameters relate directly to the shape of the signal, there are other, equivalent parameterizations that are more directly related to the characteristics of a radar signal. Specifically, the impulse response model can be written as

$$Y(r) = \sum_{i=1}^{na} \frac{d_i}{e^{j\pi(1-2r/R)} - p_i} \tag{2.17}$$

where the p_i are the roots of $A(z)$, and the d_i are the partial fraction expansion coefficients. The representation (2.17) is equivalent to (2.15) if $nc = na - 1$; the only difference between the representations is in the parameters used to represent the model.

The advantage of representation (2.17) over (2.15) is that each pole p_i directly corresponds to a scattering center, and the residue relates to the amplitude associated with this scattering center. Thus, this parameterization is more directly related to the underlying physical properties of the target than (2.15) is.

Each "pole" p_i corresponds to a scattering center on the target. The argument of p_i ($\arg p_i$) relates to the range r_i of this scattering center by

$$r_i = \pi(1 - 2\frac{\arg p_i}{R})$$

It can be seen from (2.17) that r_i is the range at which the ith component of the impulse response achieves maximum amplitude. The magnitude of the pole p_i relates to the distribution in range of the energy received from this scattering center; as $|p_i| \to 1$, the scattered energy becomes more tightly concentrated at range r_i; this corresponds to an ideal point scatterer. For $|p_i| \neq 1$, the energy is spread over some range centered at r_i. The d_i parameter gives the amplitude of the ith scattering center return.

The above paragraph relates the structure of the ARMA model to properties of the impulse response of the target, i.e. properties in the time domain. It is useful to consider the properties of the model in the frequency domain as well, since these properties represent implicit assumptions on the radar data. The inverse Fourier transform of (2.17), yields:

$$y(f_k) = \sum_{i=1}^{na} d_i p_i^k \qquad (2.18)$$

In other words, the ARMA representation assumes that the radar data can be modeled as a number (na) of damped exponentials. Each exponential term corresponds to a scattering center. The energy P_i associated with the ith scatterer can be found from (2.18)

$$P_i = \sum_{k=0}^{N} d_i d_i^*(p_i p_i^*)^k = |d_i|^2 \frac{1 - |p_i|^{2N}}{1 - |p_i|^2} \qquad (2.19)$$

2.4 Formulation of a Pole-Residue Estimator

The pole-residue model formulated in the previous section can be computed directly from the discrete frequency measurements, as detailed below. This sec-

tion gives the formulae for estimating poles and residues from a given data set $\{y(f_k)\}_{k=0}^{N-1}$.

In order to find an estimate for $Y(r)$, we need to find the A and C polynomials or, equivalently, the p_i and d_i coefficients. Below we present a method adapted from the time series analysis literature [15,16].

The first step involves estimating the a_i coefficients and finding the roots of the resulting $A(z)$ polynomial. First a standard estimate for the autocorrelation sequence corresponding to the data is found; here we use the standard unbiased autocorrelation estimates:

$$\tilde{r}_k = \frac{1}{N-k} \sum_{t=0}^{N-1-k} y(f_t)^* y(f_{t+k}) \quad k = 0, 1, \ldots, K \tag{2.20}$$

$$\tilde{r}_{-k} = \tilde{r}_k^* \tag{2.21}$$

Next, the a parameters are estimated from the r parameters by solving the well-known overdetermined Yule Walker equation [17]:

$$\begin{bmatrix} r_{nc} & \cdots & r_{nc+1-na} \\ \vdots & & \vdots \\ r_{K-1} & \cdots & r_{K-na} \end{bmatrix} \cdot \begin{bmatrix} a_1 \\ \vdots \\ a_{na} \end{bmatrix} = - \begin{bmatrix} r_{nc+1} \\ \vdots \\ r_K \end{bmatrix}, \quad K \geq na + nc \tag{2.22}$$

Now we can find the roots $\{p_i\}_{i=1}^{na}$ of $A(z)$ using standard complex polynomial root finding techniques.

Once the poles are obtained, the amplitudes d_i can be estimated using a least squares technique. From equation (2.18), such an estimator is given by minimizing e in

10

$$\begin{bmatrix} p_1^1 & \cdots & p_{na}^1 \\ \vdots & & \vdots \\ p_1^N & & p_{na}^N \end{bmatrix} \begin{bmatrix} d_1 \\ \vdots \\ d_{na} \end{bmatrix} - \begin{bmatrix} y(f_0) \\ \vdots \\ y(f_{N-1}) \end{bmatrix} = \begin{bmatrix} e_0 \\ \vdots \\ e_{N-1} \end{bmatrix} \tag{2.23}$$

or

$$Pd - y = e$$

This gives the formula

$$d = (P^*P)^{-1}P^*y \tag{2.24}$$

where P^* is the complex conjugate transpose of the matrix P. Equations (2.20), (2.22), and (2.24) comprise the ARMA estimation procedure.

2.5   Comparison of the ARMA and DFT Methods

Both the Discrete Fourier Transform and the ARMA modeling methods perform the task of transforming frequency domain radar data into a downrange impulse response. In this section we compare and contrast the two methods.

The finite Fourier Transform is given by [8]

$$Y_{FT}(r) = \sum_{k=0}^{N-1} y(f_k) e^{j\pi(1-2\frac{r}{R})}$$

Note that the finite FT is a continuous function of r just as the ARMA representation is. The Fast Fourier Transform is a computationally efficient method of computing $Y(r)$ at the N equally spaced points:

$$r_n = \frac{n}{(N-1)} R$$

11

from the N frequency measurements. If more points are desired, the data can be zero padded; in the limit of infinite zero padding, the FFT gives the finite Fourier Transform. The ARMA method gives an equation for $Y(r)$, which we can then evaluate at as many points as we need.

One advantage of the ARMA method is that it is not limited in resolution by the bandwidth of the frequency measurements, as the FT is [8]; that is, the ARMA methods are capable of resolving two scatterers no matter how close they are together, irrespective of the bandwidth of the measurements. The resolution limit of the DFT is caused by the implicit assumption of the DFT that the data is identically zero outside the measurement interval. The ARMA method, on the other hand, implicitly assumes that the data outside the measurement interval is a continuation of the data in that interval, that is the equation (2.18) is assumed to hold for all k, not just $0 \leq k \leq N - 1$ (see chapter 3 for details).

Another advantage of the ARMA methods is that it produces the estimates in the form of a (small) set of parameters, while the FT yields as many points as the original data set. Target identification techniques generally require a small number of data elements in order to be computationally feasible [18]. ARMA techniques supply a small number of parameters (the $2na$ p_i and d_i coefficients). FT methods are nonparametric, and the number of output data points produced is the same as the number of frequency measurements (N).

3. Data Length and Decimation Effects

This chapter considers the effects of the number of data points (frequency samples) N and of the frequency separation δ_f of these samples on the estimation results.

3.1 Finite Data Effects

First we consider the effect of the number of data points, i.e. in the following discussion we assume δ_f to be a constant.

Both the ARMA methods and the FT methods are theoretically formulated for the infinite data case, which means that they have to be adapted for the case of a finite number of data points. One way of looking at these adaptations is as follows: given a (finite) sequence $\{y(f_k)\}_{k=0}^{N-1}$, find an infinite sequence $\{\hat{y}(f_k)\}_{k=0}^{\infty}$ such that $y(f_k) = \hat{y}(f_k) : \forall k \epsilon 0 \ldots N - 1$, and such that the finite transform (FT or ARMA) of y equals the infinite transform of $\hat{y}$.

For the FT methods this is very simple: one chooses $\hat{y}(f_k) = 0$ for all $k < 0$ or $k \geq N$ [7]; that is to say, a finite FT implicitly assumes that all measurements outside the given data range are identically zero. It is physically obvious that this is not a very good assumption.

The ARMA methods, on the other hand, assume that the data outside the known range is a continuation of the known data [17]. In particular, the extension $\hat{y}(f_k)$ is given by equation (2.18) for $k < 0$ or $k \geq N$. This assumption gives a smooth extension of the frequency data, and is much more in keeping with the physical properties of the problem than is the FT assumption. However, this assumption

13

is valid only if the bandwidth of the radar measurements is small enough for the measurements to be stationary.

A second way of looking at the finite methods is to consider the given sequence $\{y(f_k)\}_{k=0}^{N-1}$ as a subset of a (unknown) sequence $\{y(f_k)\}_{k=0}^{\infty}$ and describe how the infinite sequence y must be manipulated to get the sequence $\hat{y}$ described above. For the finite FT methods this manipulation consists of multiplication with a rectangular window

$$\{w_k\}_{k=0}^{\infty} : \begin{cases} w_k = 1 \ , \ k = 0 \ldots N-1 \\ w_k = 0 \ , \ \text{otherwise} \end{cases}$$

This means that estimated impulse response will be the actual impulse response convolved with the transform $W(z)$ of the window w_k.

$$W(z) = \sum_{k=0}^{N-1} z^{-k} = \frac{1 - z^{-N}}{1 - z^{-1}} \tag{3.1}$$

Evaluated on the unit circle, $W(z)$ is a sinc function, so the convolution will have the effect of smearing the estimate: this accounts for the resolution limit of the finite FT methods. For proofs and details about the various finite FT properties referred to above, see [7,8].

The ARMA method does not assume that the data points outside the known range are zero; instead, a smooth continuation of the known data is assumed. As a result, there is no windowing effect, and hence no corresponding resolution limit for the ARMA method. Of course, with both ARMA and finite FT methods, any information contained in the unknown data will not be taken into account, so the ARMA estimates will improve in quality as the amount of available data increases.

For the FT methods, the statistical behaviour of the estimates has been well-studied, and various methods for trading off bias for variance have been developed

14

[14]. For the ARMA method, the estimated parameters in the model become random variables. The statistical behaviour of parameter estimates have also been studied (see [19,20]). One important result is that the variance of the estimates decreases as the number of data points increases; this is another argument supporting the use of more data points in the estimates.

3.2 Decimation Effects

In this section we discuss decimation effects; here the value of $N\delta_f$ is assumed constant throughout the following discussion.

If we decimate our data, i.e. increase δ_f (and therefore decrease N), we decrease the maximum unambiguous range R, since $R = c/(2\delta_f)$ (2.14). For the finite FT method this does not change the resolution in meters, which is determined only by the number of data points. For the ARMA methods there is an advantage to choosing the maximum unambiguous range as small as possible: if R is much larger than the size of the target, the impulse response will look like a number of closely spaced peaks, surrounded by stretches of zero signal ("empty space"). Since zero intervals are not well represented by a sum of complex exponentials, ARMA methods will work best when the target fills the unambiguous range. Therefore, decimation techniques (which decrease the unambiguous range) are of interest.

The simplest method of decimating is to use only one out of every n data points, where n is the decimation factor. Of course, this has the disadvantage that only a fraction of the available data is used. An alternative method is to compute the autocorrelation sequence (equation (2.20)) using all available data, and then decimate the autocorrelation sequence, instead of the data sequence. This method has

15

the advantage of using all data, thus producing more accurate parameter estimates. This method is equivalent to averaging n adjacent data points to produce one decimated point. In other words, this is convolution by a rectangular window, followed by decimation. From the signal processing literature [8] it is well known that the rectangular window, while computationally simple, produces strong sidelobes in the resulting estimate. Other, more complicated windows produce far weaker sidelobes, and thus give better quality estimates from the same data. Therefore we have decided to use a Hamming window in all our estimates. Using windows has the added advantage that any spurious effects in the data will tend to be averaged out.

4. Application of the ARMA Techniques to the ESL Compact Range Data

In this chapter we describe the application of the techniques developed above to the OSU ESL Compact Range radar data. As described in Section 2.1, we have radar measurements in the 5–92 MHz range for five commercial aircraft, namely the Boeing 707, 727 and 747, the DC10 and the Concorde. This data has been obtained by measuring the response of scaled models of these aircraft; the measurement frequencies span the 1–12 GHz range.

4.1 Explanation of the Figures

This section describes the figures referred to in the next sections; it discusses the meaning of the various quantities shown and the meaning of the scales on the axes.

The figures that display actual data as it is stored in the database are in units of Volts/meter (in other words signal strength, not power) on the vertical axis, with the index into the database file on the horizontal axis. The frequency corresponding to index k is f_{k+1}.

The plots that give FFT results direct from the data are in units of the signal power (in dB meter^2) on the vertical axis, with the FFT index on the horizontal axis The FFT index k corresponds to range $\frac{k-1}{N-1}R$. All FFT are obtained by padding the data with zeroes to obtain 256 points.

The other plots all are in units of power (in dB meter^2) on the vertical axis, and range (in meters) on the horizontal axis. The range is corrected for the two-way

propagation effect, and has been plotted such that the physical center of the target is at half range; that is, if the horizontal scale runs from zero to 72 meters, then the center of the target is at 36 meters. The center of the target is the point on the model where it was attached to the pedestal in the Compact Range facility; this mounting point has been chosen to be approximately the target's geometrical center. All ranges have been corrected for the target scale factor, that is the ranges given are in meters for the actual aircraft, not for the model.

For the ARMA results we show two plots per figure, namely the estimated response and the estimated scattering centers (labelled "response" and "scatterers", respectively). Both are to the same horizontal scale to make comparisons easy. The "response" plot is the impulse response magnitude, and compares to the FFT. The "scatterers" plot is a graphical presentation of the pole and residue coefficients: each horizontal line represents a scattering center; the vertical tick mark gives the estimated range of the scattering center, and the width of the horizontal line represents the 3dB spatial dispersion of the scattering center (analogous to 3 dB bandwidth). The height of each horizontal line gives the energy associated with the scattering center.

4.2 Preliminary Modeling Results

In this section we study a few preliminary modeling and estimation issues. In particular, we study the effect of the frequency range used on the quality of the resulting estimates, the effect of model order, and we verify that the various data preprocessing strategies do not cause undesirable side effects on the results. In addition, we compare the ARMA modeling results with FT estimates for verification.

All results shown in this section were obtained with vertical polarization transmitted and received (VV data), and using targets at an aspect angle of 10°.

4.2.1 Data Decimation Effects

To see the effect of using all available data, we need to calculate the maximum unambiguous range R. To do this we need δ_f, which can be found by dividing the δ_f of the database by the scale factor of the aircraft under consideration; for the case of the Boeing 707 data this gives $\delta_f = 50 \cdot 10^6/150 = .33 \cdot 10^6$ Hz. From equation (2.14), with $\delta_f = 0.33$ MHz we have that using all available data gives an unambiguous range of about 450 m, see Figs A.1 and A.2. Both the FT and the ARMA result clearly show the presence of the target (Boeing 707) in the middle of the range, and no response to either side of it. To improve resolution, we need to decimate our data until we have decreased the unambiguous range to approximately equal the length of the aircraft. Since the aircraft is about 70 m long, decimation of $450/70 \approx 6.49$ is needed; thus, we need to use about $211/6.49 = 32$ data points for full bandwidth cases (using all frequency data), or about 16 for half bandwidth cases (using either the upper or the lower half of the measurements).

4.2.2 Hamming Window Data Averaging

The next set of figures shows the effects of averaging the data with a three-point Hamming window. Hamming window averaging is equivalent to multiplying the target response (in the range domain) with the inverse FT of a Hamming window. it is readily verified that a three point Hamming window has a main lobe width which is wider than any target of interest. Thus, this averaging has the effect of

attenuating any spurious response outside the target range [2].

Fig A.3 is the raw data (amplitude and phase) for one of the targets (code name target 32) The horizontal axis shows the value of the index into the data array, the lowest index corresponds to 1 GHz, the highest index to 12 GHz (these are the scaled data base frequencies, not the frequencies for a full-size target). Fig. A.4 shows the windowed data (three point Hamming window) in the same format. As can be seen by comparing the two Figures, the Hamming window does not greatly alter the data. Figure A.5 shows the decimated data (decimated by a factor of 6). The frequency range is the same; i.e., index 1 corresponds to 1 GHz, and index 36 to 12 GHz. The values in this plot are obtained through the same Hamming window as used in Fig. A.4; the effect of the decimation can be readily seen by comparing the two Figures: Figure A.5 has the same overall shape as figure A.4, but does not have the more rapid variations seen in the latter figure.

Figure A.6 shows the result of an FT on the raw data of Fig. A.3. This clearly shows the target (the bumps at the edges of the plot), and the expected empty space around it (the low region in the middle). Figure A.7 shows the result of an FT on the windowed data of Figure A.4. By comparing with the FT result for the raw data (Fig. A.6), it is clear that the window achieves its intended function of reducing the spurious responses in "empty space" region without altering the response in the "aircraft" region: this will reduce aliasing effects when the data is decimated. Finally, Figure A.8 shows the FT of Figure A.5, the windowed and decimated data. We can clearly see that the "aircraft" region has now expanded to occupy the entire plot range, as intended.

4.2.3 Stationarity of the Data

Going back to the previous example (the Boeing 707), Figure A.9 shows the ARMA results when we use frequency data in the 6.67–40 MHz range, about half of the available bandwidth; Figure A.10 is the corresponding FT. Figure A.11 shows the ARMA, and Figure A.12 shows the FT results for data from the 40– 80 MHz range, the upper half of the frequency band. Comparison between the ARMA response curves and the FT curves shows that they agree only marginally well. One reason for this is that the FT curve represents the ideal response convolved with a window function; the ARMA response does not contain this windowing operation. Second, it is the *area* under a peak in the ARMA curve that represents its energy; thus, sharp peaks with little energy seem to disagree with FT results, when in fact the agreement is far better. We have found it more helpful to compare the scatterers plots with the FT plots; here one sees direct correspondence between scattering centers of significant energy and peaks in the FT curves.

To consider "data stationarity", compare the lower frequency plots with the higher frequency plots. It can be seen that the ARMA estimates for the lower frequency range give much more spatially distributed scatterers (that is scatterers that are not point-like, but occupy a non-zero range). These results imply that:

- the data is not stationary with respect to frequency. This is to be expected from electromagnetic theory, but we have now observed that the effect is significant in the frequency ranges and bandwidths used in this study.

- Since the ARMA model is well suited to estimating point-like scatterers (i.e. a more optical response), we should use higher frequency data whenever pos-

21

sible, because more point-like scatter-behaviour is seen in this range. It is expected that data taken at higher frequencies will result in better performance of the ARMA techniques.

Based on these observations, all remaining experiments use data in the 40–80 MHz range.

4.2.4 Removal of Spatially Distributed Scattering Centers

To further reduce the effects of non-stationarity, and improve performance, we use a technique that has the added advantage of enabling the ARMA estimator to automatically choose the number of scattering centers to include in the model; for estimation on unknown target data this is an important and desirable property of the algorithm.

The technique uses the fact that the estimation procedure entails two main steps: first the locations and spatial distribution of the scattering centers are estimated, then their energies are computed. The modified algorithm performs the first step with a fixed number na of scattering centers. Then all centers that are too spatially distributed are eliminated. Finally, the amplitudes of the remaining centers are estimated as before.

The spatial distribution of a scattering center is related to the magnitude of the pole estimated for that center (see (2.17)); the contribution of the center to the frequency response at frequency f_i is (C.f. (2.18))

$$d_i p_i^k \qquad 0 \le k \le N - 1$$

If $|p_i|$ is too far from unity (i.e. if the scattering center is too spatially distributed),

22

then its contribution to the frequency model is greatly different at frequency f_0 then at frequency f_{N-1}. The ratio of these contributions is:

$$
\begin{aligned}
D &= \left| \frac{p_i^{N-1}}{p_i^0} \right| = |p_i|^{N-1} \quad , \quad |p_i| > 1 \\
D &= \left| \frac{p_i^0}{p_i^{N-1}} \right| = |p_i|^{-N+1} \quad , \quad |p_i| < 1
\end{aligned}
\tag{4.1}
$$

In the modified algorithm, if $|p_i|$ is such that D is greater than some threshold, that pole is discarded.

Empirical tests showed that $D = 100$ provided good removal of highly dispersive scatterers without removing sharp scatterers. As an example, Figures A.13 and A.14 show the results for $D = 1000$ and $D = 100$, respectively. It can be seen that the results are very similar for the two cases. Also, comparing Figure A.14 with Figure A.11 (where no pole removal is used) shows that sharp scatterers are more clearly seen if $D = 100$ is used. Finally, it was found that estimation results were less sensitive to model order selection when this technique is used, as discussed below.

4.2.5 Effects of Model Order

The ARMA estimator is based on the assumption that the target can be modeled as a set of na scattering centers, where the value of na needs to be given. This section discusses the effect different choices of na has on the ARMA estimates.

Figures A.15 through A.21 show the effect of increasing the order of the ARMA estimate from 1 to 9; compare with the FT response in Figure A.12. The pole elimination procedure was used in these estimates with $D = 100$, so the number of scatterers in thew estimate is not equal to the original model order in many cases. It should be noted that for orders 1 and 3 the estimate did not contain any useful scatterers (all scatterers were too distributed) therefore, no plots are included for

these two cases. From the Figures we can clearly see that, as early as at fourth order the estimater picks out the two major peaks in the FT, which appear to correspond to the cockpit windows and the tail assembly. At sixth and higher orders we see additional peaks which seem to correspond to the leading edge of the engines and the trailing edges of the wing and the engines. At some orders (order 4, for example) we get a peak that seems to be a post-resonance.

The correspondence between the responses and the physical atributes of the target can be seen by overlaying Figure A.113 (a scaled picture of the Boeing 707), at an aspect angle of 10°, on the plots.

In evaluating these results, we should keep in mind that the Boeing 707 is a geometrically complicated target: it has four engines, a complex tail assembly, complex wing shape, and several irregularities on the body (cockpit windows, antennas). Such a complex target needs a high model order (for good modelling, we need the model order to be at least as high as the number of features, or about 15 for this plane), but, due to the small number of data points, we cannot increase the model order that far: in other words, this is a hard case for the ARMA estimator. Despite this, the ARMA estimator seems to give reasonable results, and the automatic elimination of spatially distributed scatterers seems to work well.

4.3 Aircraft Data Results

In this section we present two sets of results. The first set shows two aircraft, the Concorde and the Boeing 707, rotated through aspect angles $0° - -180°$, both at horizontal transmitted and horizontal received polarization (HH). The second set shows all five aircraft at an aspect angle of 10°, at both HH and VV polarization.

24

4.3.1 Comparison of Estimates at Different Aspect Angles

We expect from geometrical considerations that as an aircraft rotates, its response will vary more or less smoothly as a function of angle, so the aircraft will look different at different angles, but similar at similar angles. The DFT results for the Concorde (Figures A.79 through A.97) do indeed exhibit this behaviour, the DFT's for the Boeing 707 (Figures A.41 through A.59) do this to a lesser degree. The ARMA results for the Concorde (Figures A.60..A.78) show this behaviour for angles close to 0° and 180°, but not at intermediate angles. For example, the peak at range 48 m in Figure A.60 can be seen moving smoothly toward 40 m as the angle varies from 0° to 30°. Except for a few angles, the ARMA results for the Boeing 707 do not show this behaviour at all. We suspect this is caused by the fact that the ARMA model attempts to extract the most characteristic features of the response, rather than model it in its entirety, and the relative importance of various scatterers does not have to vary smoothly with the aspect angle.

Despite its non-continuous behaviour, the ARMA model seems to follow the most important peaks of the DFT rather faithfully, with exceptions at 110° and 140° for the Concorde and at 0°, 20°, 50°, 80°, 90° and 140° for the Boeing 707. Again it should be observed that the Boeing 707 is a complex plane, which is somewhat difficult to model.

4.3.2 Comparison of Estimates from Different Aircraft

The second set of results shows all five planes (Boeing 707, 727, 747; DC10 and Concorde) at 10° aspect (10° is chosen because 0° is a degenerate case where the complexity of the target is reduced through symmetry) in both Horizontal and

Vertical polarization.

As can be seen by comparing Figures A.103 through A.107 and A.108 through A.111 (the ARMA results) with Figures A.98 through A.102 (the DFT results), we again have a fairly good correspondence between the DFT and the ARMA results. It is also easy to see that the ARMA parameters for different aircraft are different, so a classifier based on ARMA results should be able to distinguish between these planes. Quantative analysis of such an ARMA-based classification procedure is a topic of future research.

5. Conclusions

From our simulations and analysis, we can conclude the following:

1. ARMA models can be used to estimate the impulse response of a radar target, given radar cross-section measurements at a number of different (evenly spaced) frequencies. Our simulations show that about 20 frequencies is enough to get satisfactory results.

2. The resulting ARMA estimates have the advantages over estimates obtained through Fourier Transform techniques that

   - They tend to concentrate on the strongest, most pointlike scattering centers in the response.

   - They are not resolution-limited by the bandwidth of the measurements.

   - They are expressed in the form of a small number of parameters, rather than as many samples of a curve.

Spacing of the frequency samples should be chosen such that the maximum unambiguous range of the target response is at least as large as the target. If the spacing of the frequency samples is chosen such that the maximum unambiguous range is much larger than the target length, modelling quality can be improved by applying data decimation techniques before the actual estimation. In a noisy environment, such a strategy could be used to improve the signal to noise ratio.

The total bandwi th of the measurements should be restricted so as to avoid violating the implicit stationarity assumption of the ARMA model. For the cases we have studied, we found that a bandwidth of 40–80 MHz works well.

27

While no formal quantative studies have been made, our simulations indicate that the ARMA modelling technique is capable of distinguishing between different aircraft, and between different aspect angles for the same aircraft. In other words, the ARMA modelling technique seems to be a suitable signal processing method to precede target classification. Future research should focus on a more formal, quantative evaluation of classification performance using ARMA parameters.

6. References

[1] T. S. Perry and P. Wallach, "A matter of margins," *Proceedings of the IEEE*, vol. 23, no. 11, pp. 38–44, November 1986.

[2] A. Kamis, F. D. Garber, and E. K. Walton, "Radar target classification studies – software development and documentation," Technical Report 716559-1, Generated under Contract No 00014-84-K-0705, for the Department of the Navy, Office of Naval Research, Arlington, VA, September 1985.

[3] Ögmundur Snorrason and F. D. Garber, "Feature selection applied to radar target identification," Technical Report 717220-3, Generated under Contract No 00014-85-K-0321, for the Department of the Navy, Office of Naval Research, Arlington, VA, July 1987.

[4] I. Jouny and F. D. Garber, "On M-ary sequential hypothesis testing for the classification of radar targets," Technical Report 717220-4, Generated under Contract No 00014-85-K-0321, for the Department of the Navy, Office of Naval Research, Arlington, VA, July 1987.

[5] O. S. Sands and F. D. Garber, "Syntactic pattern recognition for radar target identification," Technical Report 718048-2, Generated under Contract No 00014-86-K-0202, for the Department of the Navy, Office of Naval Research, Arlington, VA, May 1987.

[6] D. L. Mensa, *High Resolution Radar Imaging*. Dedham, MA: Artech House, 1981.

[7] A. Oppenheim and R. Schafer, *Digital Signal Processing*. Englewood Cliffs, New Jersey: Prentice-Hall, 1975.

[8] J. A. Cadzow, *Foundations of Digital Signal Processing and Data Analysis*. New York: MacMillan, 1987.

[9] M. G. Bellanger, "New applications of digital signal processing in communications," *IEEE ASSP Magazine*, vol. 3, no. 3, pp. 6–11, July 1986.

[10] A. J. Berkhout, "The seismic method in the search for oil and gas: current techniques and future developments," *Proceedings of the IEEE*, vol. 74, no. 8, pp. 1133–1159, August 1986.

[11] J. M. Mendel, "Some modeling problems in reflection seismology," *IEEE ASSP Magazine*, vol. 3, no. 2, pp. 4–17, April 1986.

[12] J. Makhoul, "Linear prediction: A tutorial review," *Proceedings of the IEEE*, vol. 63, no. 4, pp. 561–580, April 1975.

[13] A. V. Oppenheim and R. W. Schafer, *Digital Signal Processing*. Englewood Cliffs: Prentice–Hall, 1975.

[14] L. H. Koopmans, *The Spectral Analysis of Time Series*. New York: Academic Press, 1974.

[15] A. A. Beex, "Covariance sequence approximation with applications to spectrum analysis and digital filter design," Ph.D. Thesis, Colorado State University, 1979.

[16] J. Li, "On the estimation of damped and undamped sinusoids with application to speech analysis," M.S. Thesis, The Ohio State University, 1987.

[17] G. Box and G. Jenkins, *Time Series Analysis: Forecasting and Control.* San Fransisco: Holden-day, 1976.

[18] H. L. van Trees, *Detection, Estimation, and Modulation Theory; Part 1, Detection, Estimation, and Linear Modulation Theory.* New York: Wiley, 1968.

[19] L. Marple, *Digital Spectral Analysis with Applications.* Englewood Cliffs: Prentice-Hall, 1987.

[20] R. Carrière and R. L. Moses, "Short data length effects in an asymptotically efficient ARMA spectral estimator," Technical Report 717220-5, Generated under Contract No 00014-85-K-0321, for the Department of the Navy, Office of Naval Research, Arlington, VA, 1987.

A. Figures

The following pages contain the Figures for this report

scatterers
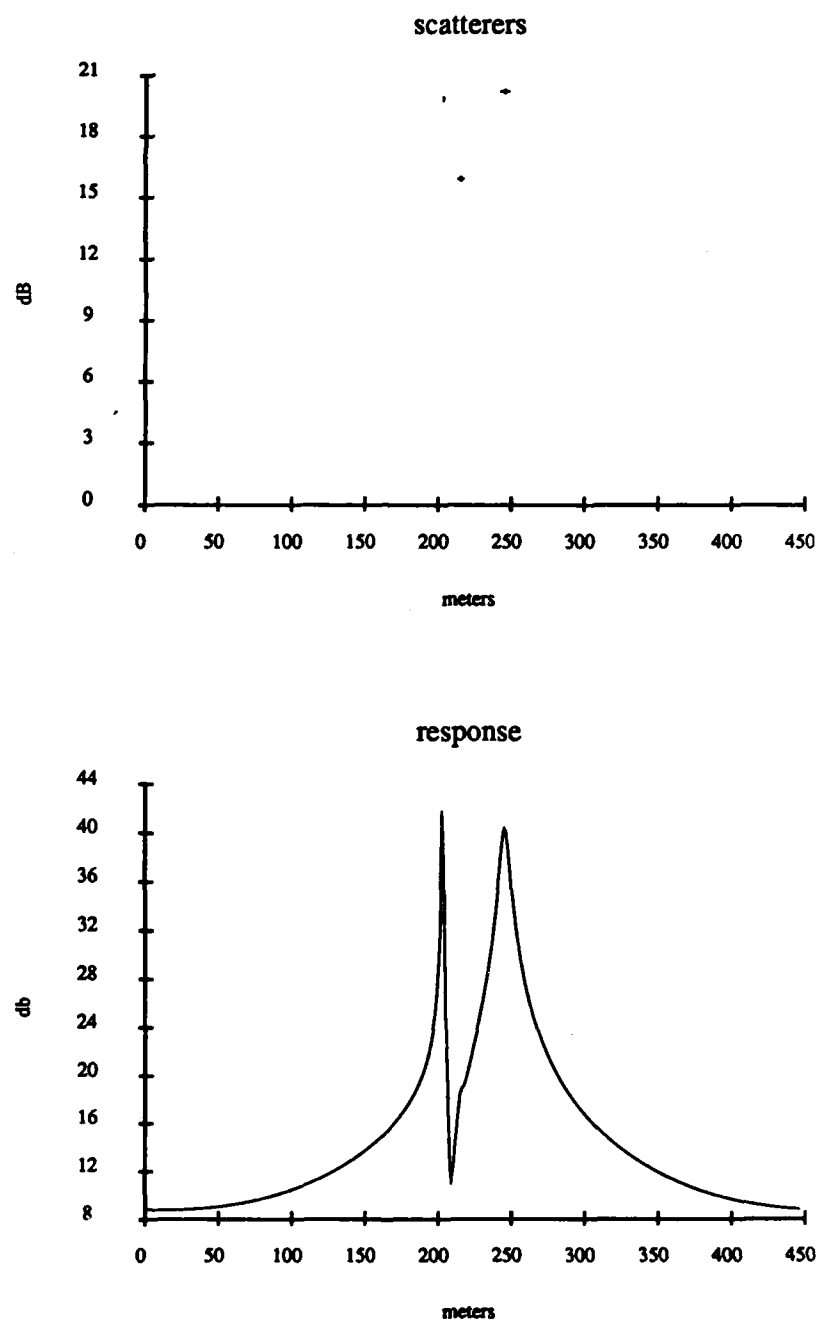
response

Figure A.1: ARMA Response of Boeing 707 at Vertical Polarization, 10° aspect angle, 40–80 MHz, 120 frequency samples used
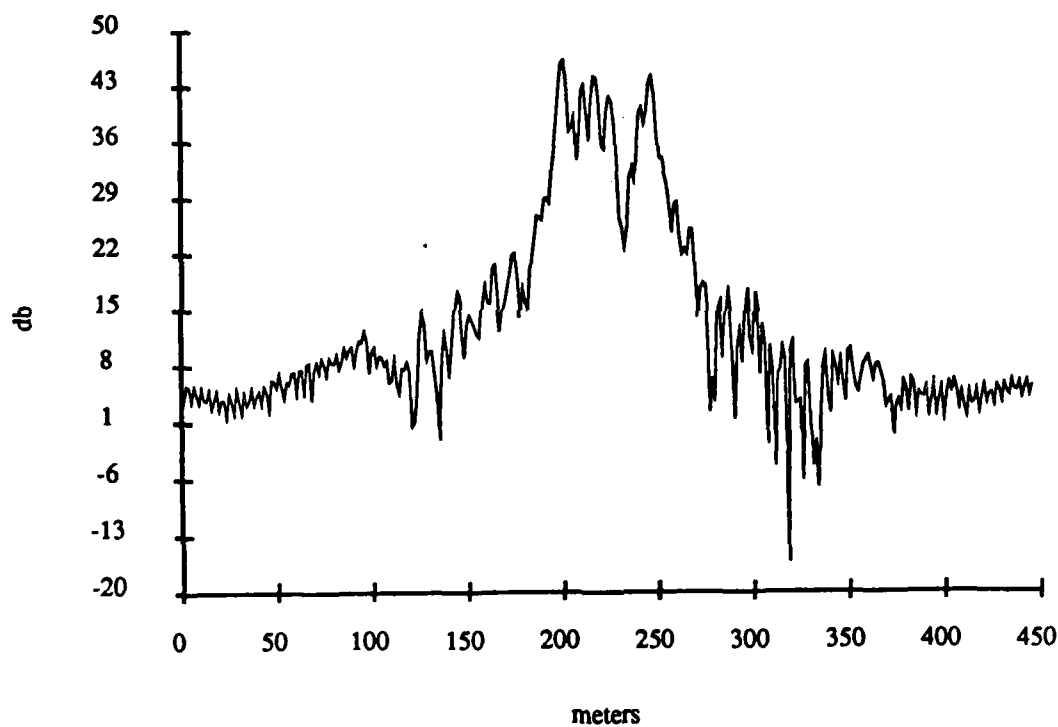
Figure A.2: FT of Boeing 707 at Vertical Polarization, 10° aspect angle, 40–80 MHz, 120 frequency samples used (zero padded to 340)

Raw Data --- Amplitude

Raw Data --- Phase
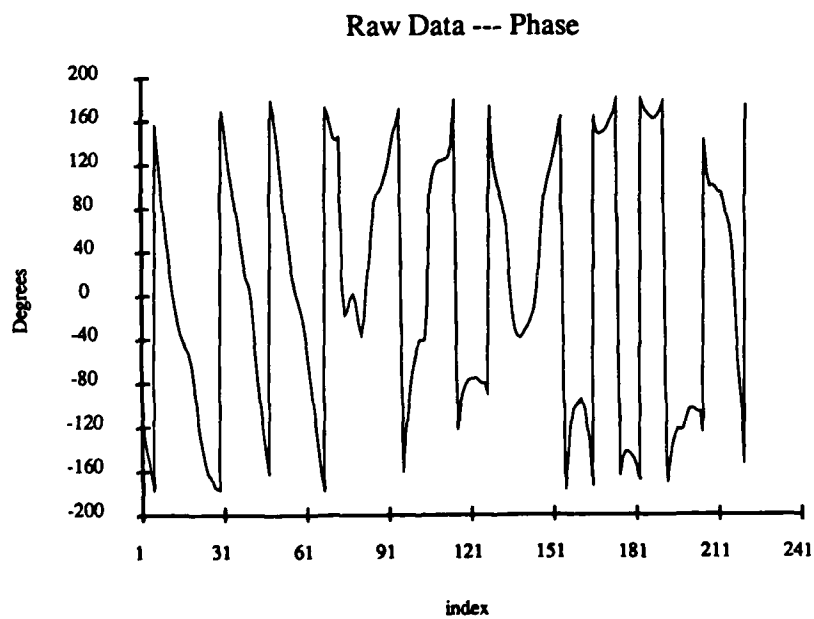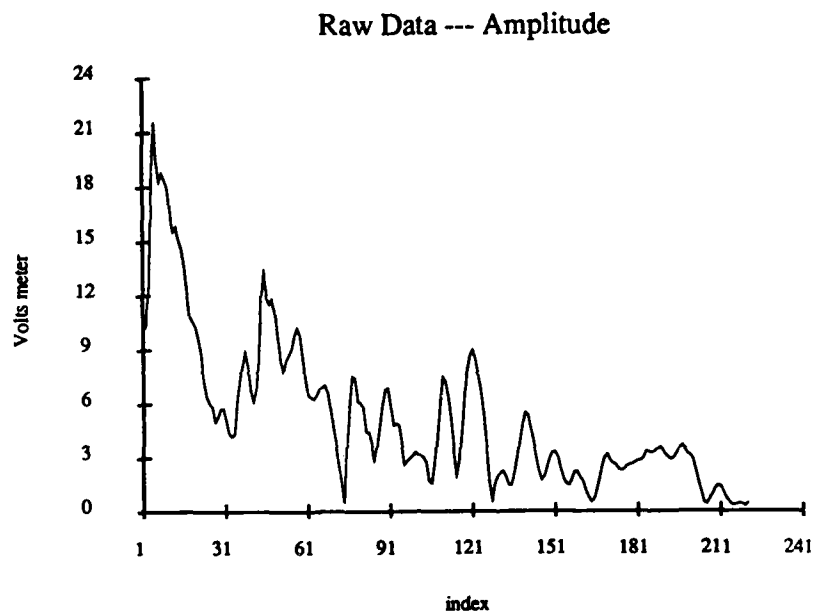
Figure A.3: Target number 32, Vertical Polarization, 10° aspect angle, 1–12GHz model frequencies, all frequency samples used.

Windowed Data --- Amplitude

Windowed Data --- Phase
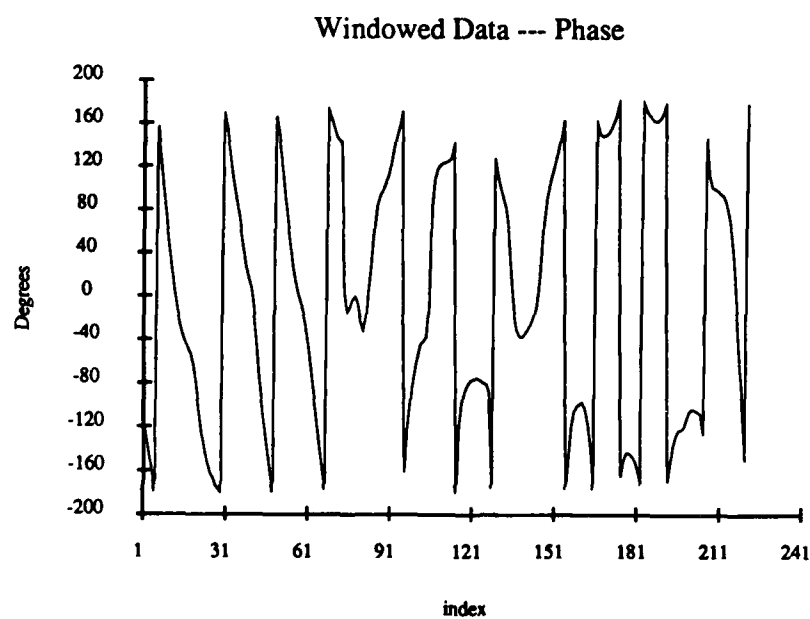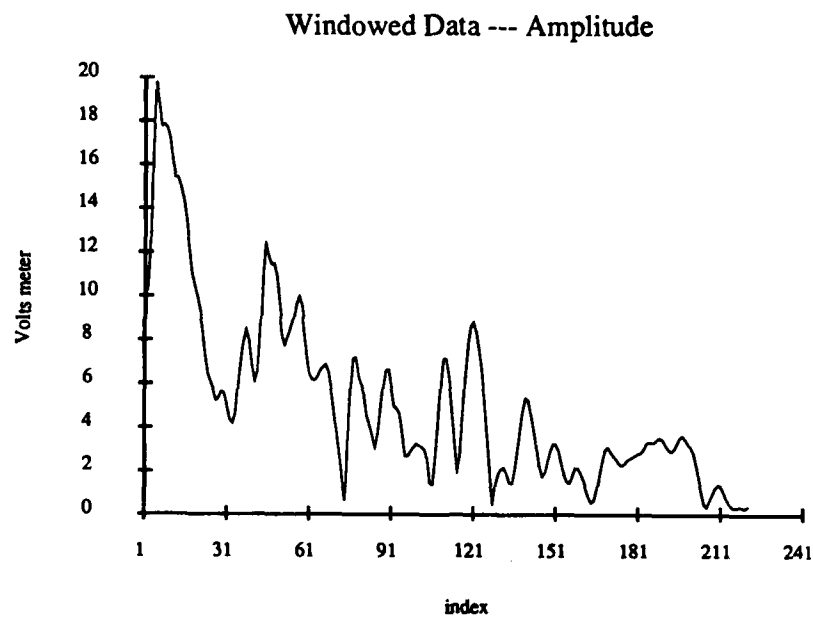
Figure A.4: Target number 32, Vertical Polarization, 10° aspect angle, 1–12GHz model frequencies, with 3-point Hamming window, all frequency samples used.

36
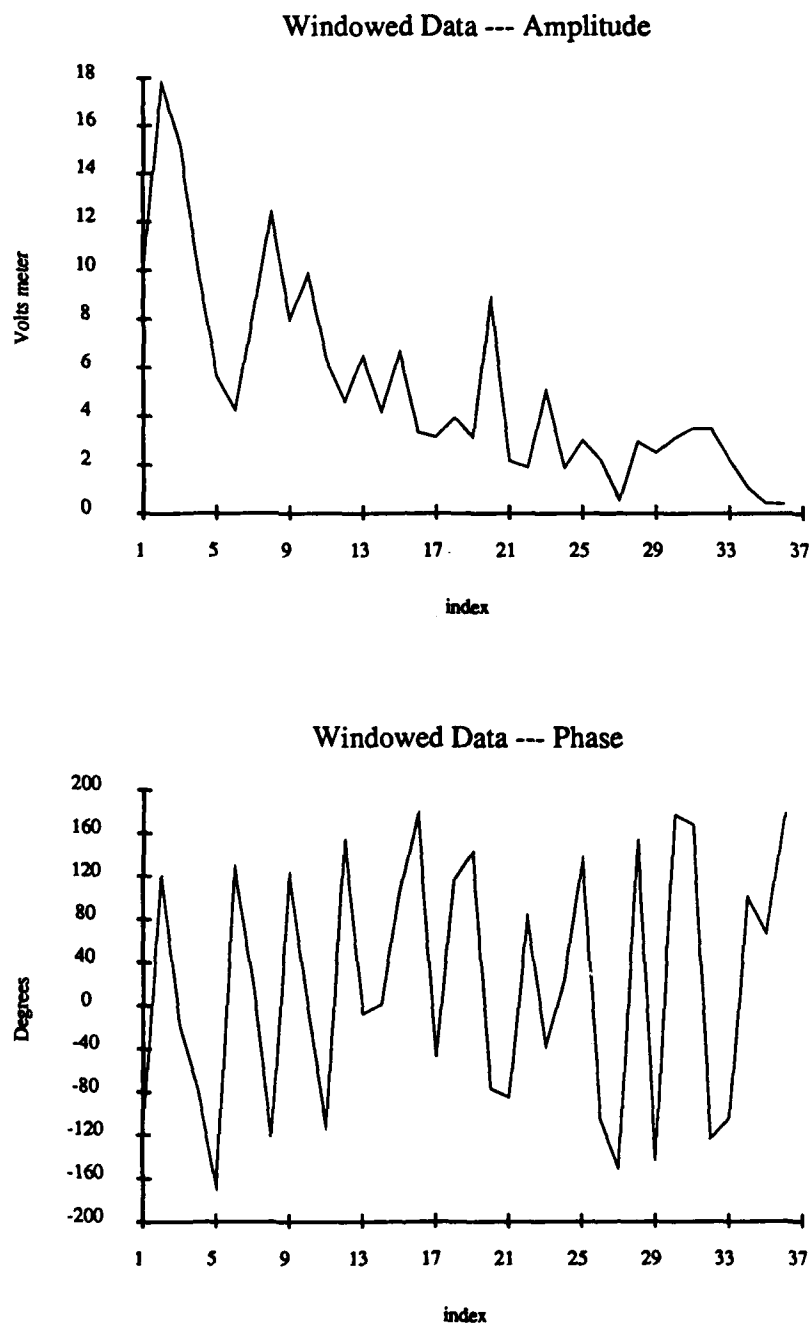
Figure A.5: Target number 32, Vertical Polarization, 10° aspect angle, 1–12GHz model frequencies, with 3-point Hamming window, 36 frequency samples used.
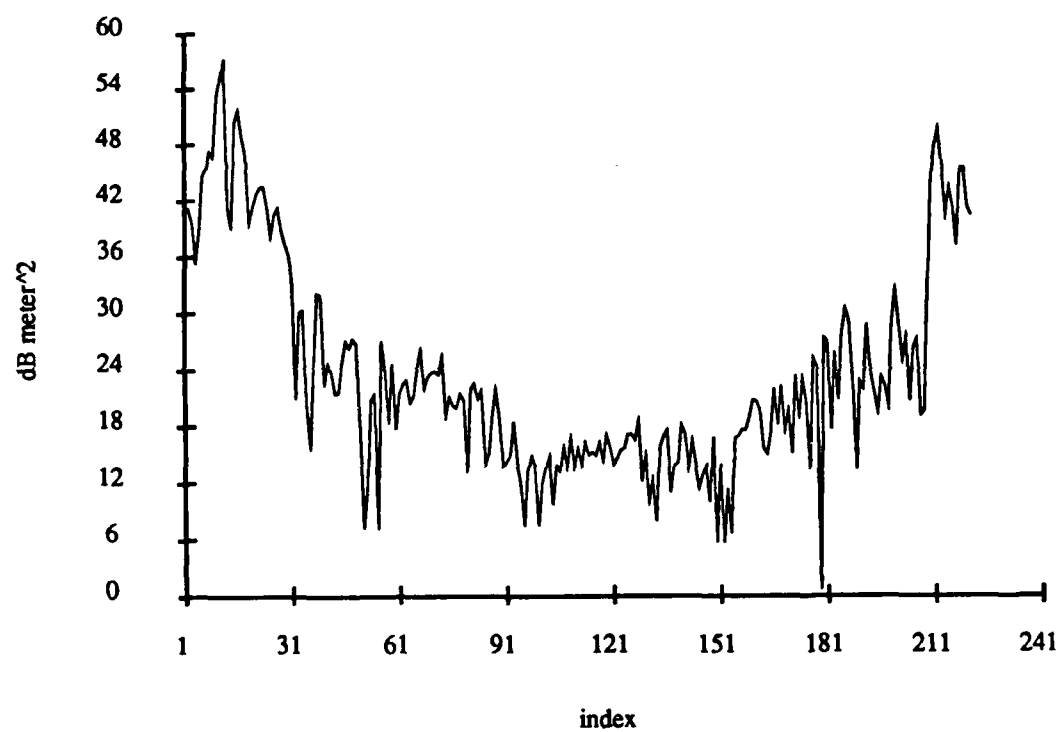
Figure A.6: FT of Target number 32, Vertical Polarization, 10° aspect angle, 1–12GHz model frequencies, all frequency samples used.
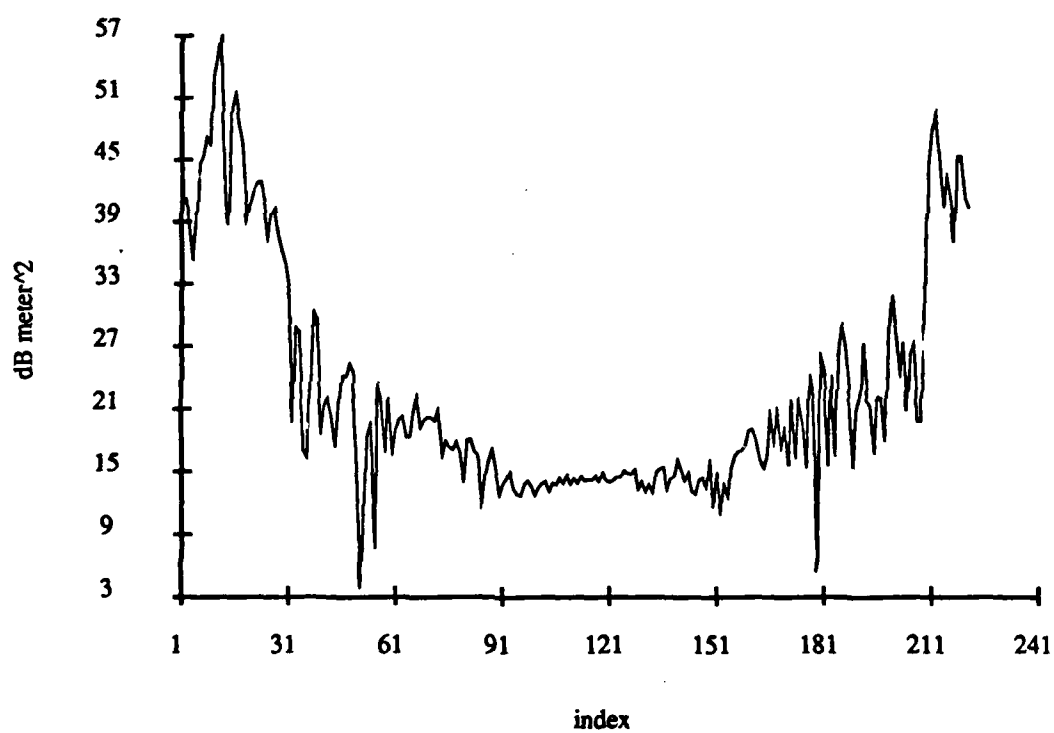
Figure A.7: FT of Target number 32, Vertical Polarization, 10° aspect angle, 1–12GHz model frequencies, with 3-point Hamming window, all frequency samples used.

39
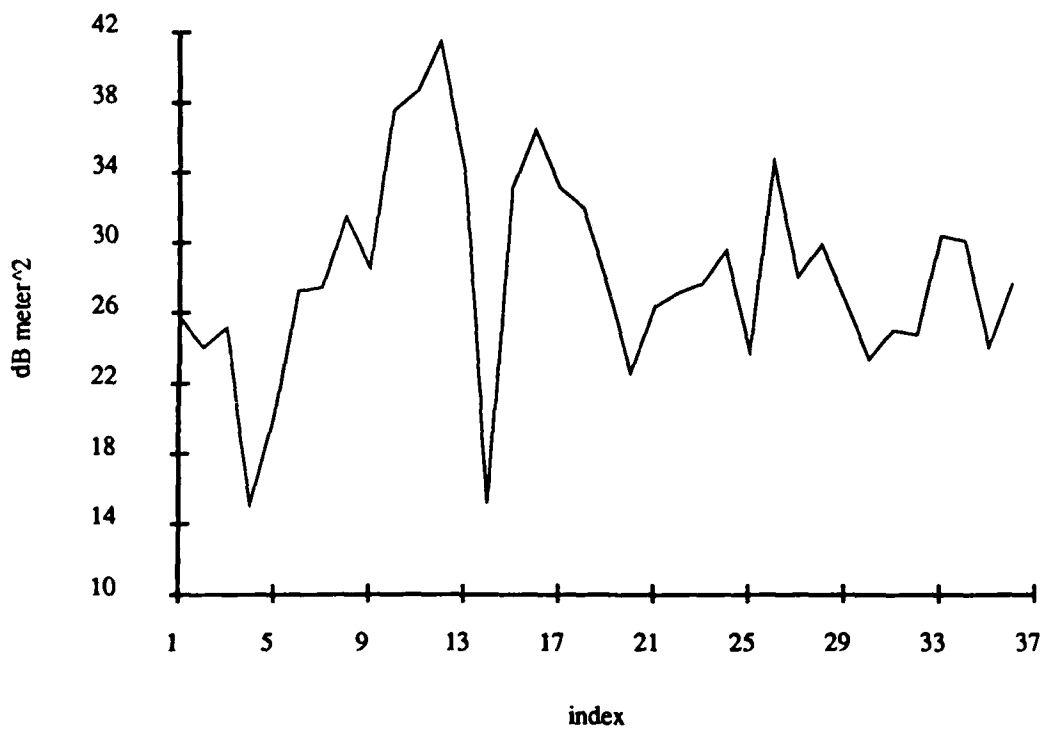
Figure A.8: FT of Target number 32, Vertical Polarization, 10° aspect angle, 1–12GHz model frequencies, with 3-point Hamming window, 36 frequency samples used.
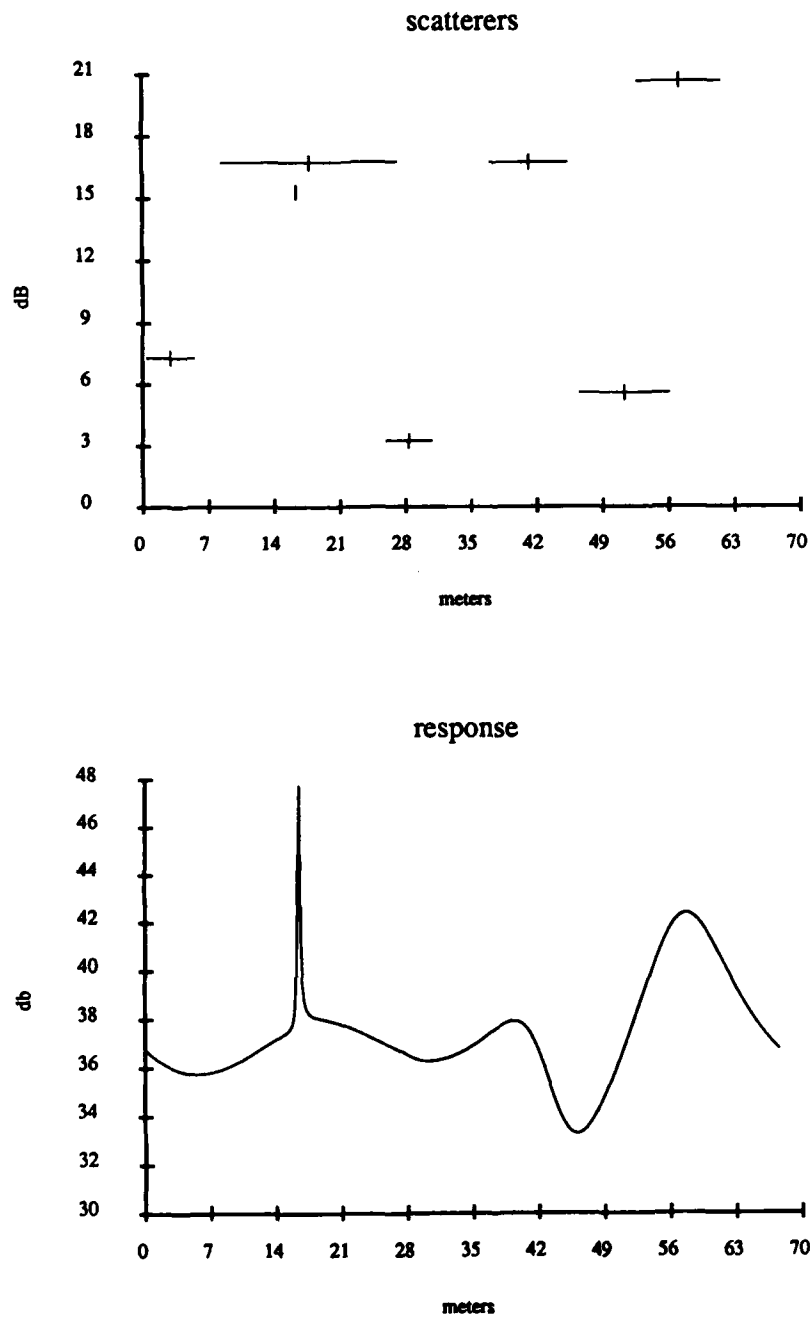
Figure A.9: ARMA Response of the Boeing 707 at Vertical Polarization, 10° aspect angle, 16 frequency samples used, 6.67–40 MHz.
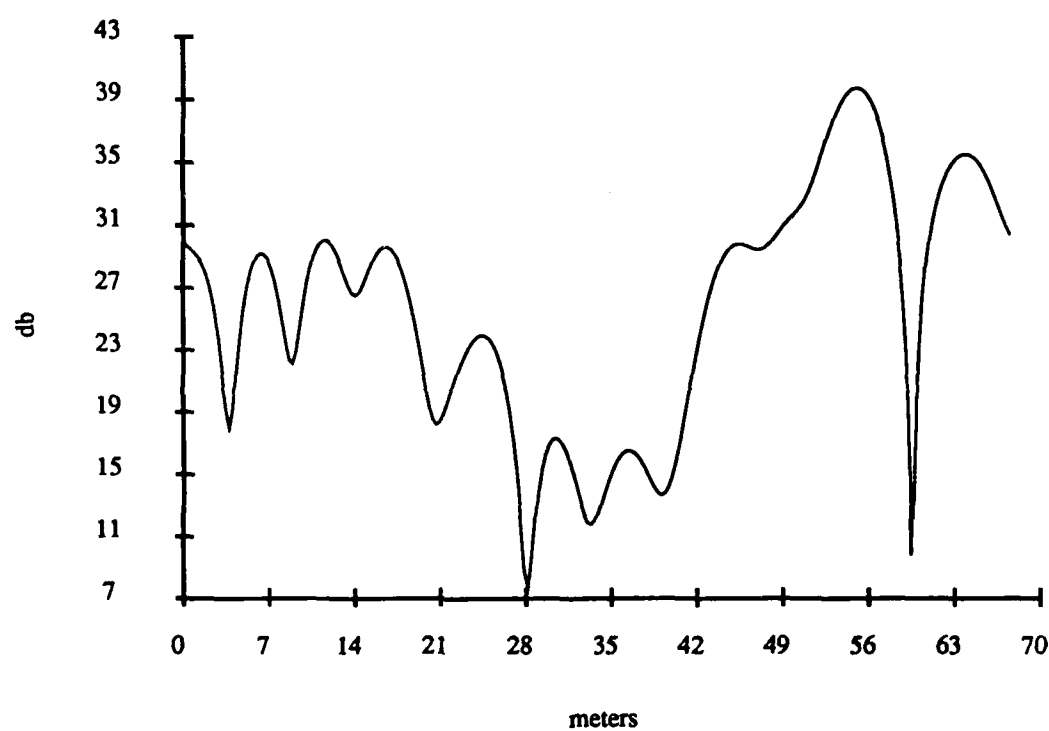
Figure A.10: FT of the Boeing 707 at Vertical Polarization, 10° aspect angle, 16 frequency samples used, zero padded to 256, 6.67–40 MHz.
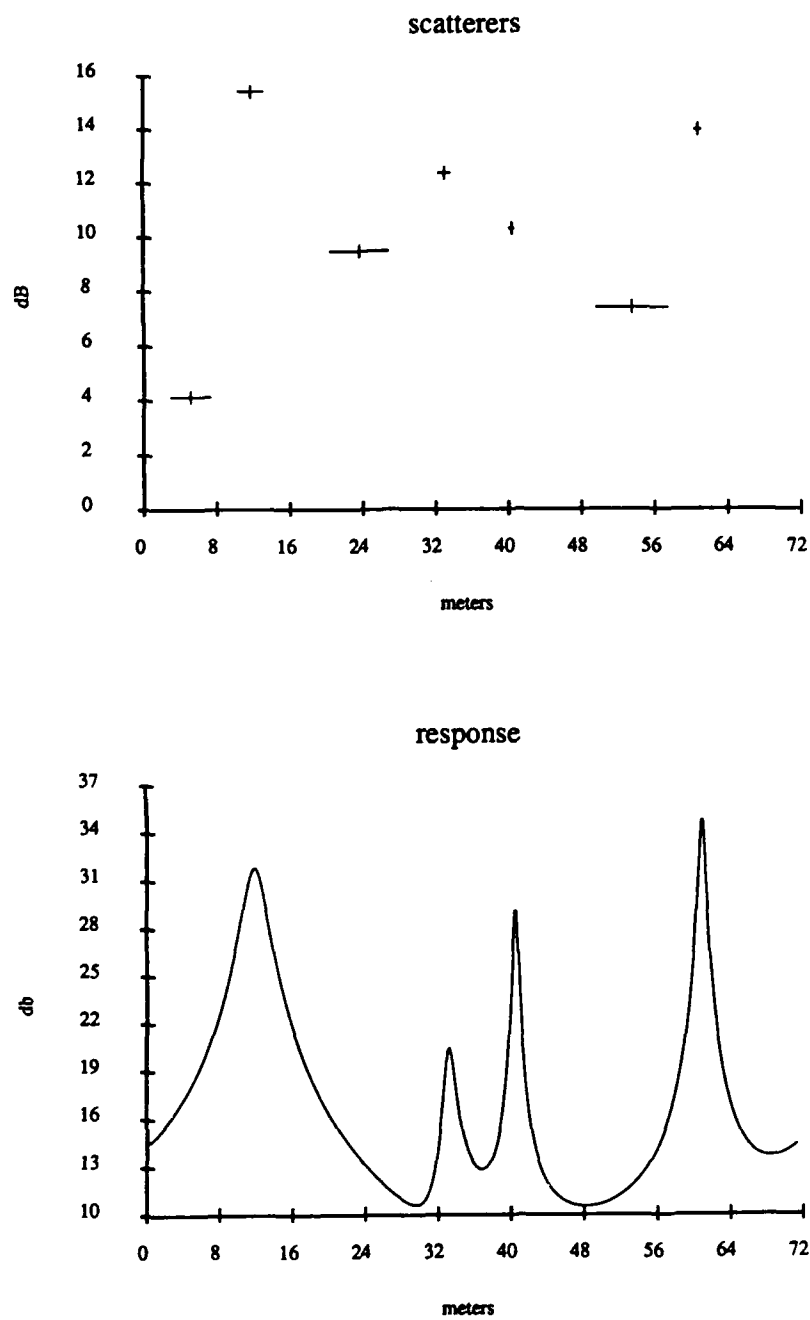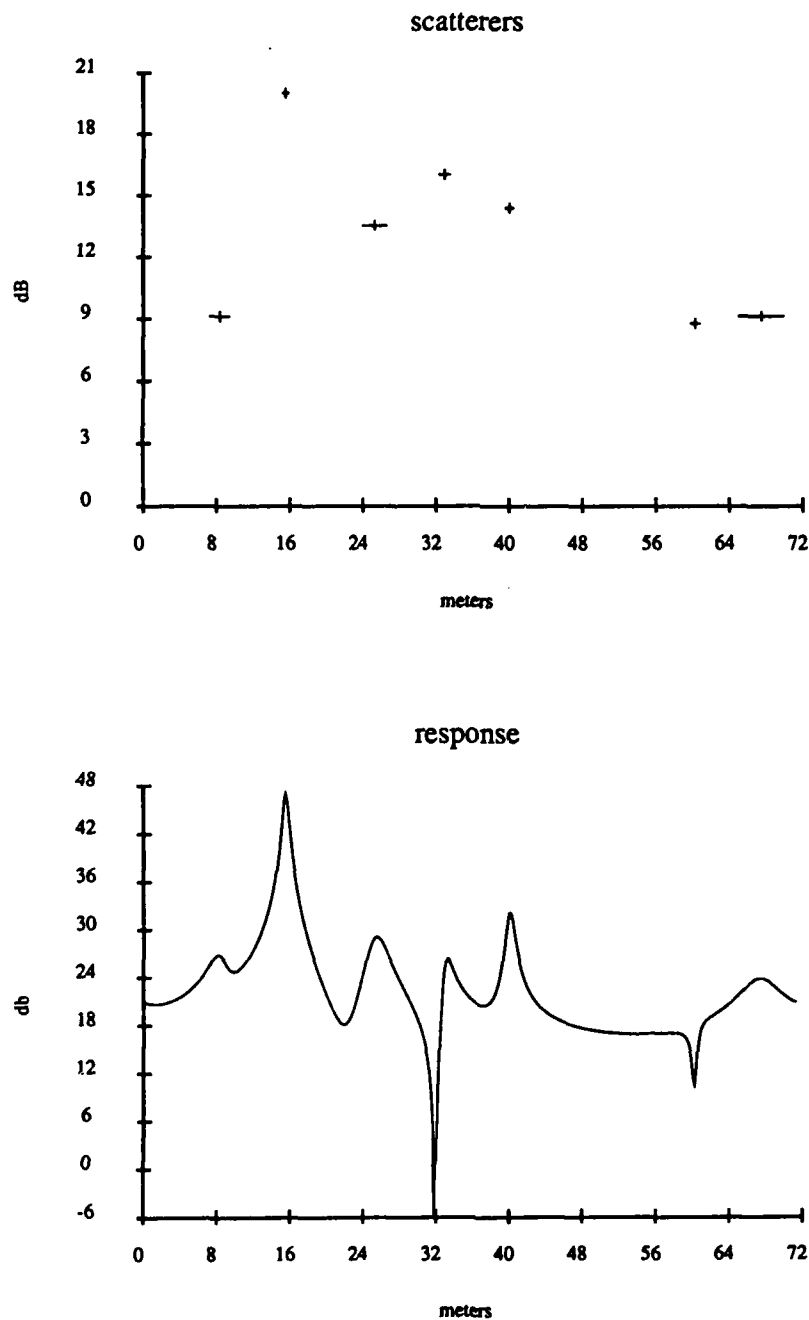
Figure A.11: ARMA Response of the Boeing 707 at Vertical Polarization, 10° aspect angle, 20 frequency samples used, 40–80 MHz.
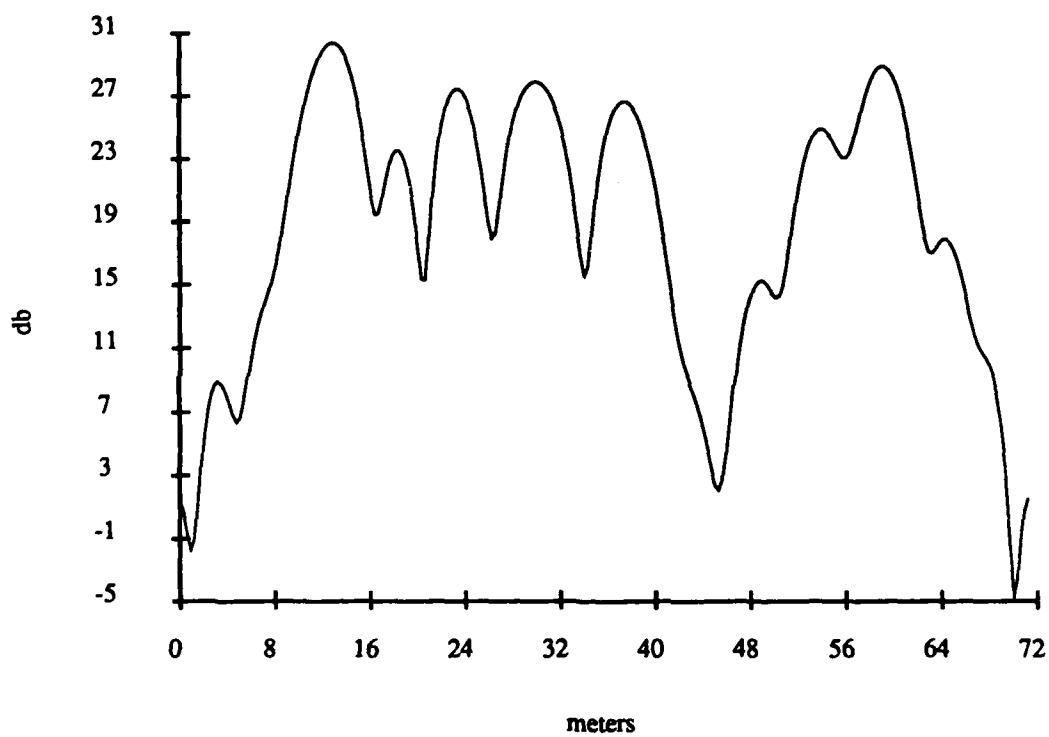
Figure A.12: FT of the Boeing 707 at Vertical Polarization, 10° aspect angle, 20 frequency samples used, zero padded to 256, 40–80 MHz.

44
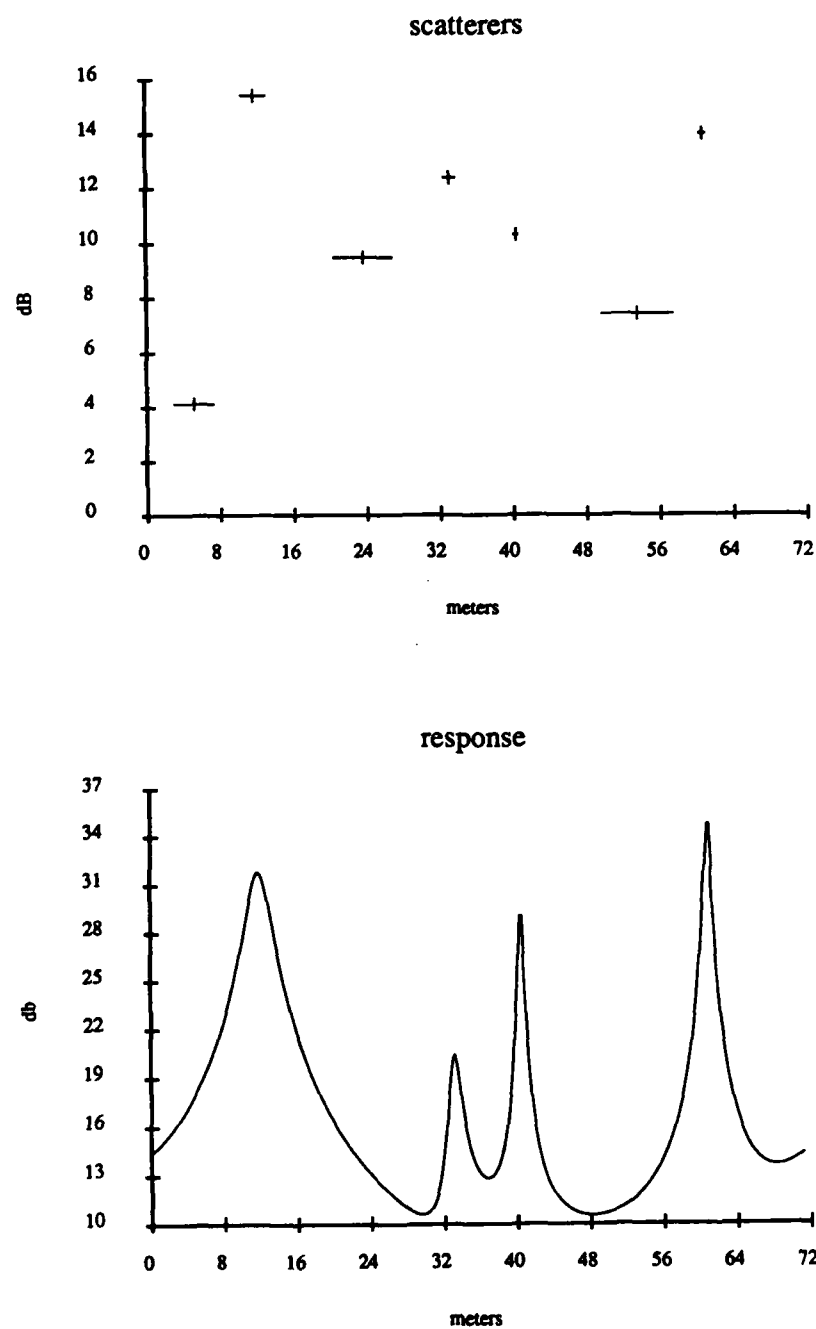
Figure A.13: ARMA Response of the Boeing 707 at Vertical Polarization, 10° aspect angle, 20 frequency samples used, 40–80 MHz, rejection factor=1000

45
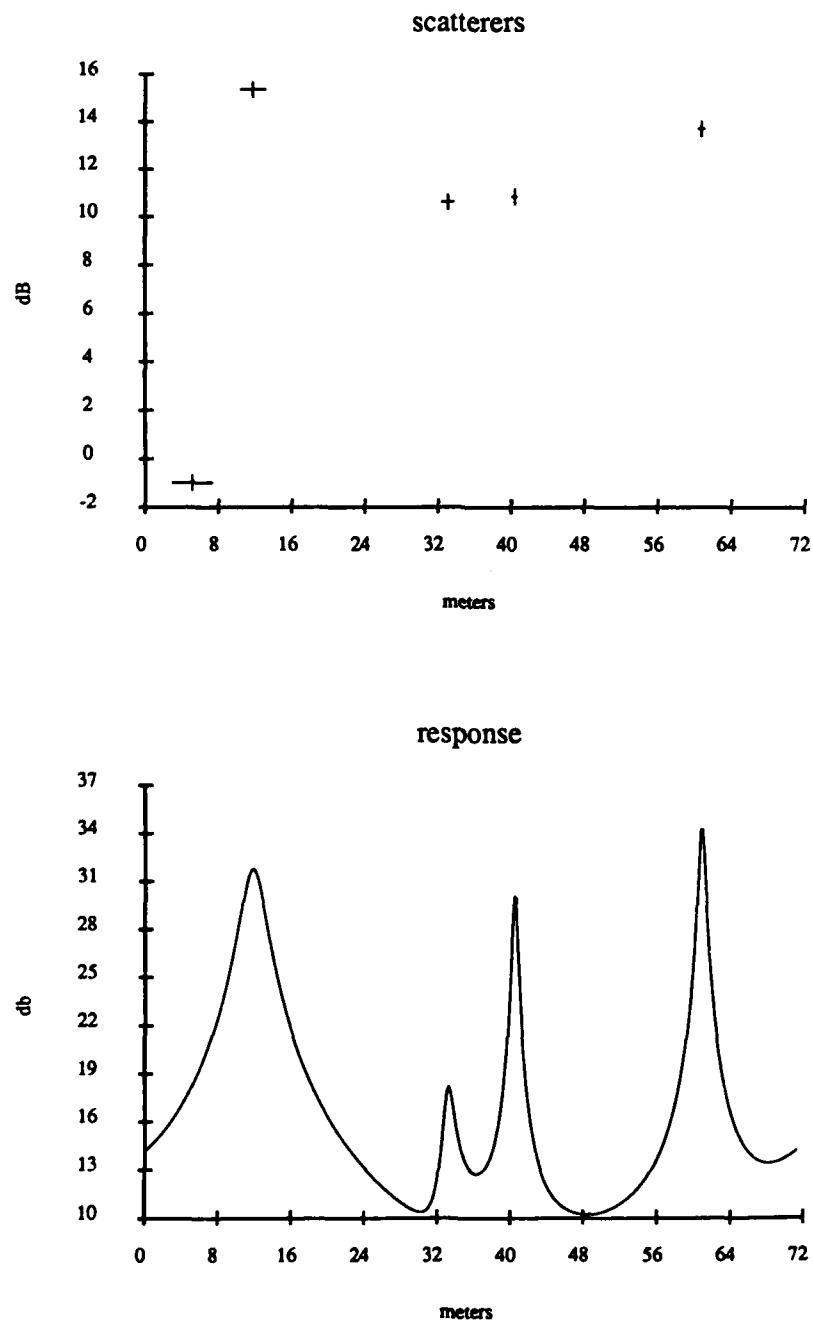
Figure A.14: ARMA Response of the Boeing 707 at Vertical Polarization, 10° aspect angle, 20 frequency samples used, 40–80 MHz, rejection factor=100
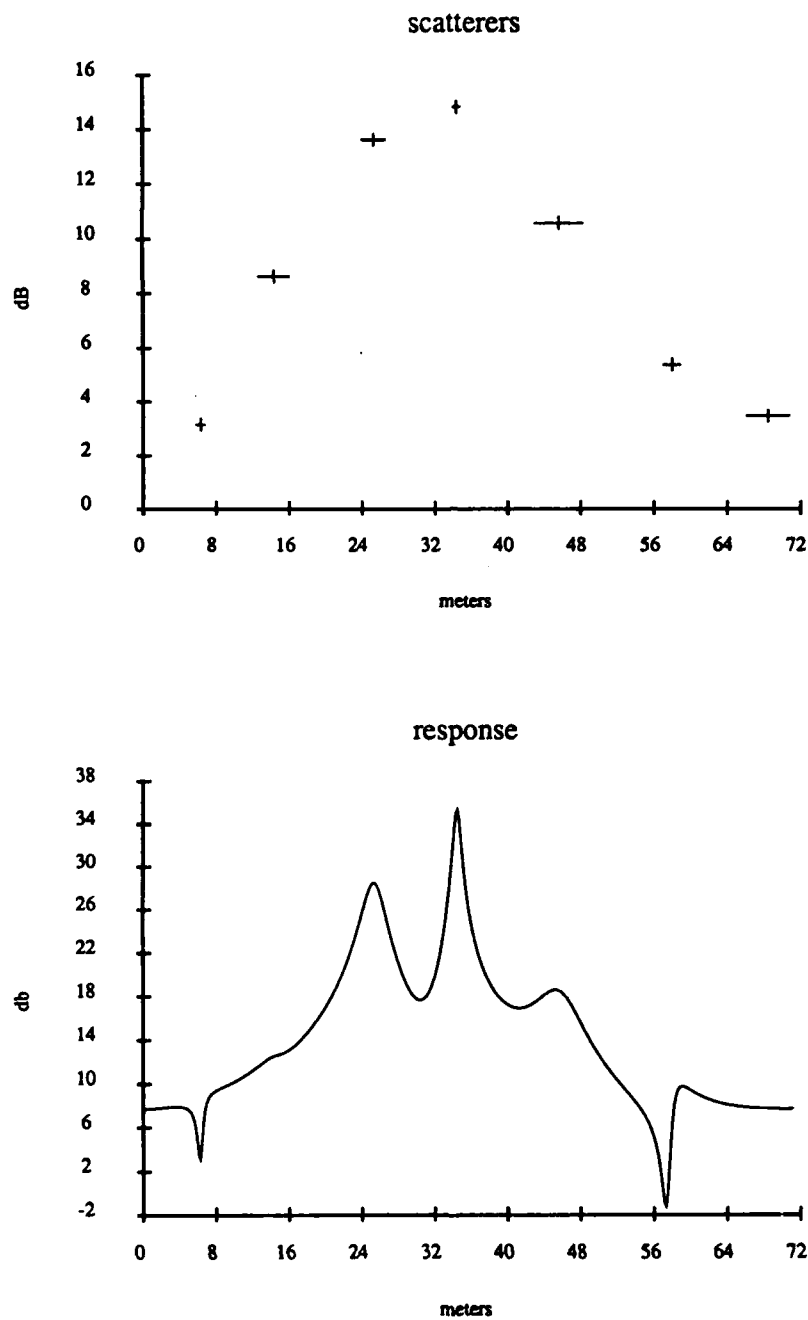
scatterers
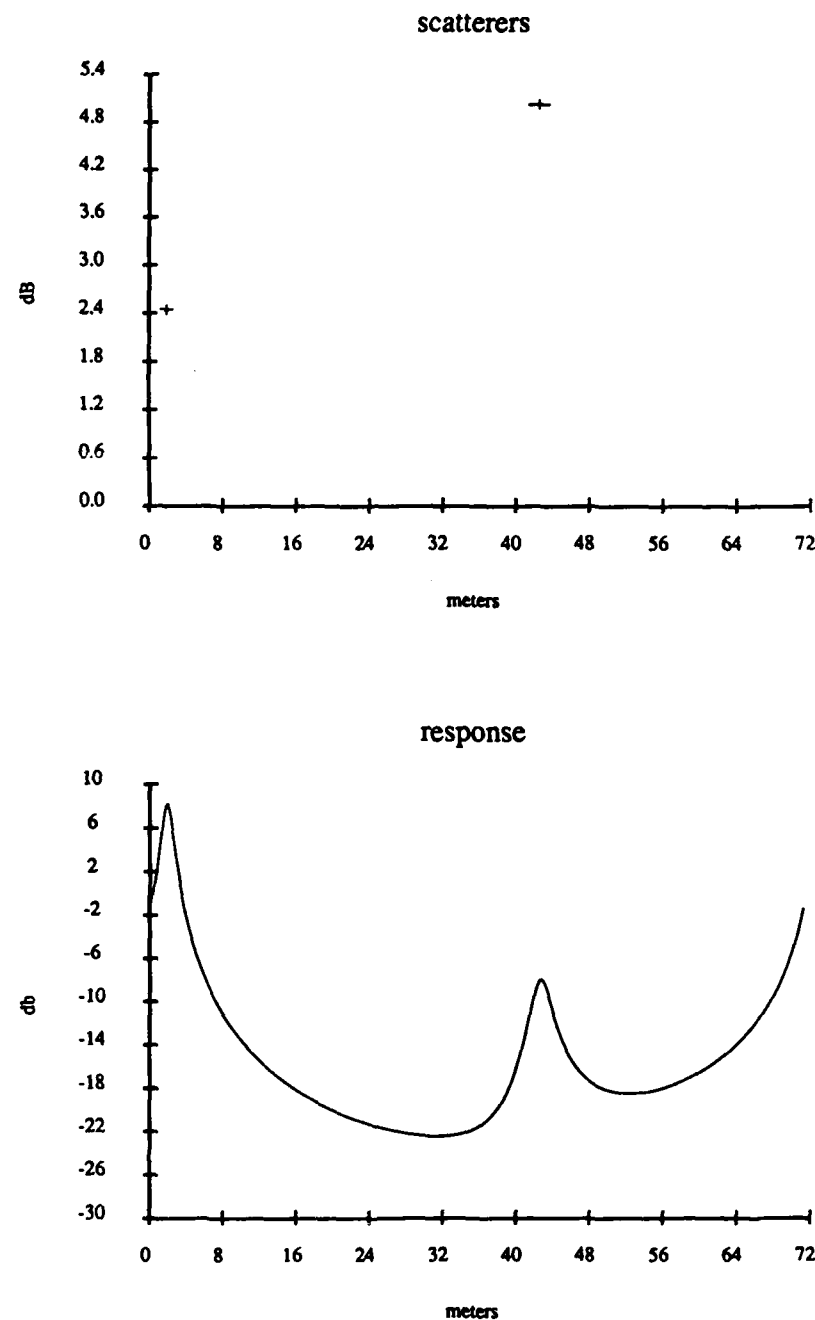
response

Figure A.15: ARMA Response of the Boeing 707 at Vertical Polarization, 10° aspect angle, 20 frequency samples used, 40–80 MHz, 2nd order model

47
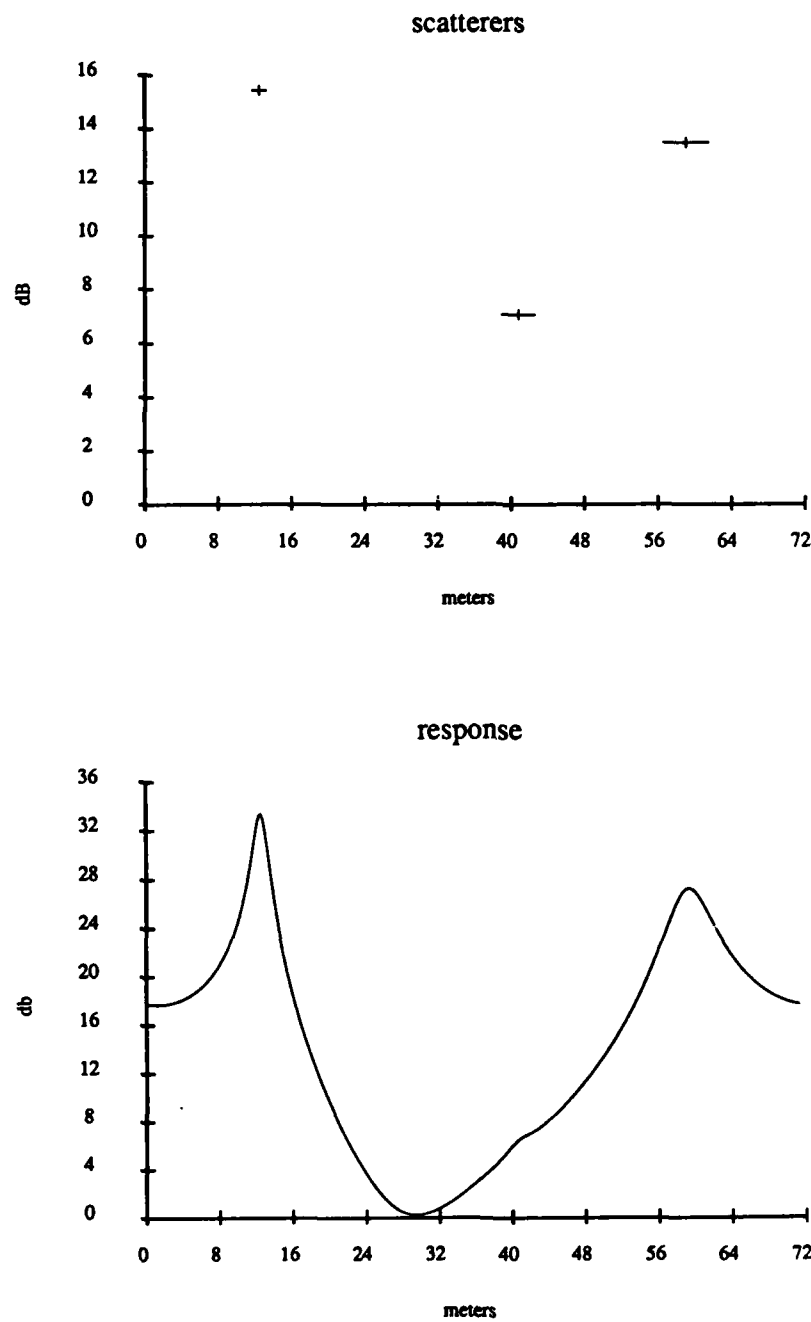
Figure A.16: ARMA Response of the Boeing 707 at Vertical Polarization, 10° aspect angle, 20 frequency samples used, 40–80 MHz, 4th order model

48

scatterers
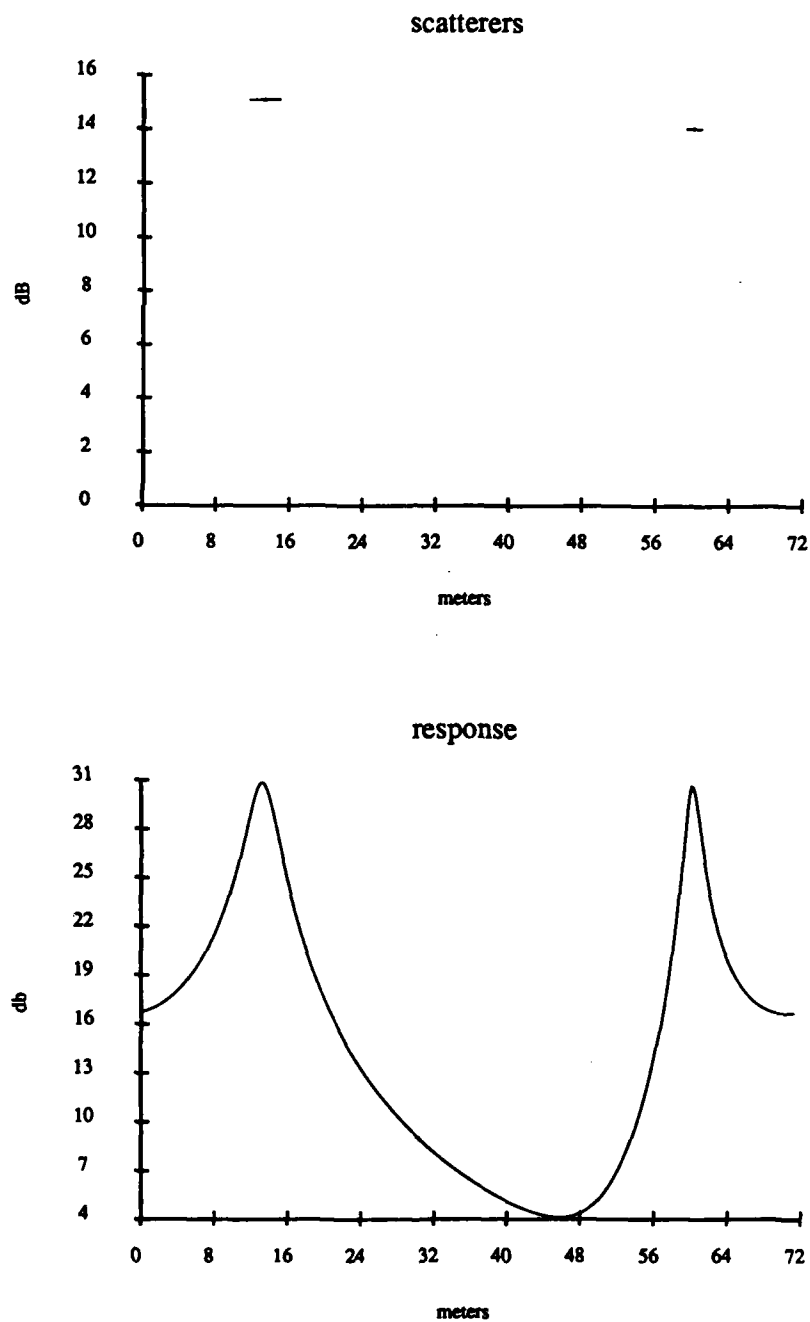
response

Figure A.17: ARMA Response of the Boeing 707 at Vertical Polarization, 10° aspect angle, 20 frequency samples used, 40–80 MHz, 5th order model

49
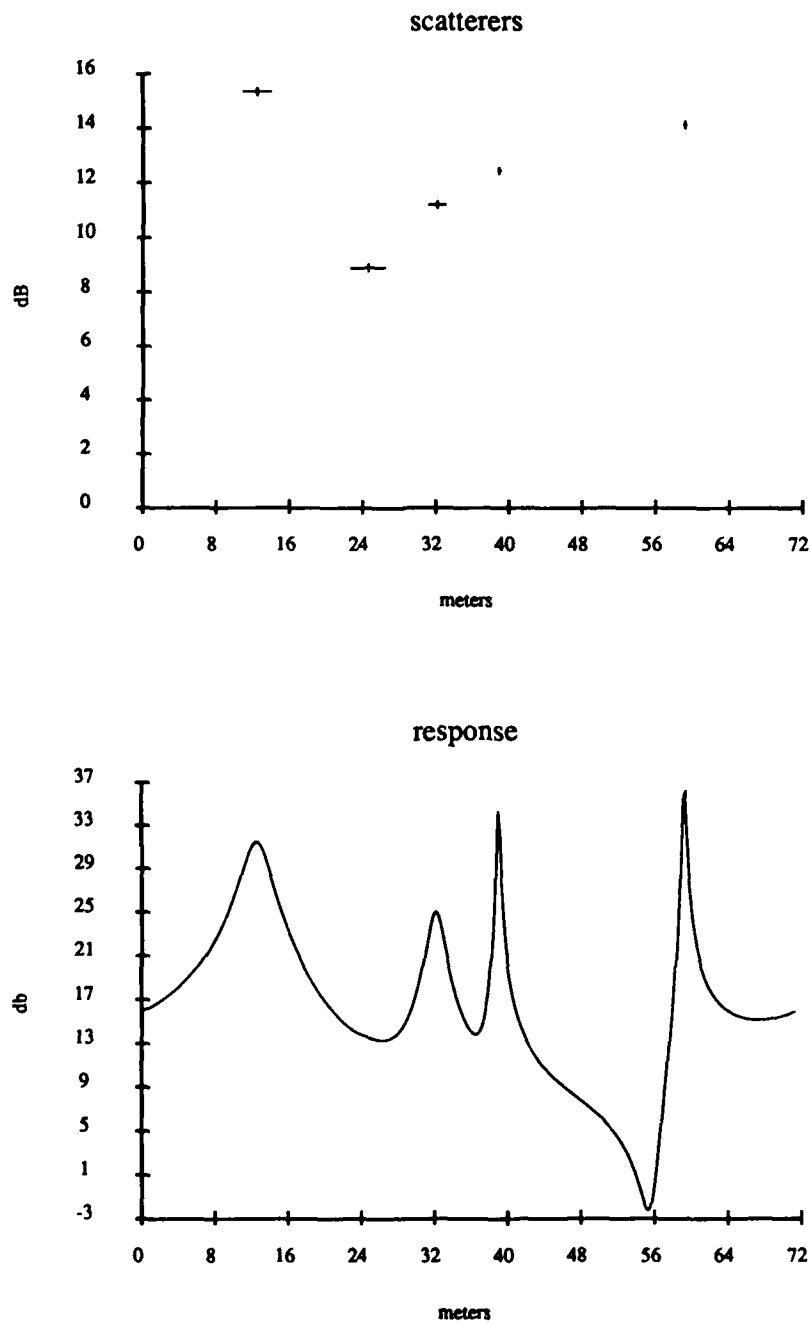
Figure A.18: ARMA Response of the Boeing 707 at Vertical Polarization, 10° aspect angle, 20 frequency samples used, 40–80 MHz, 6th order model

50
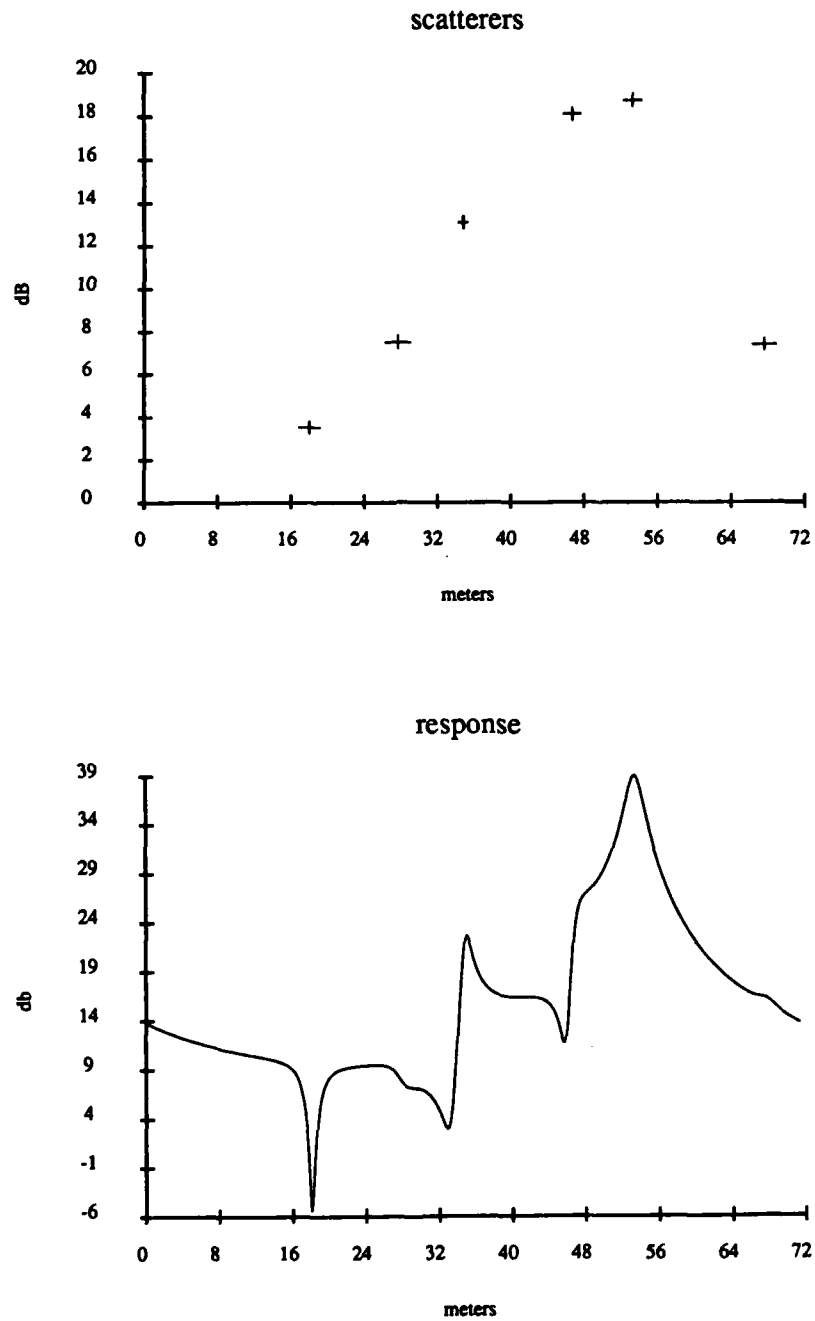
Figure A.19: ARMA Response of the Boeing 707 at Vertical Polarization, 10° aspect angle, 20 frequency samples used, 40–80 MHz, 7th order model

scatterers
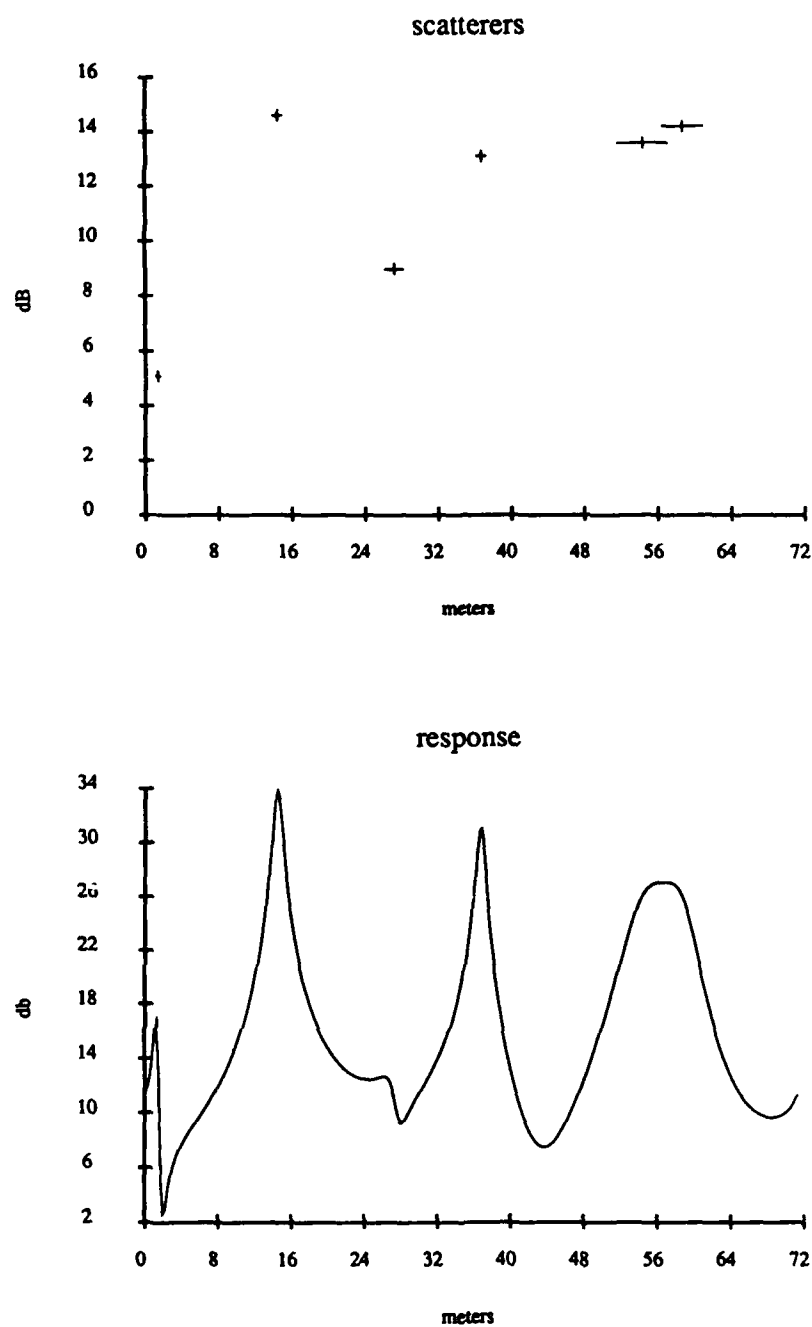
response

Figure A.20: ARMA Response of the Boeing 707 at Vertical Polarization, 10° aspect angle, 20 frequency samples used, 40–80 MHz, 8th order model

52
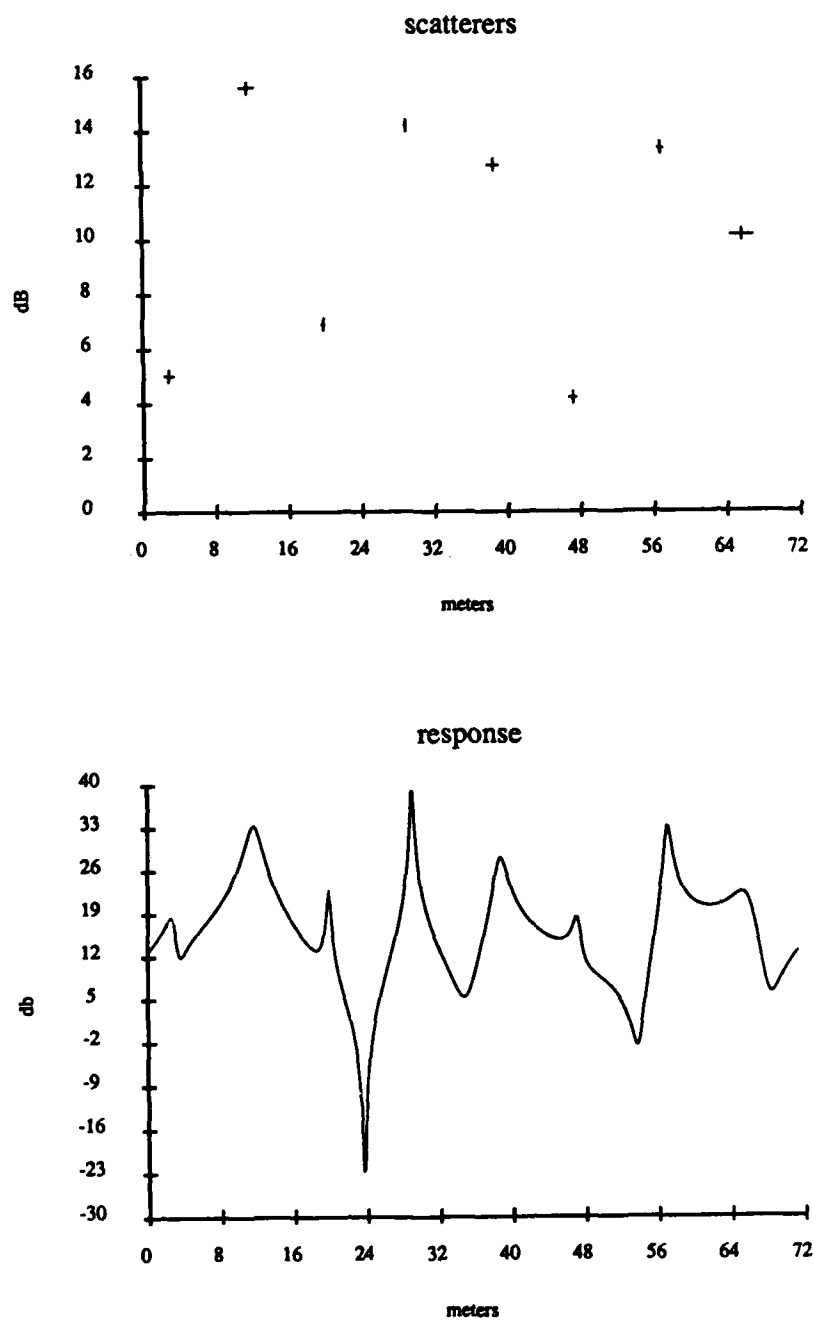
Figure A.21: ARMA Response of the Boeing 707 at Vertical Polarization, 10° aspect angle, 20 frequency samples used, 40–80 MHz, 9th order model

53

scatterers
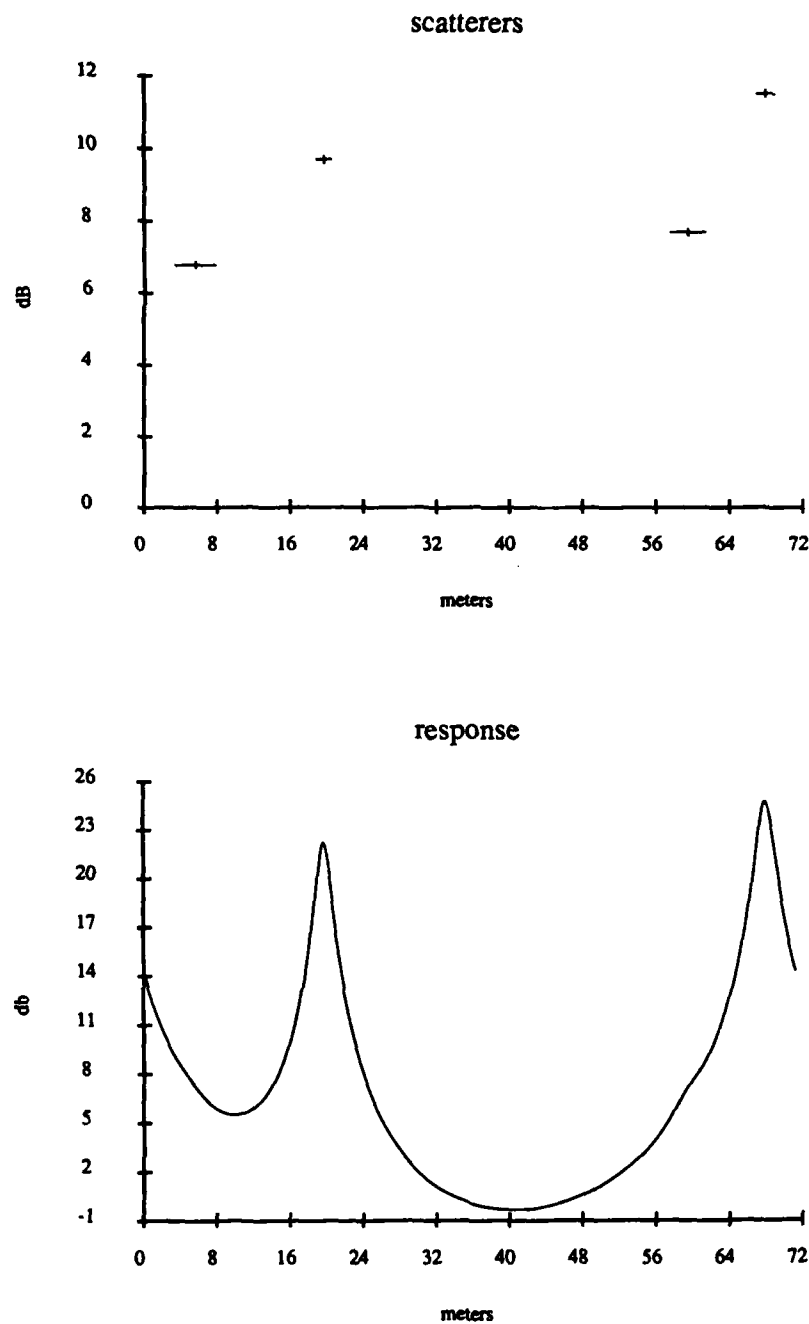
response

Figure A.22: ARMA Response of the Boeing 707 at Horizontal Polarization, 0° aspect angle, 20 frequency samples used, 40–80 MHz, 9th order model

54

scatterers
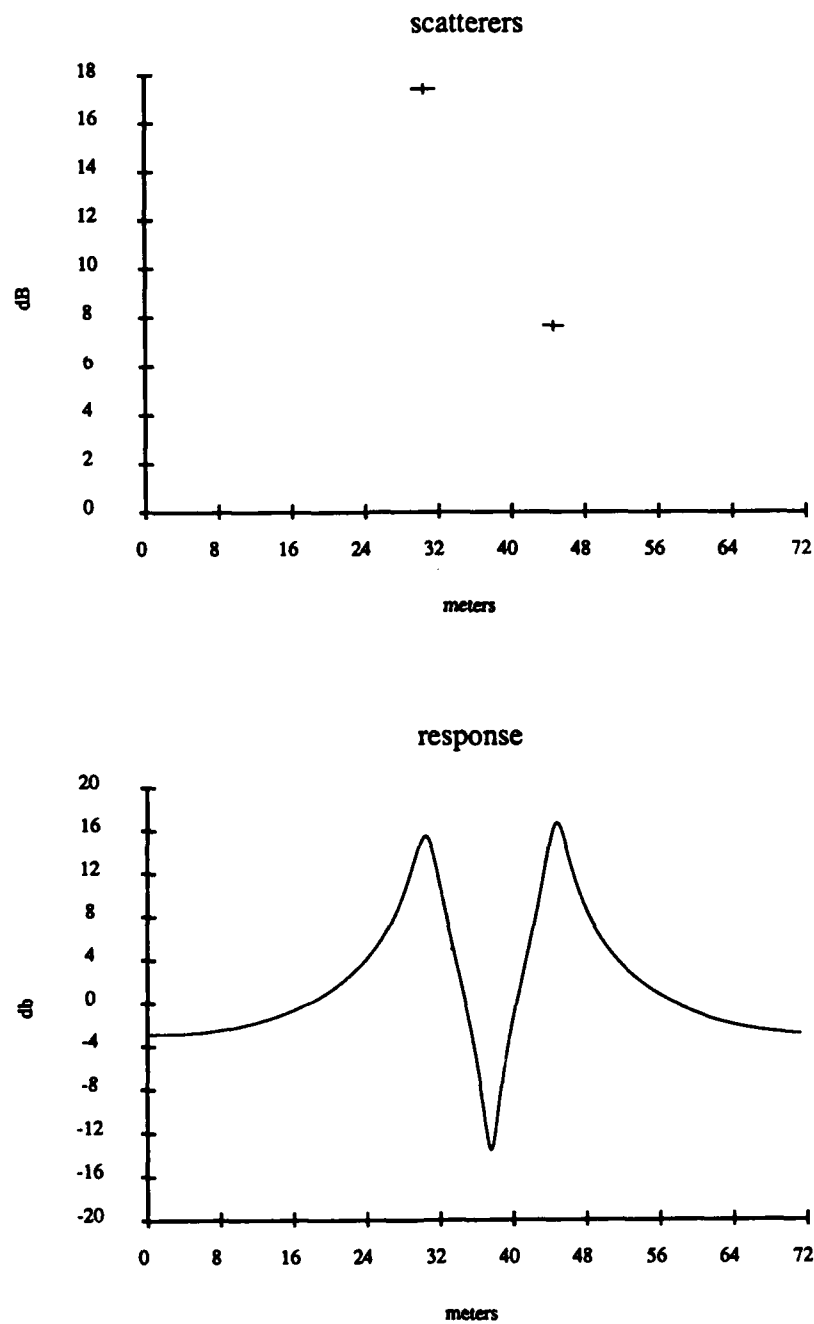
response

Figure A.23: ARMA Response of the Boeing 707 at Horizontal Polarization, 10° aspect angle, 20 frequency samples used, 40–80 MHz, 9th order model
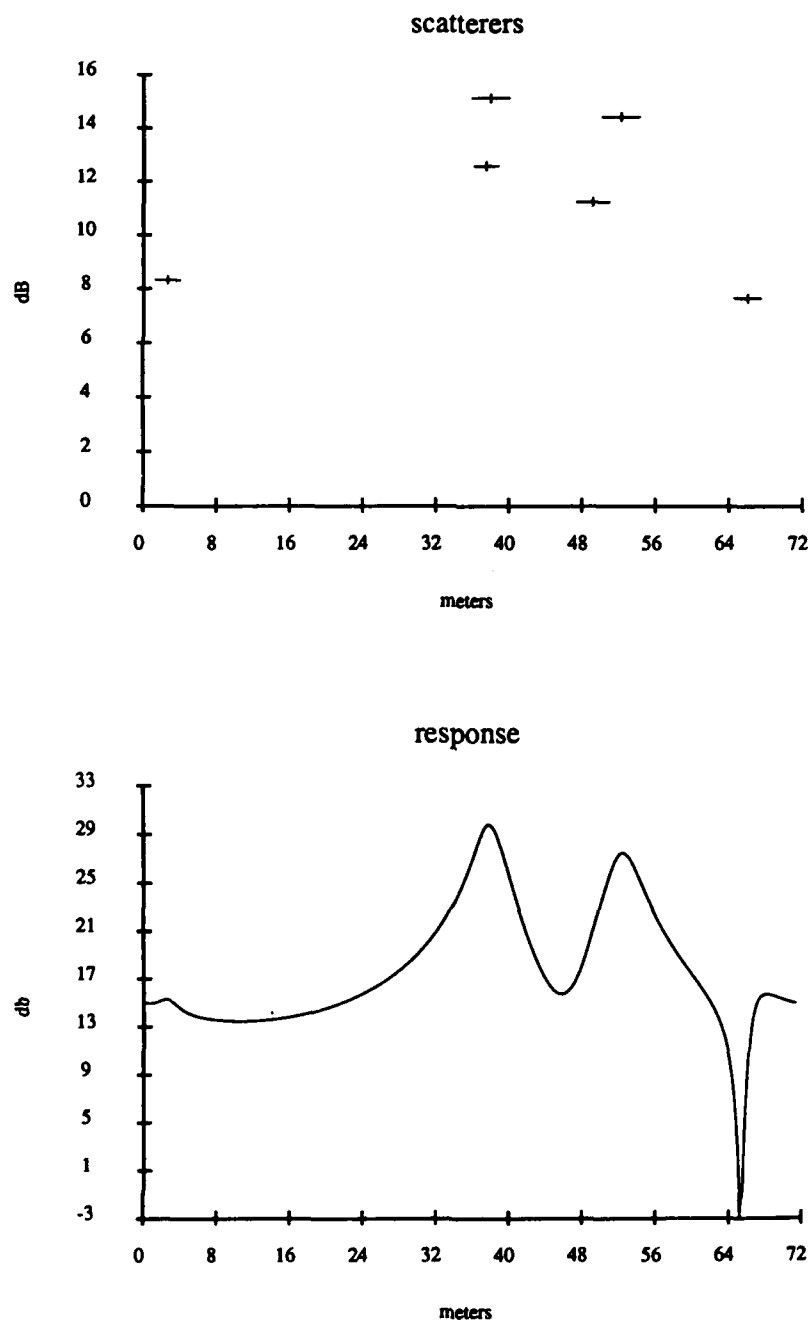
Figure A.24: ARMA Response of the Boeing 707 at Horizontal Polarization, 20°
aspect angle, 20 frequency samples used, 40–80 MHz, 9th order model

56

scatterers
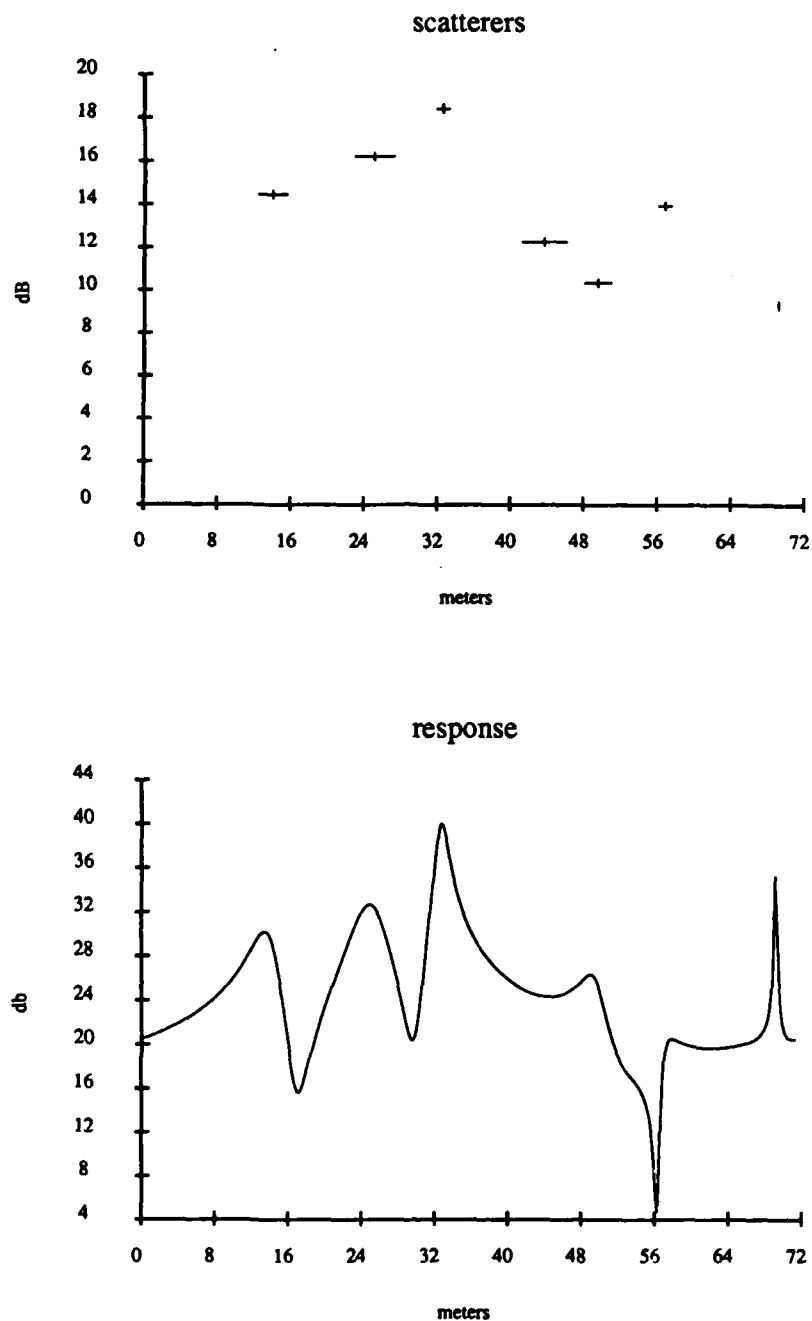
response

Figure A.25: ARMA Response of the Boeing 707 at Horizontal Polarization, 30° aspect angle, 20 frequency samples used, 40–80 MHz, 9th order model

57
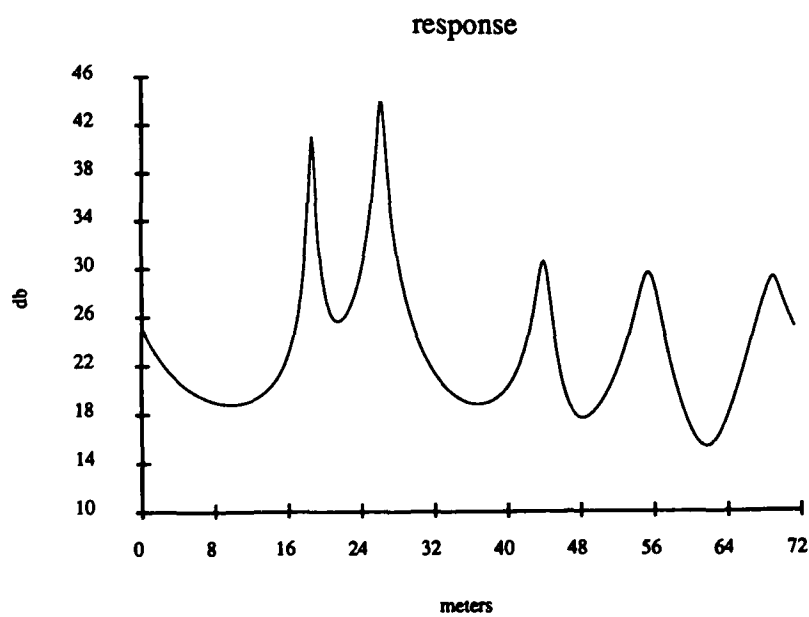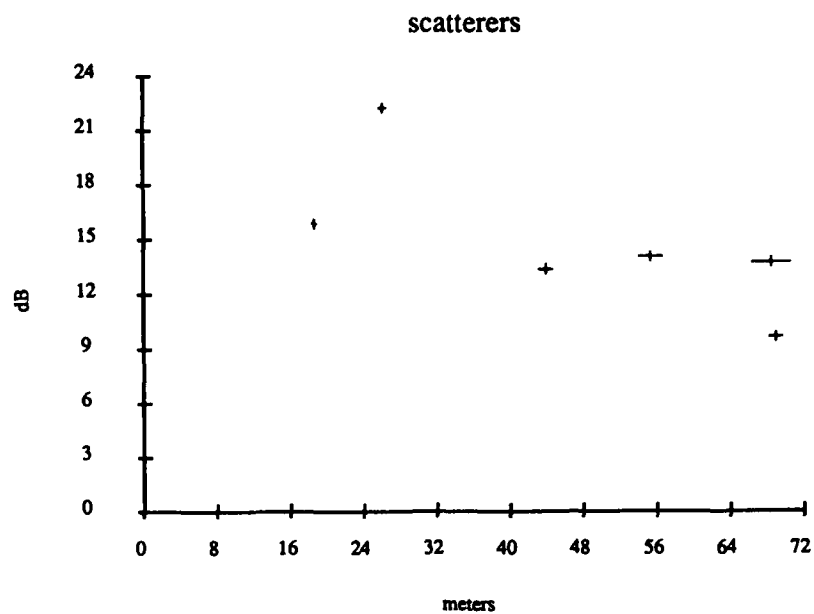
Figure A.26: ARMA Response of the Boeing 707 at Horizontal Polarization, 40°
aspect angle, 20 frequency samples used, 40–80 MHz, 9th order model

58
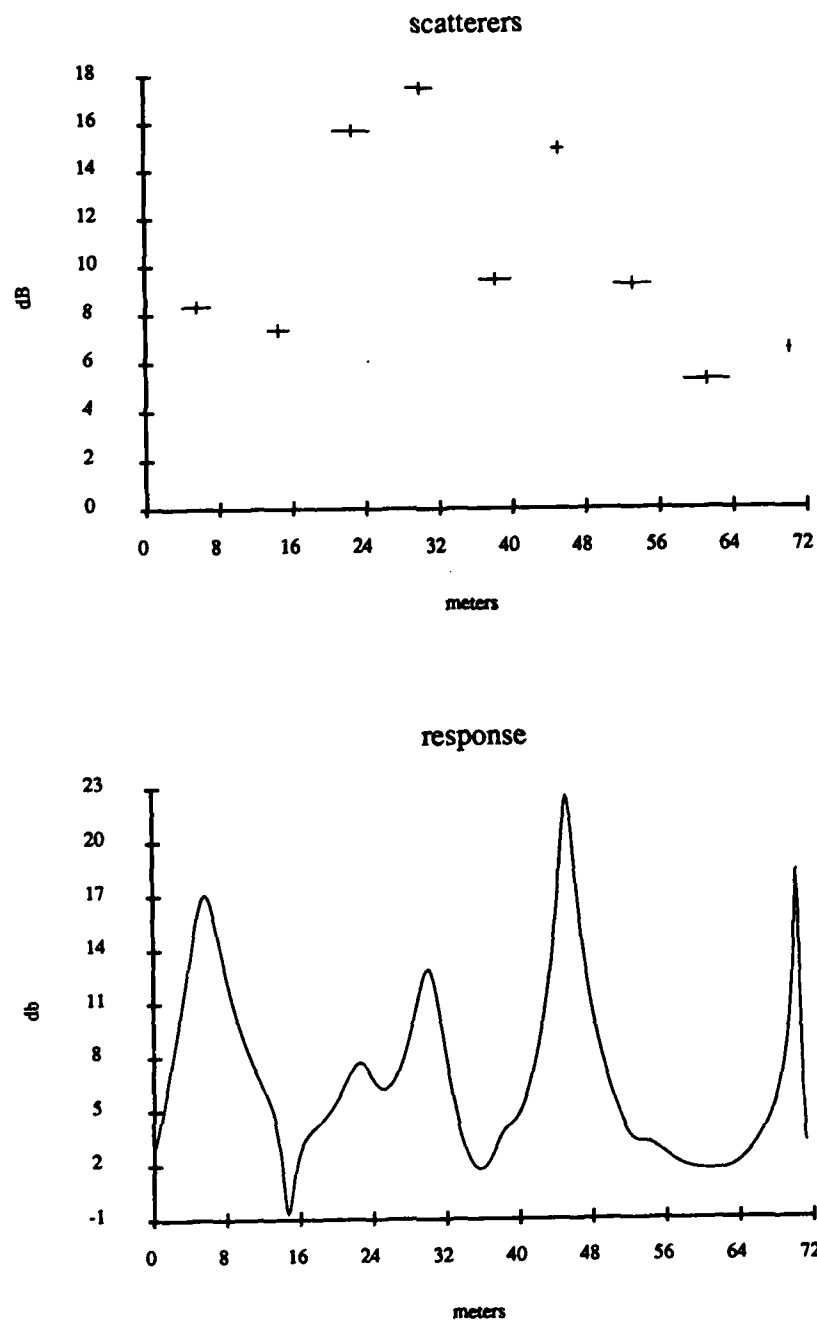
Figure A.27: ARMA Response of the Boeing 707 at Horizontal Polarization, 50° aspect angle, 20 frequency samples used, 40–80 MHz, 9th order model

scatterers
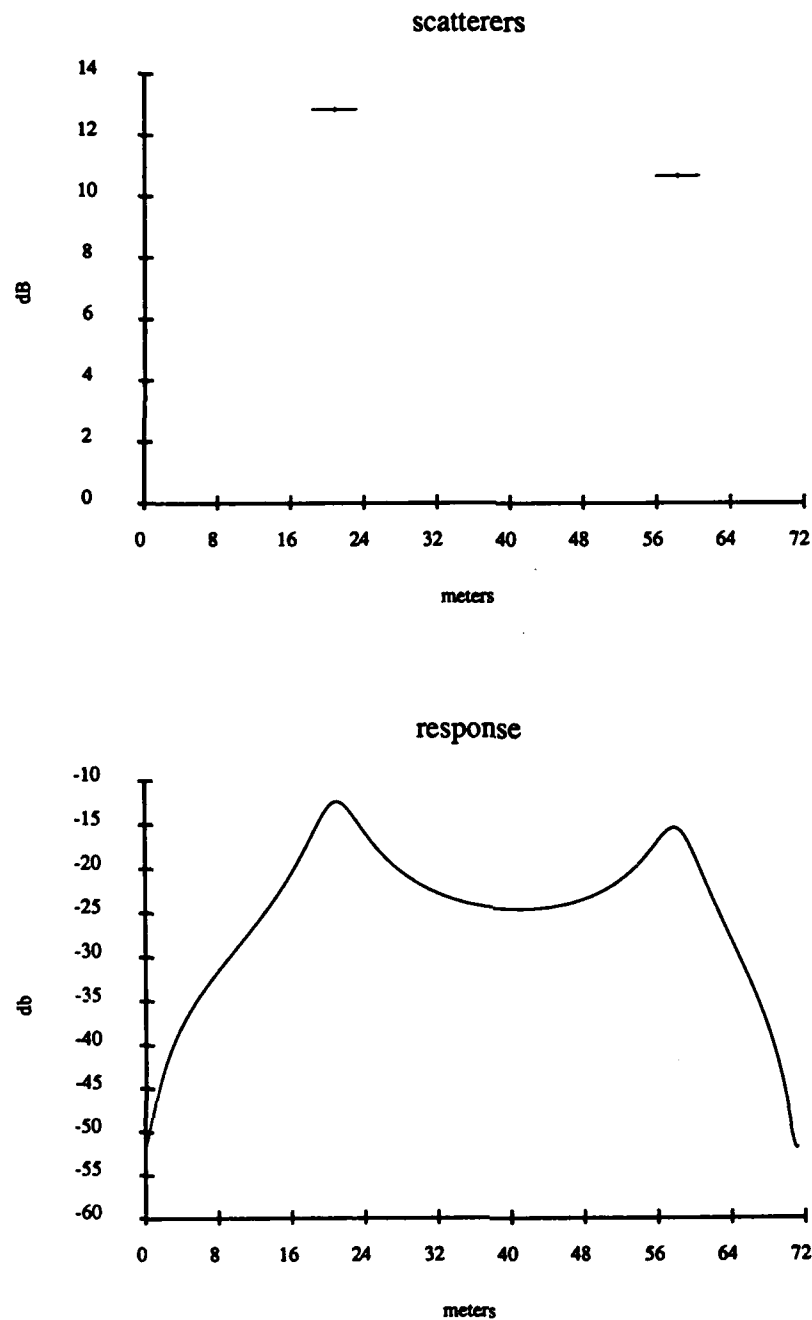
response

Figure A.28: ARMA Response of the Boeing 707 at Horizontal Polarization, 60°
aspect angle, 20 frequency samples used, 40–80 MHz, 9th order model

60

scatterers
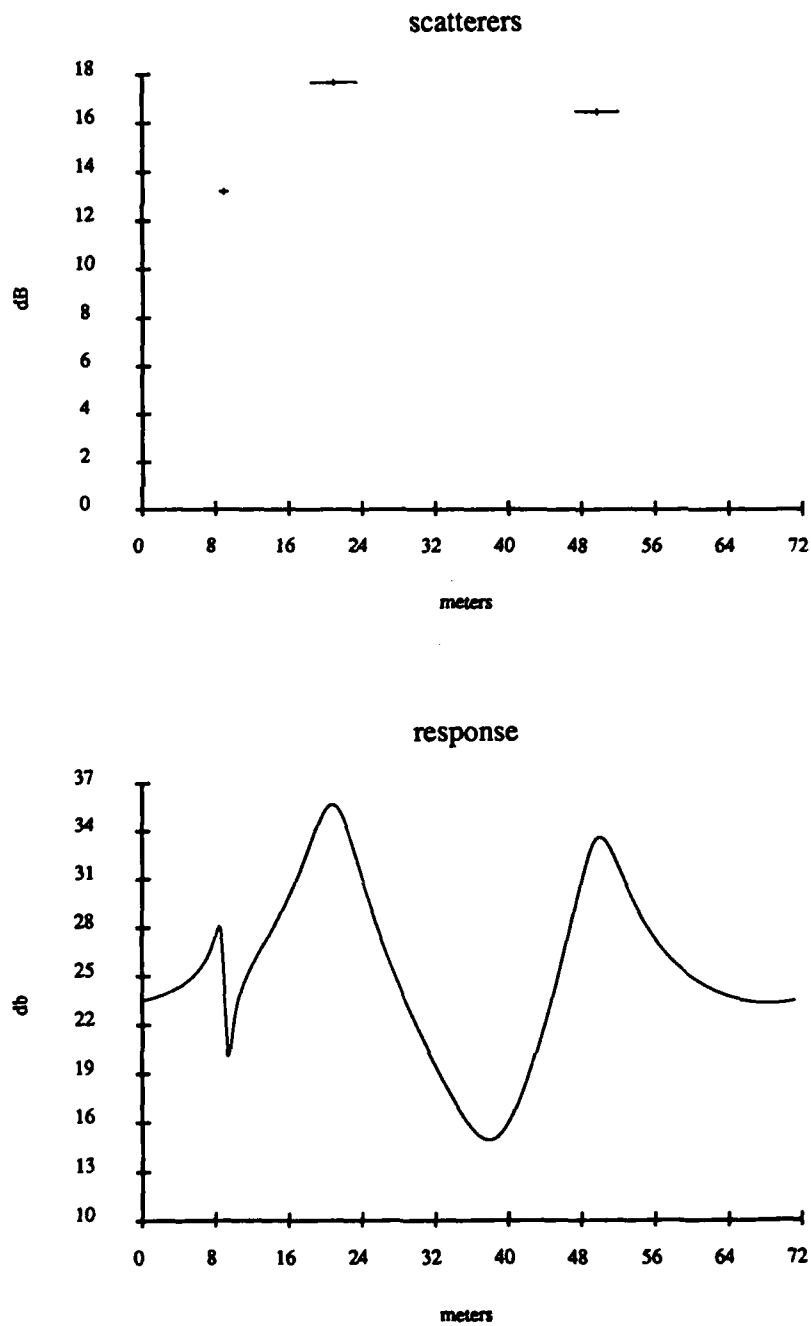
response

Figure A.29: ARMA Response of the Boeing 707 at Horizontal Polarization, 70° aspect angle, 20 frequency samples used, 40–80 MHz, 9th order model

scatterers
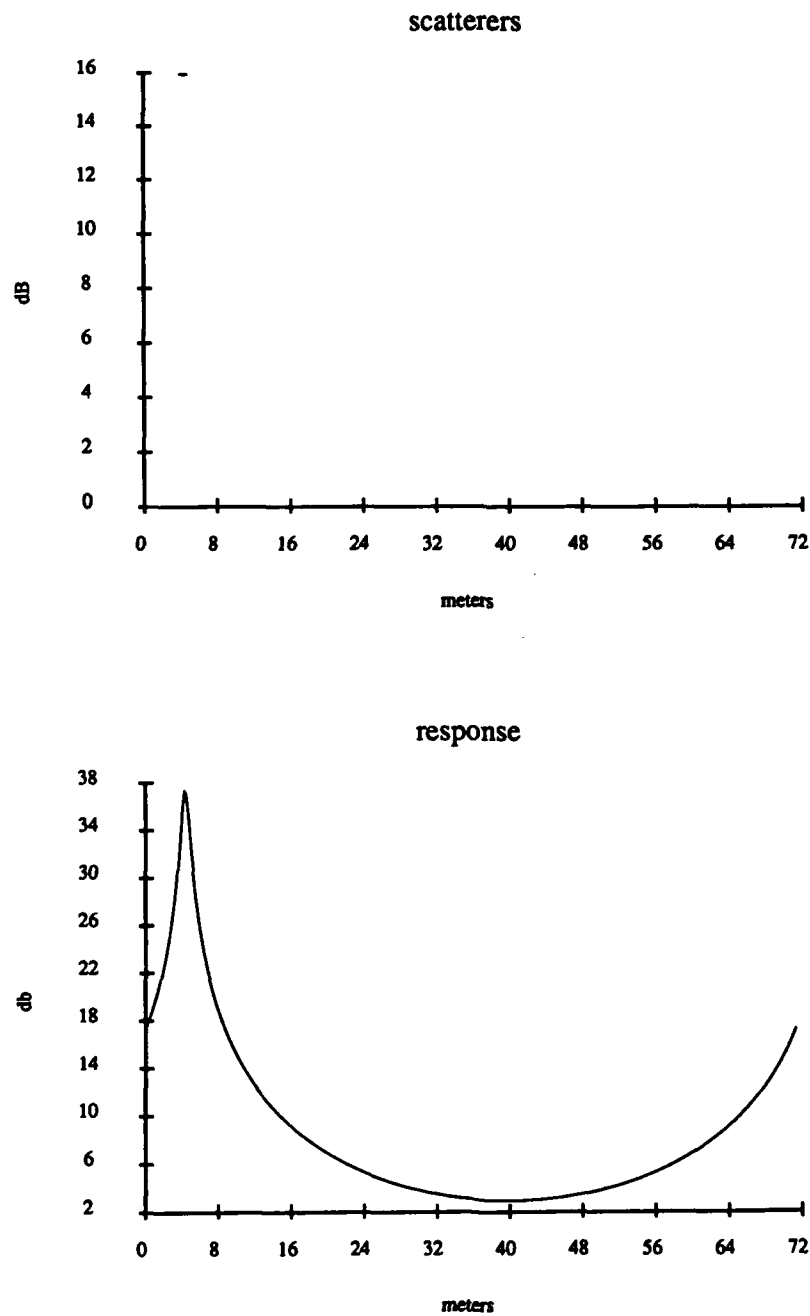
response

Figure A.30: ARMA Response of the Boeing 707 at Horizontal Polarization, 80°
aspect angle, 20 frequency samples used, 40–80 MHz, 9th order model
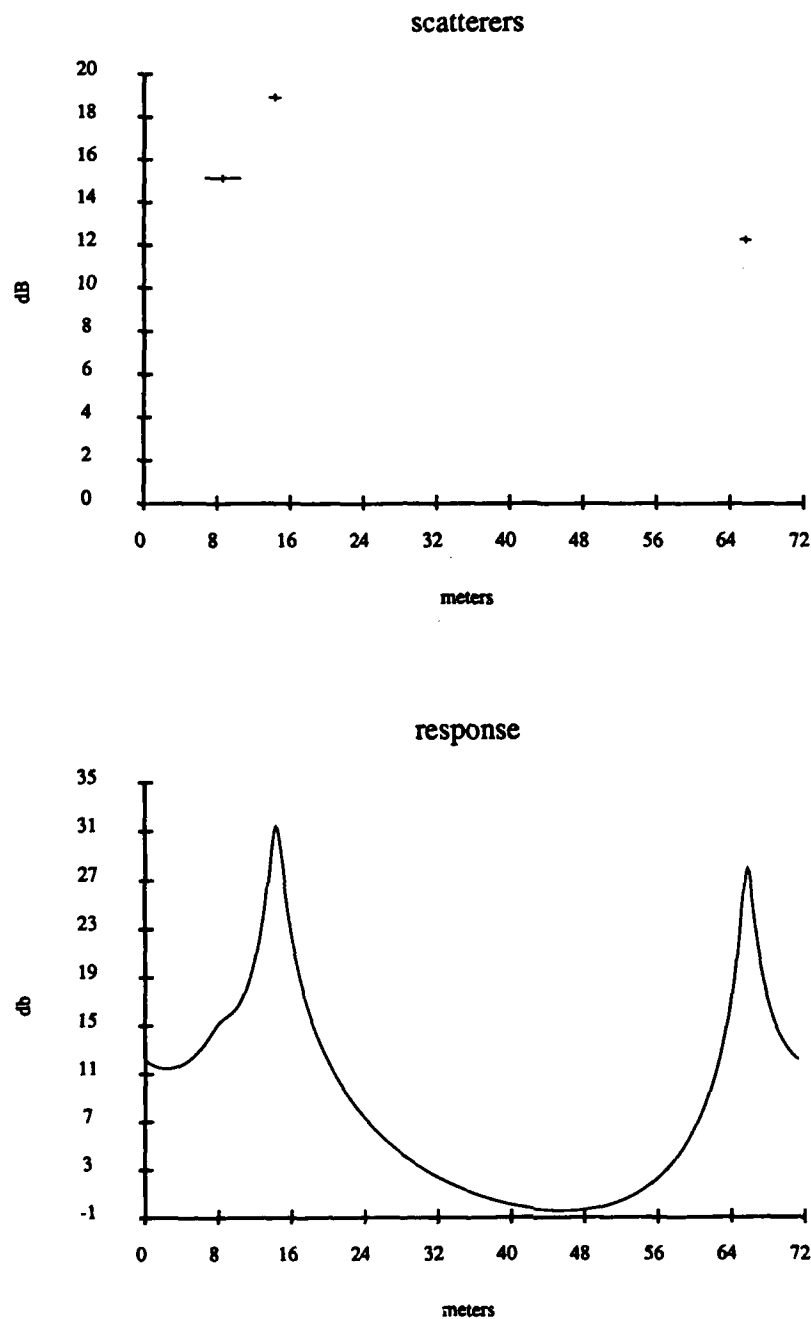
Figure A.31: ARMA Response of the Boeing 707 at Horizontal Polarization, 90° aspect angle, 20 frequency samples used, 40–80 MHz, 9th order model
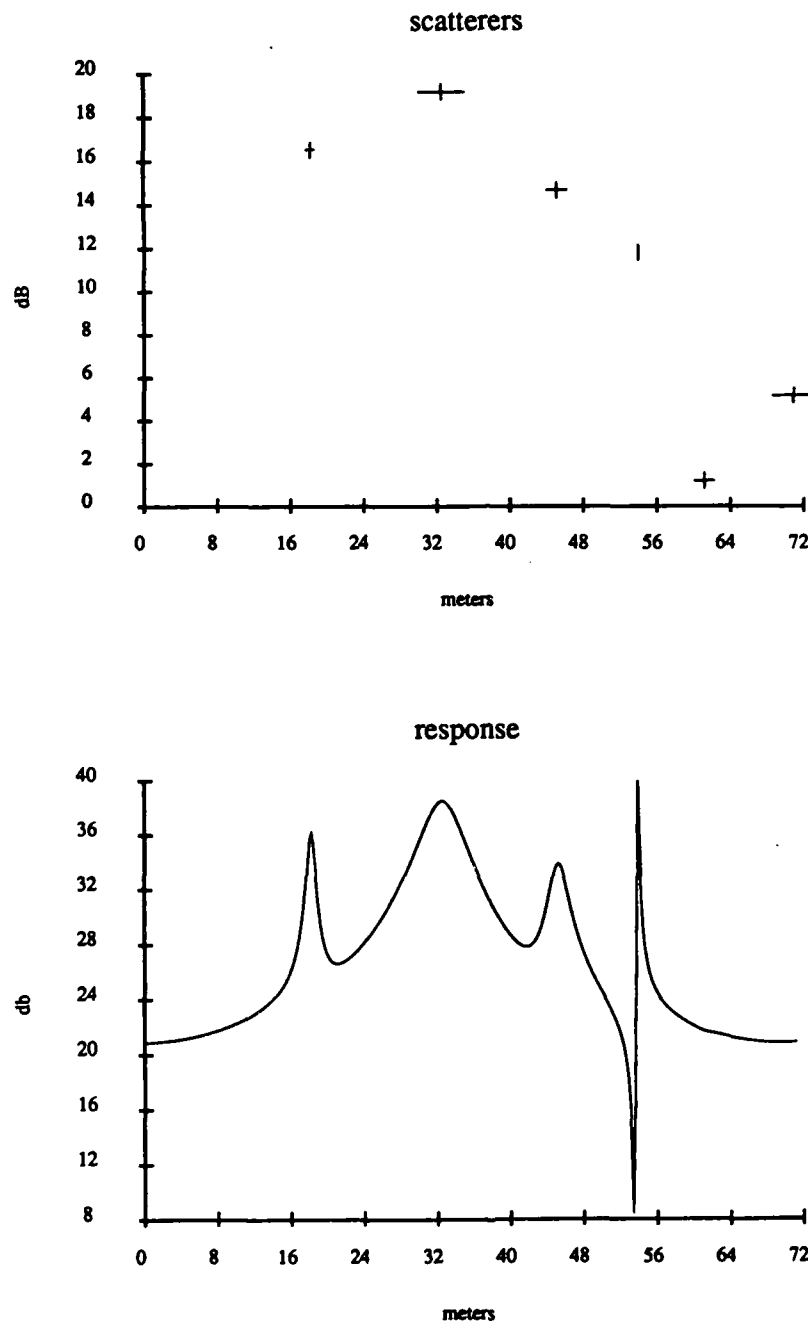
Figure A.32: ARMA Response of the Boeing 707 at Horizontal Polarization, 100°
aspect angle, 20 frequency samples used, 40–80 MHz, 9th order model

scatterers
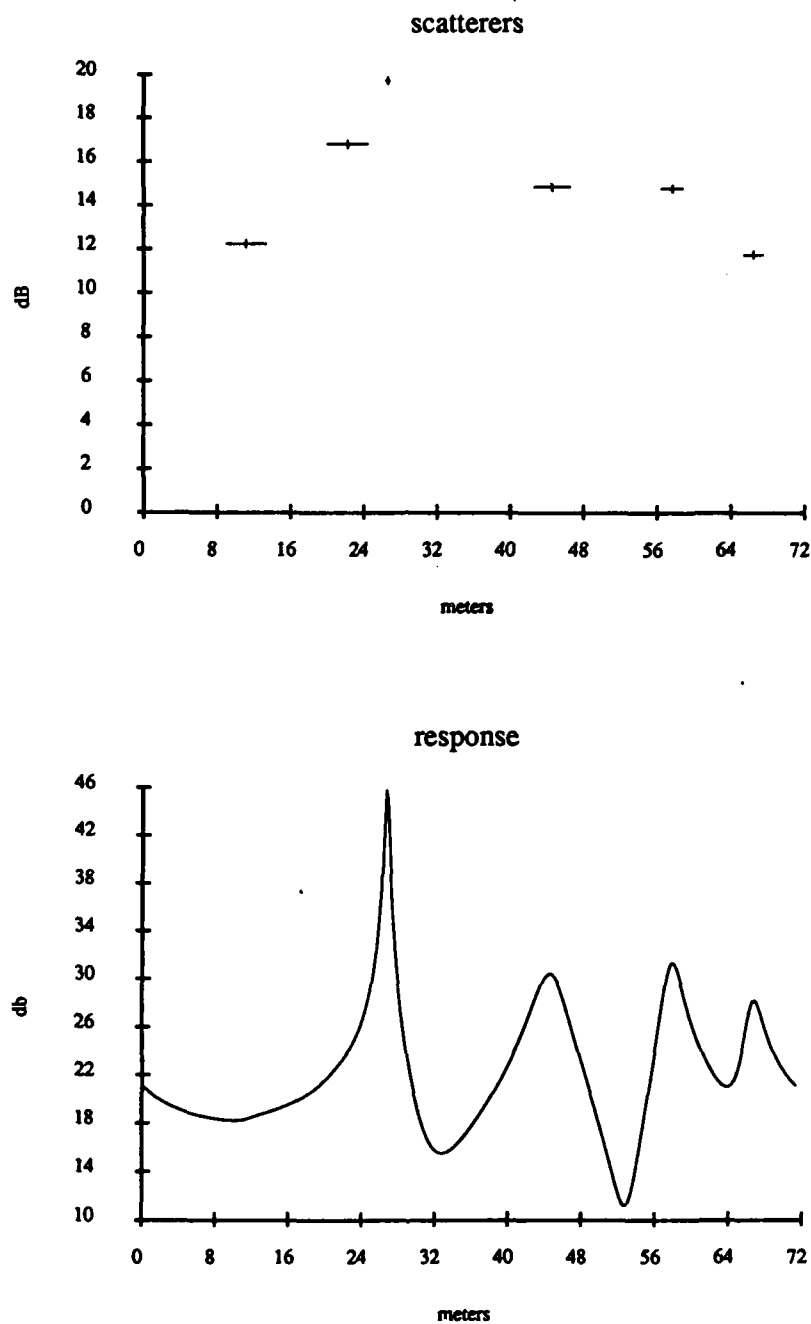
response

Figure A.33: ARMA Response of the Boeing 707 at Horizontal Polarization, 110°
aspect angle, 20 frequency samples used, 40–80 MHz, 9th order model
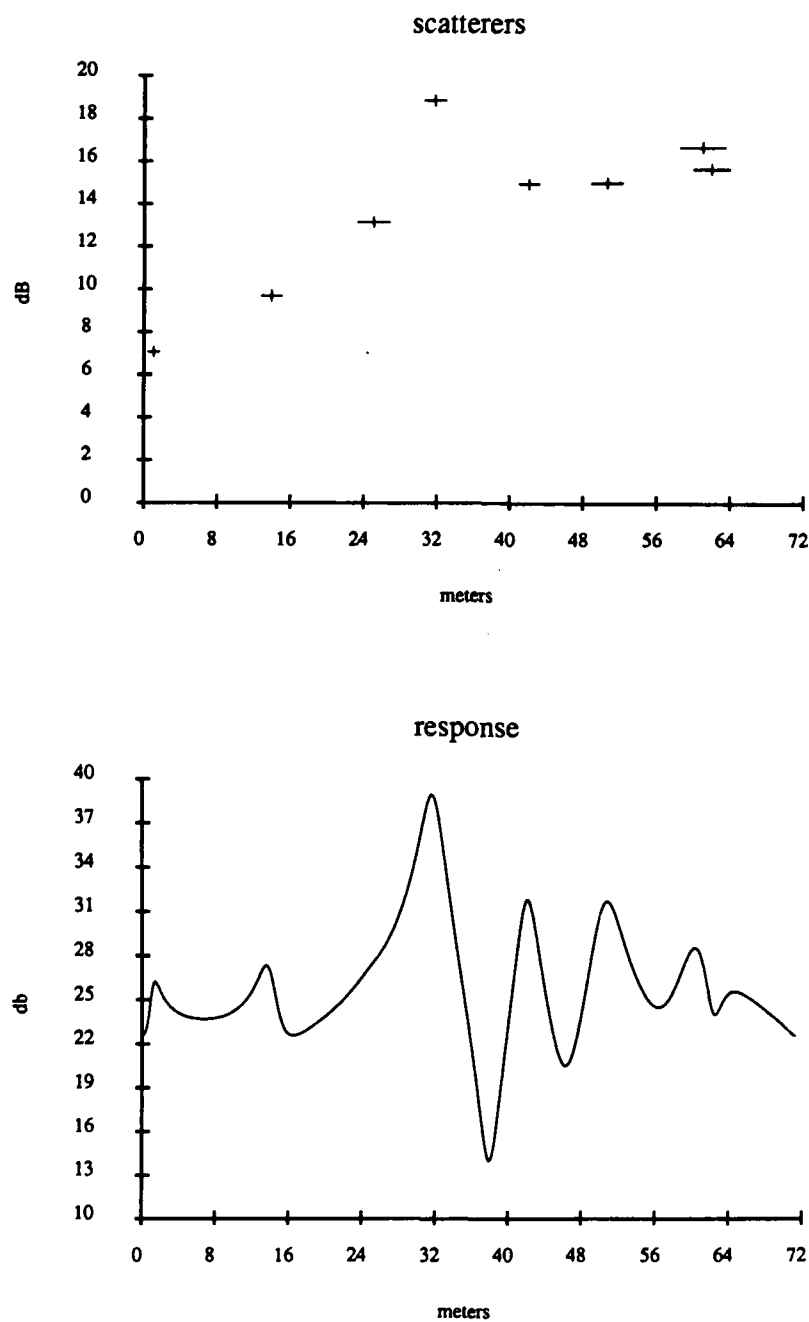
Figure A.34: ARMA Response of the Boeing 707 at Horizontal Polarization, 120° aspect angle, 20 frequency samples used, 40–80 MHz, 9th order model

66
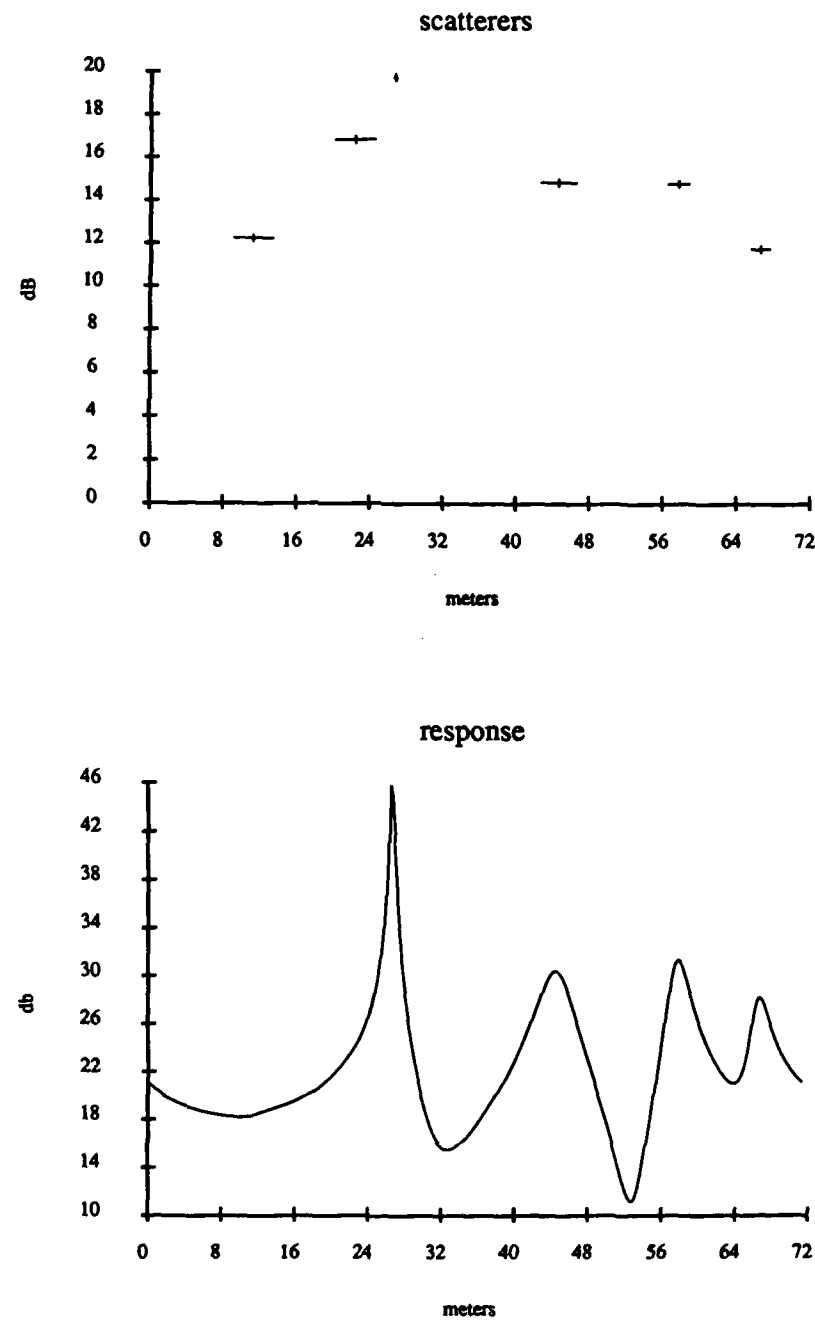
Figure A.35: ARMA Response of the Boeing 707 at Horizontal Polarization, 130°
aspect angle, 20 frequency samples used, 40–80 MHz, 9th order model
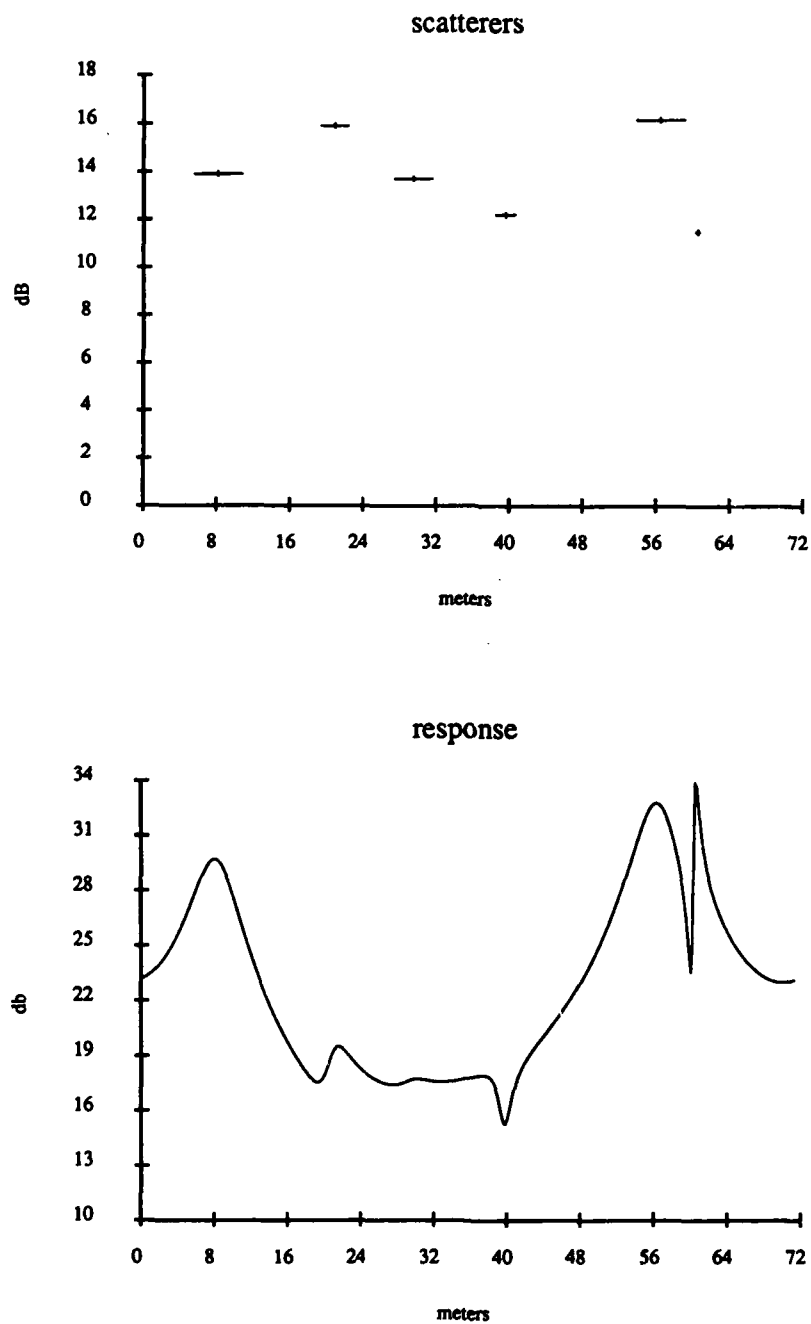
Figure A.36: ARMA Response of the Boeing 707 at Horizontal Polarization, 140° aspect angle, 20 frequency samples used, 40–80 MHz, 9th order model

68

scatterers
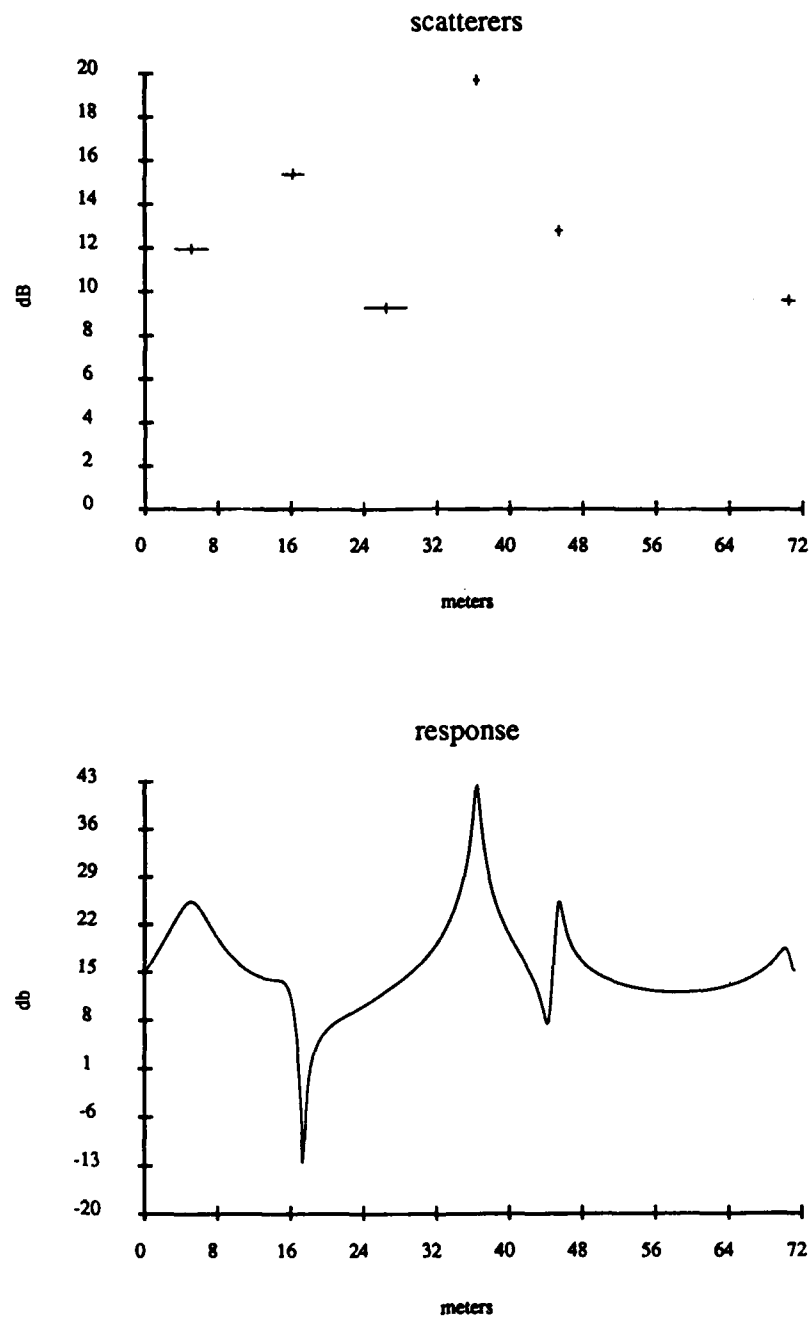
response

Figure A.37: ARMA Response of the Boeing 707 at Horizontal Polarization, 150° aspect angle, 20 frequency samples used, 40–80 MHz, 9th order model

scatterers

dB

21
18
15
12
9
6
3
0

0   8   16   24   32   40   48   56   64   72

meters

response

db

48
42
36
30
24
18
12
6
0
-6

0   8   16   24   32   40   48   56   64   72

meters

Figure A.38: ARMA Response of the Boeing 707 at Horizontal Polarization, 160° aspect angle, 20 frequency samples used, 40–80 MHz, 9th order model

70

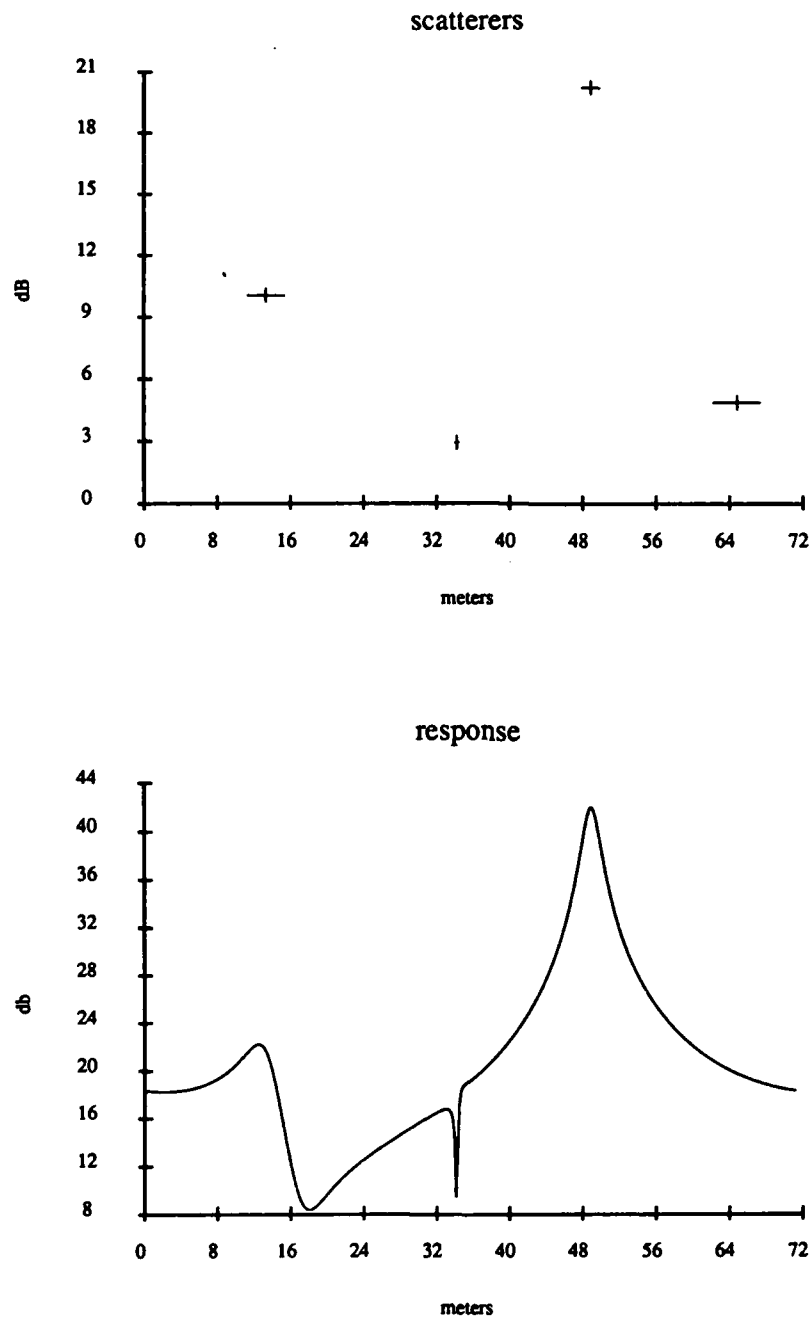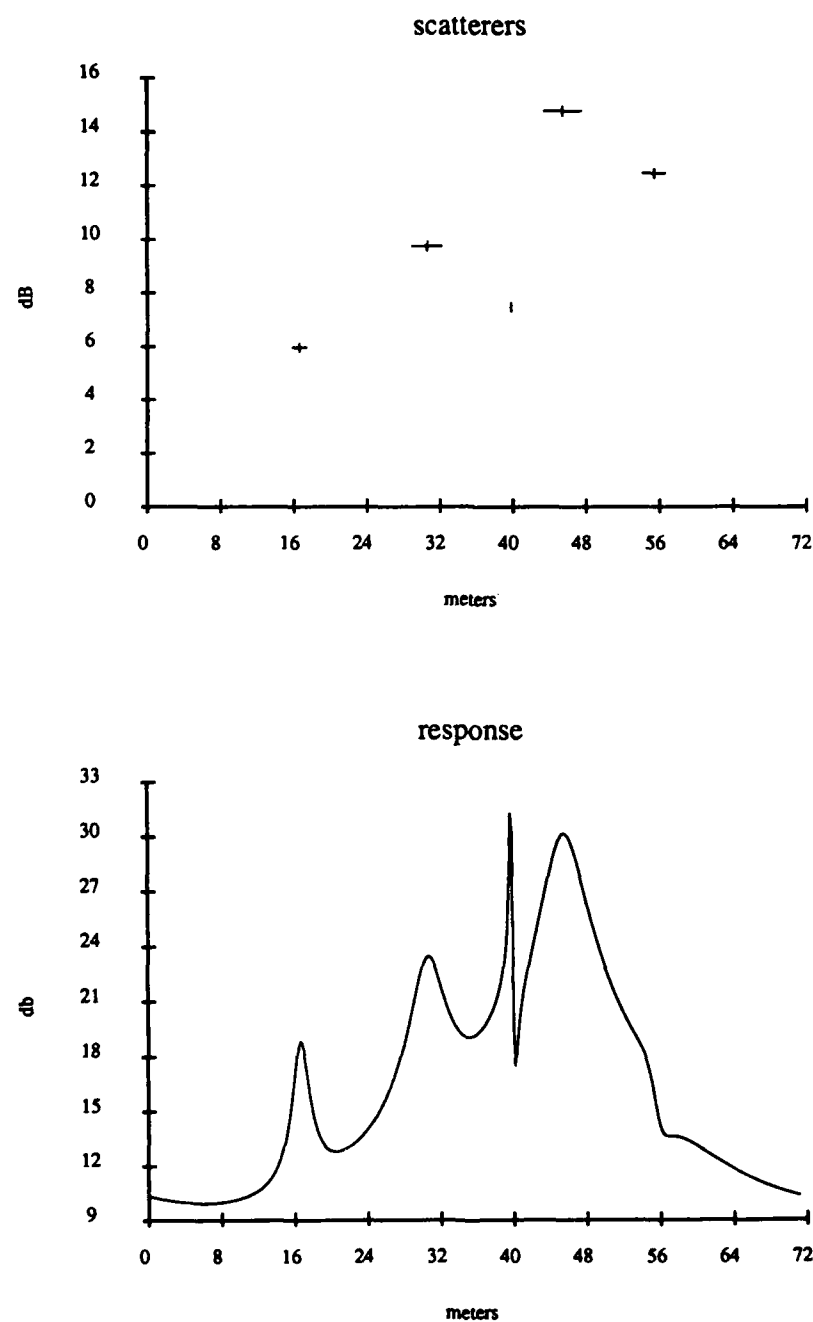## scatterers
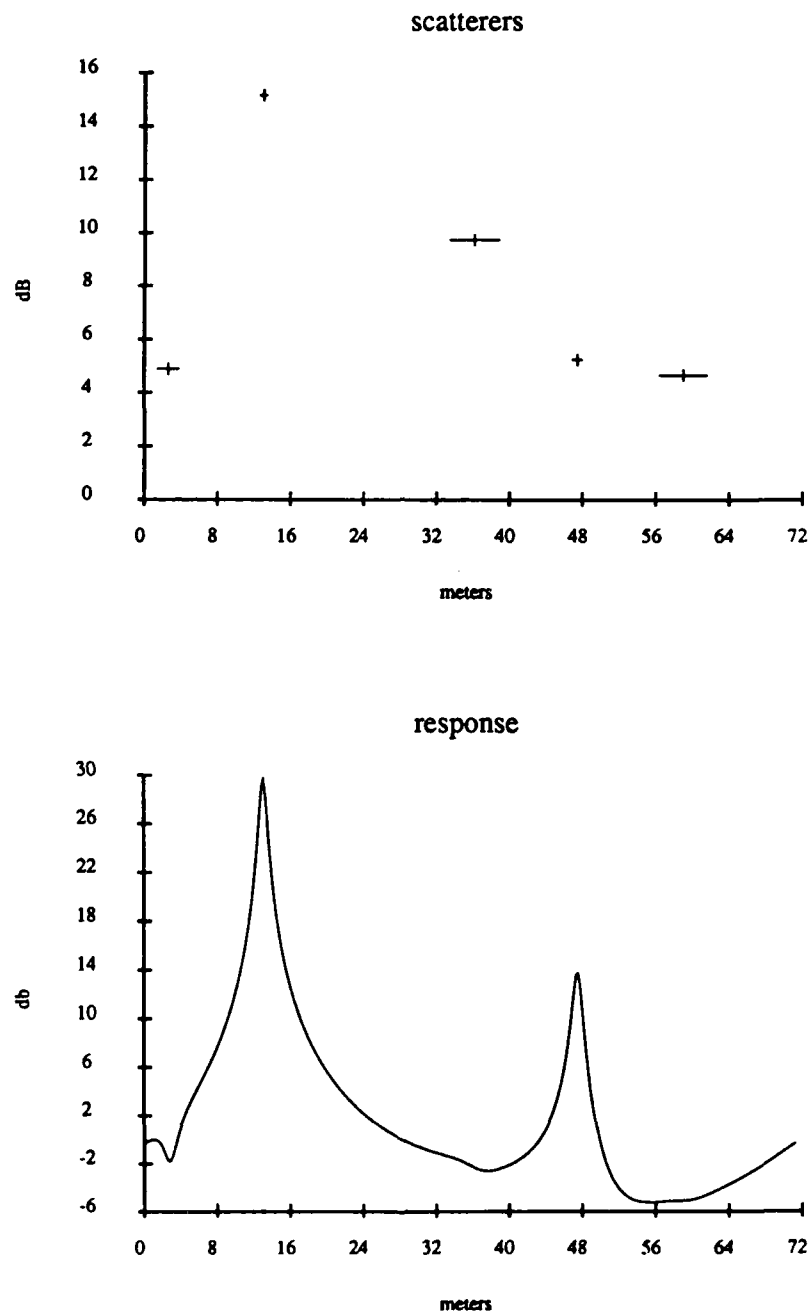
response

Figure A.39: ARMA Response of the Boeing 707 at Horizontal Polarization, 170°
aspect angle, 20 frequency samples used, 40–80 MHz, 9th order model

Figure A.40: ARMA Response of the Boeing 707 at Horizontal Polarization, 180°
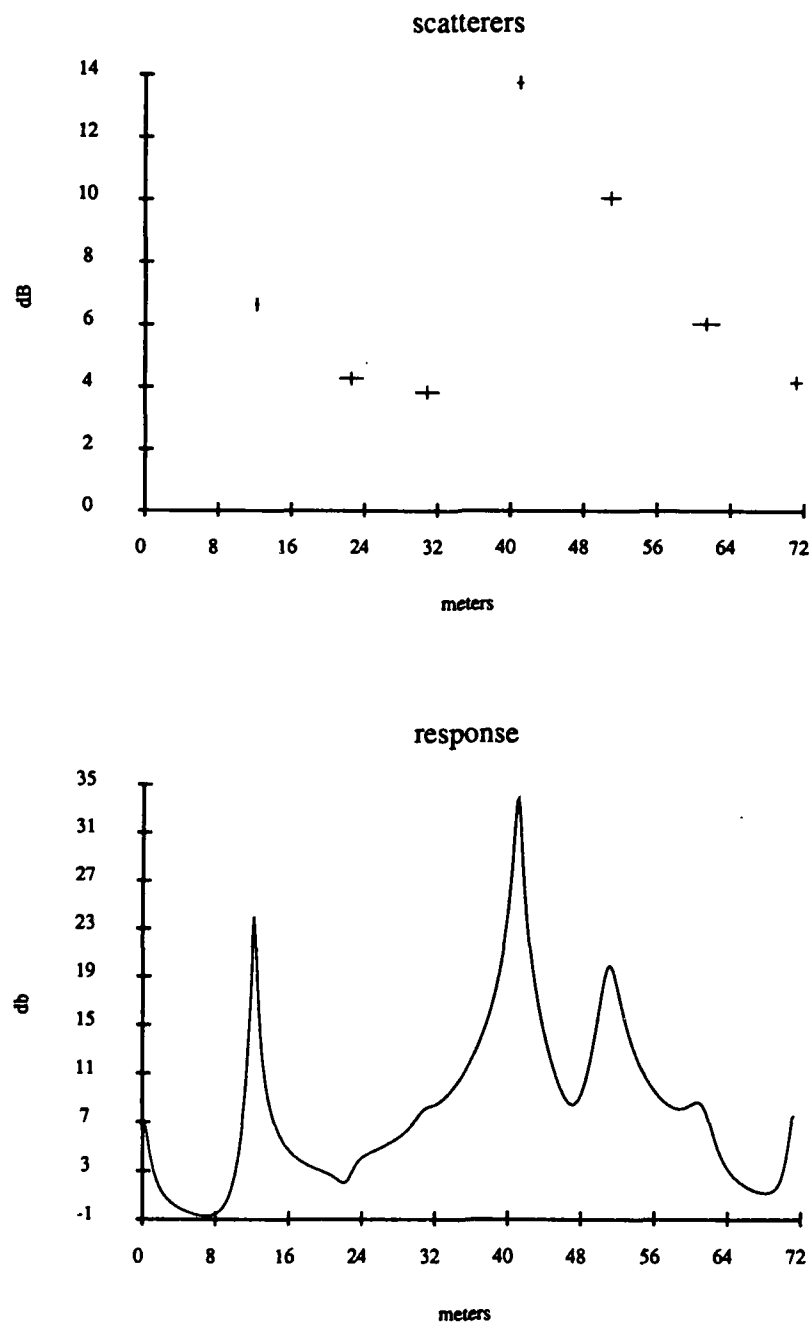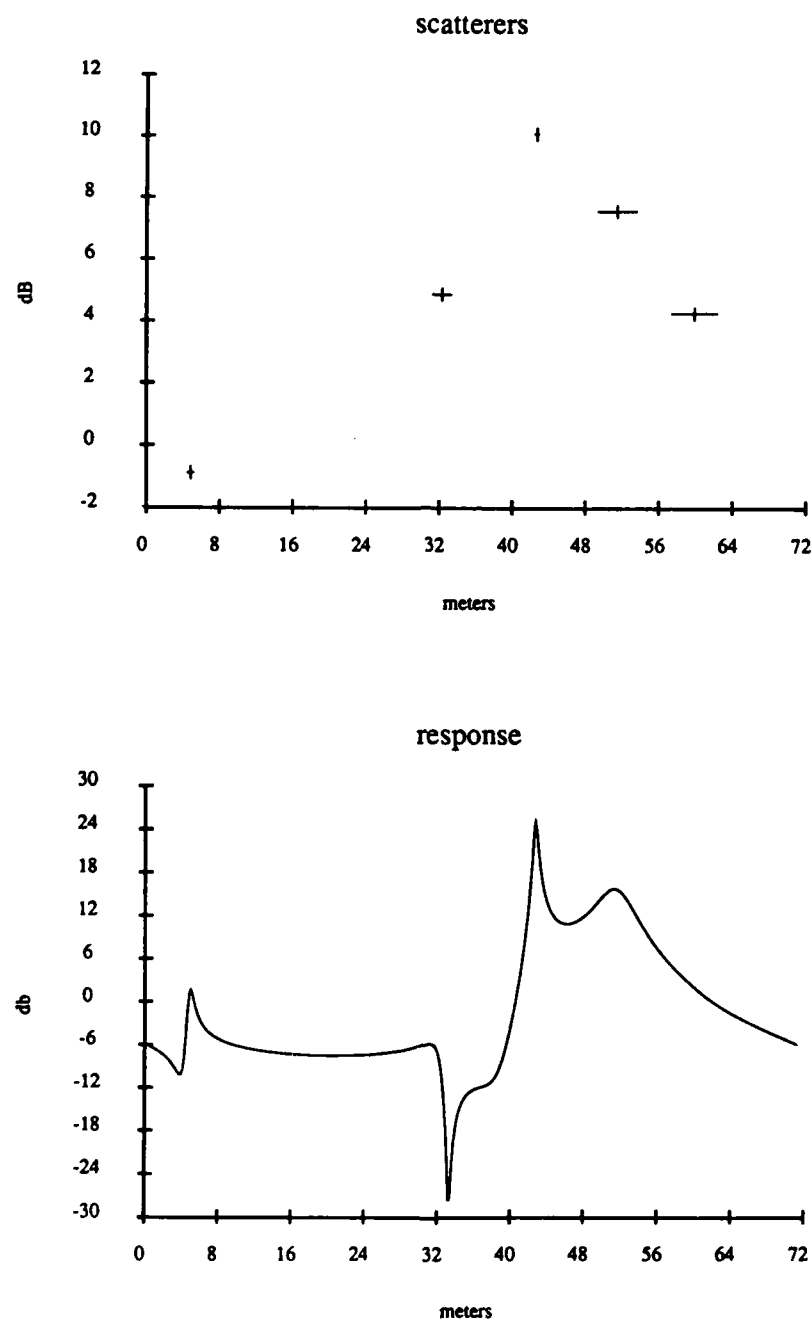aspect angle, 20 frequency samples used, 40–80 MHz, 9th order model

72
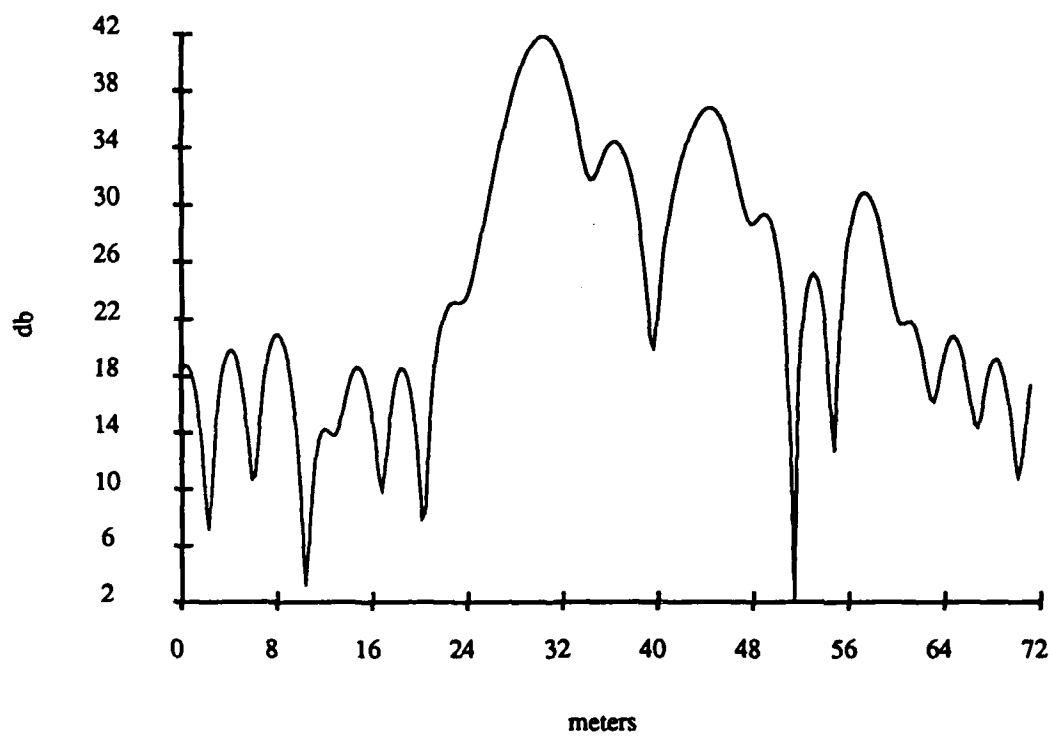
Figure A.41: FT of the Boeing 707 at Horizontal Polarization, 0° aspect angle, 20 frequency samples used, 40–80 MHz
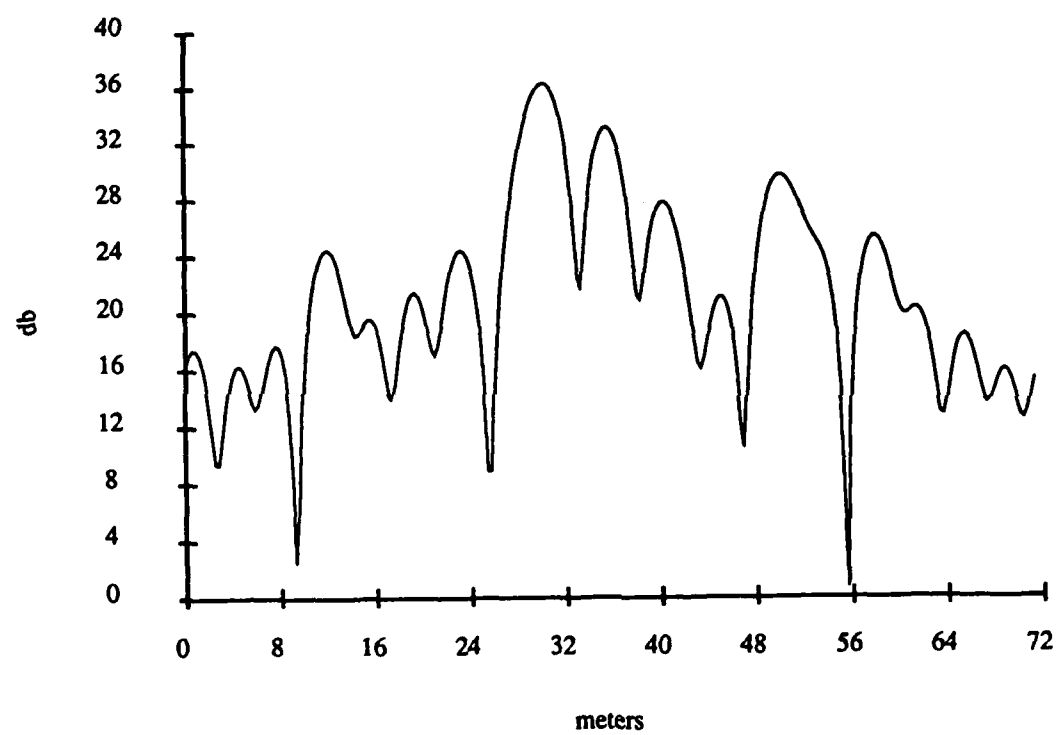
Figure A.42: FT of the Boeing 707 at Horizontal Polarization, 10° aspect angle, 20 frequency samples used, 40–80 MHz

74
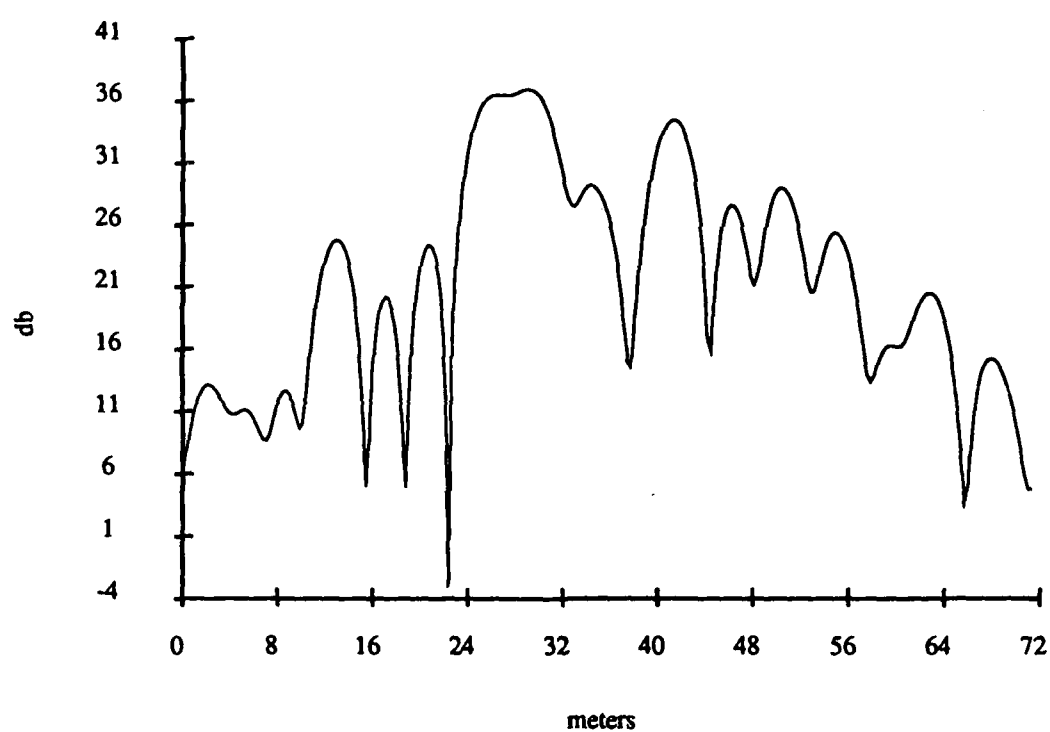
Figure A.43: FT of the Boeing 707 at Horizontal Polarization, 20° aspect angle, 20 frequency samples used, 40–80 MHz
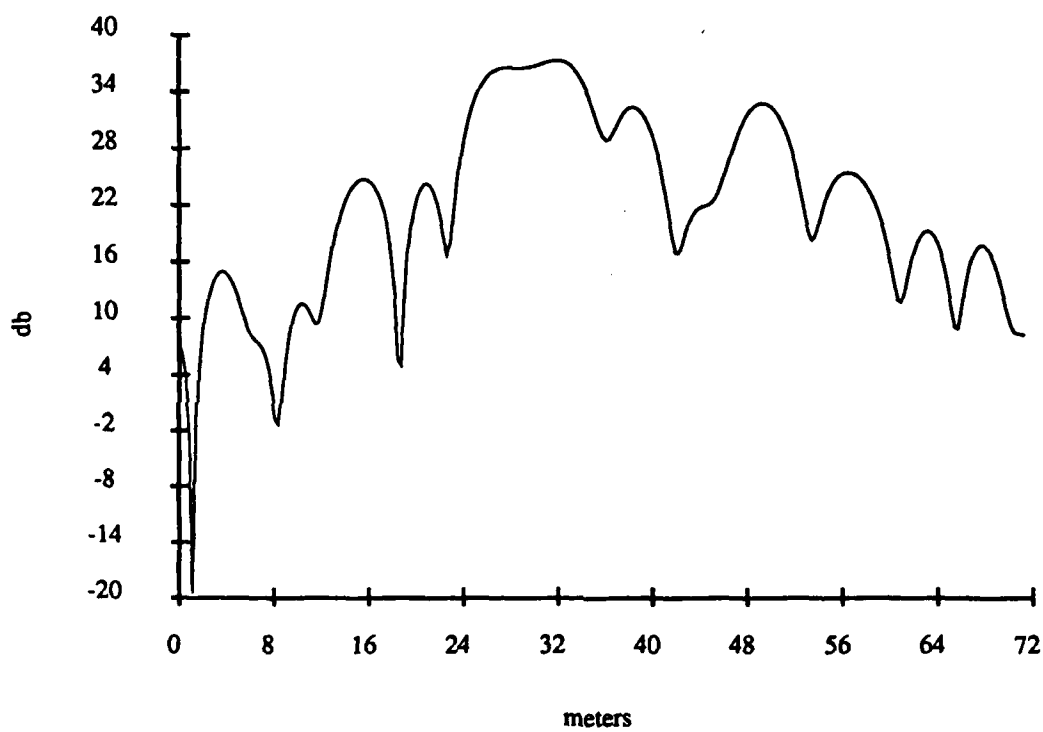
Figure A.44: FT of the Boeing 707 at Horizontal Polarization, 30° aspect angle, 20 frequency samples used, 40–80 MHz
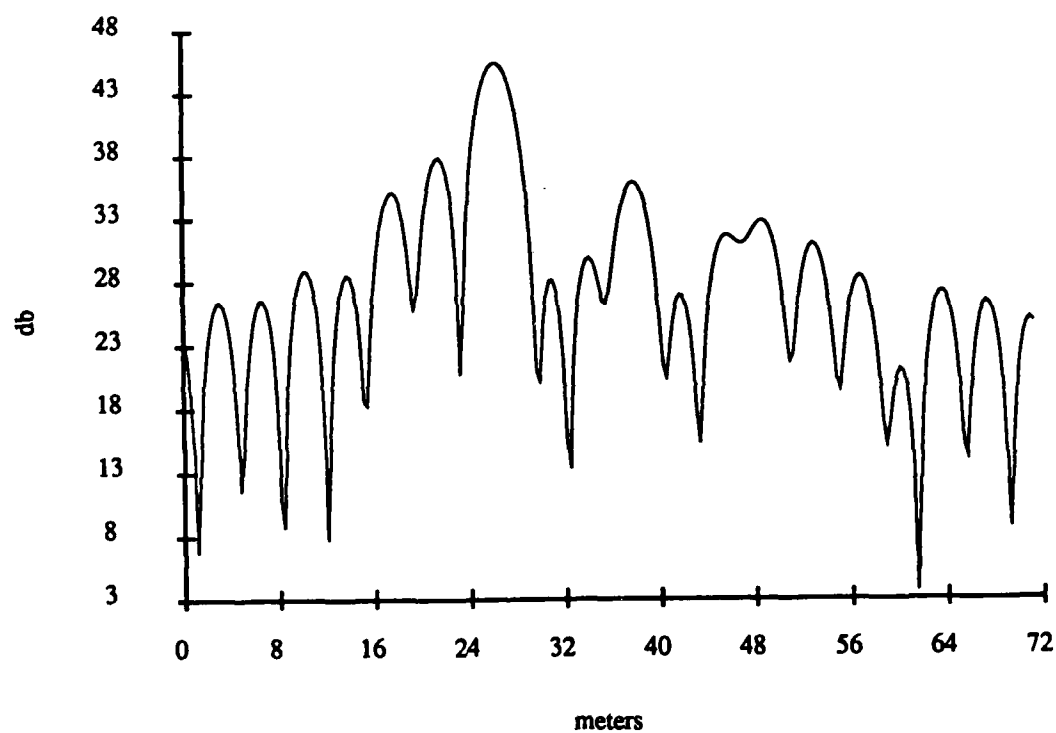
Figure A.45: FT of the Boeing 707 at Horizontal Polarization, 40° aspect angle, 20 frequency samples used, 40–80 MHz
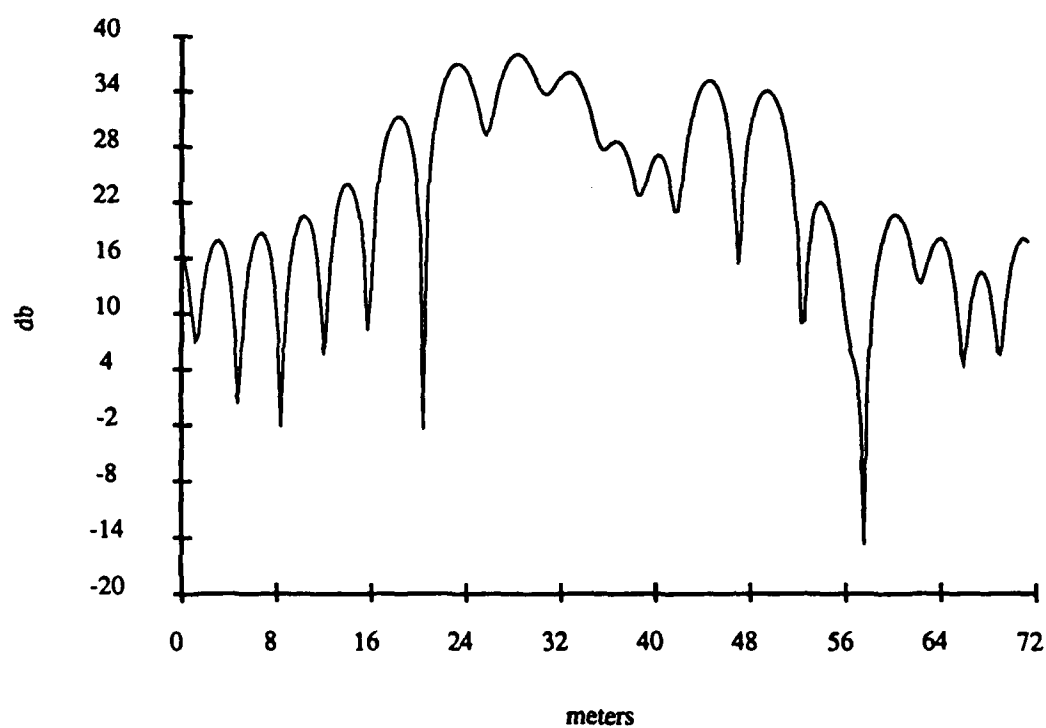
Figure A.46: FT of the Boeing 707 at Horizontal Polarization, 50° aspect angle, 20 frequency samples used, 40–80 MHz
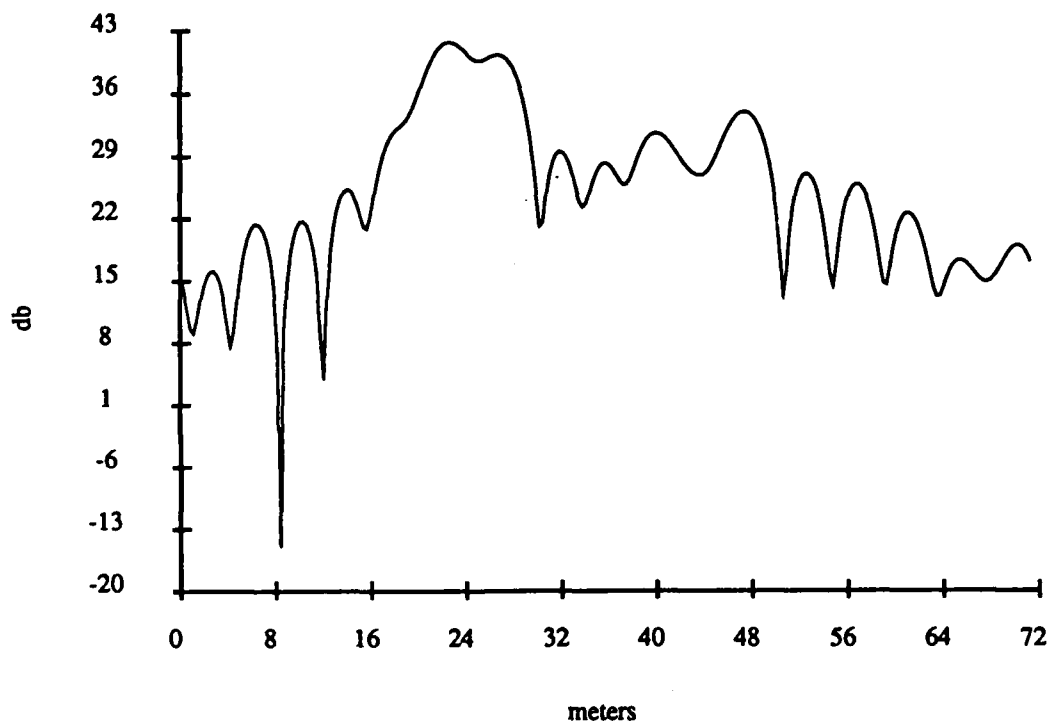
Figure A.47: FT of the Boeing 707 at Horizontal Polarization, 60° aspect angle, 20 frequency samples used, 40–80 MHz
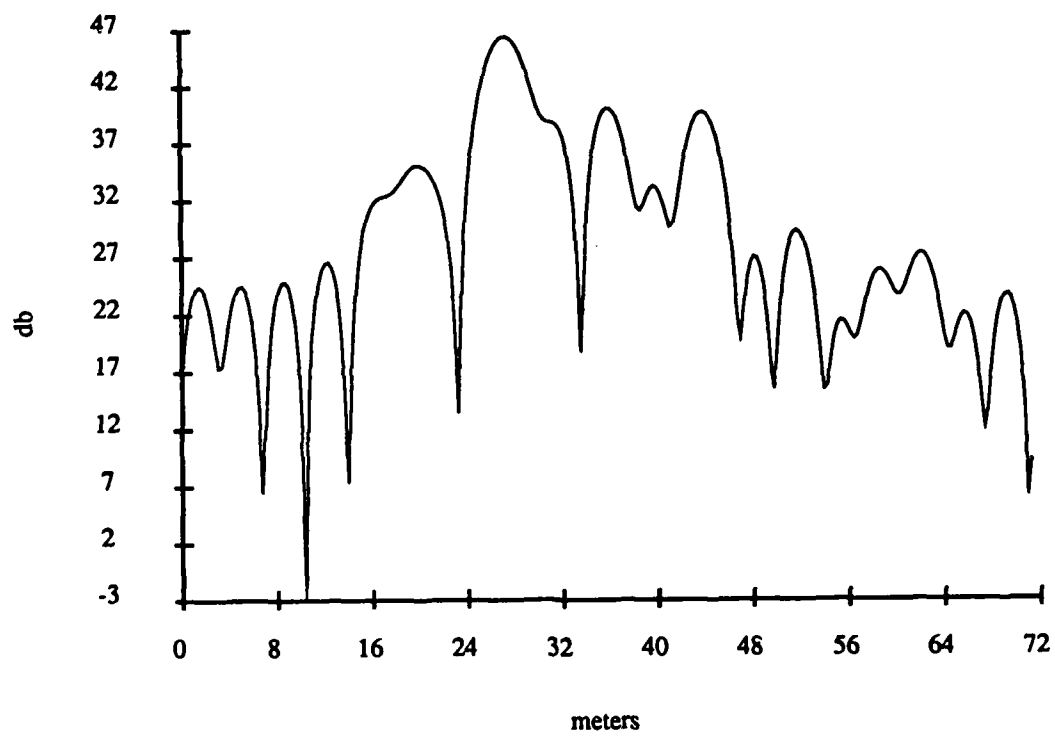
Figure A.48: FT of the Boeing 707 at Horizontal Polarization, 70° aspect angle, 20 frequency samples used, 40–80 MHz
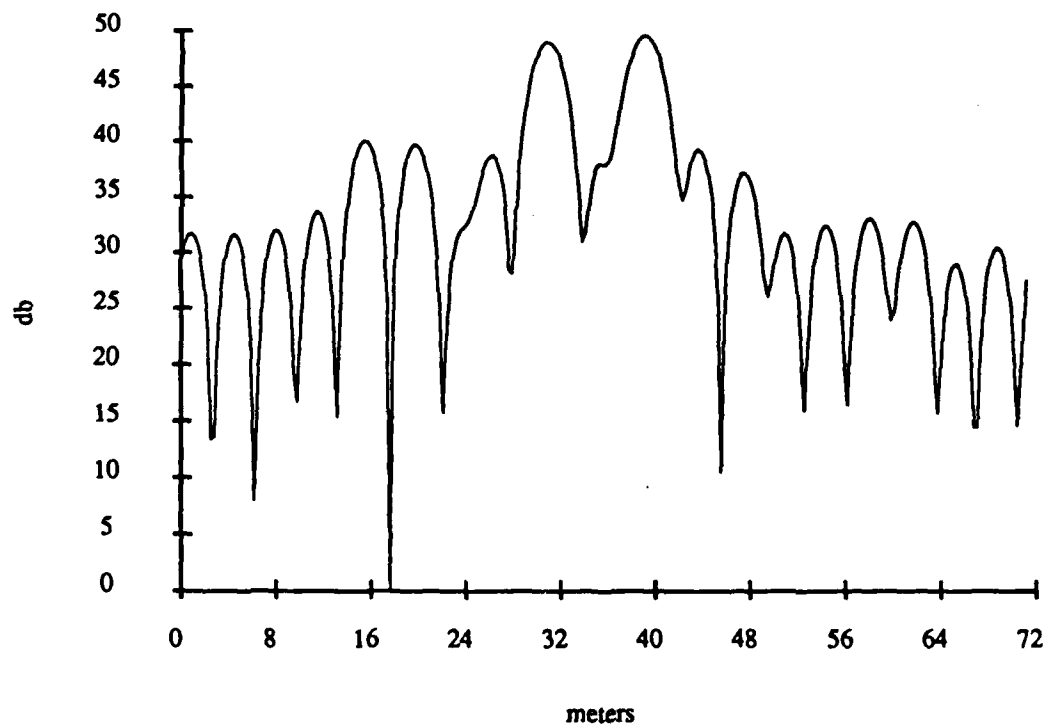
Figure A.49: FT of the Boeing 707 at Horizontal Polarization, 80° aspect angle, 20 frequency samples used, 40–80 MHz
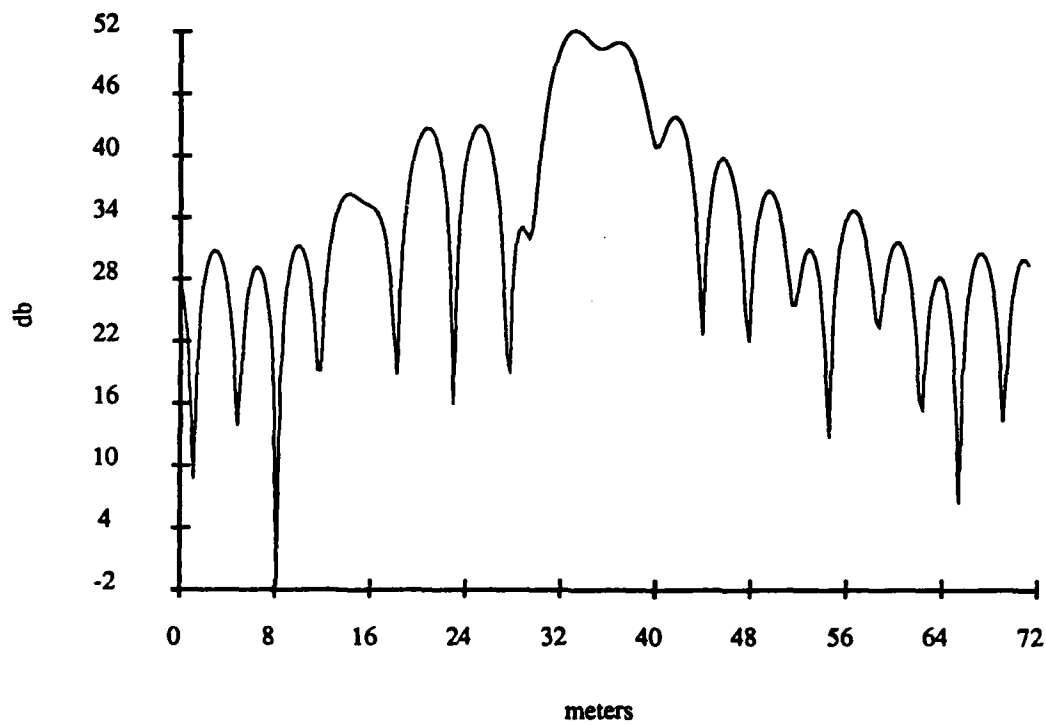
Figure A.50: FT of the Boeing 707 at Horizontal Polarization, 90° aspect angle, 20 frequency samples used, 40–80 MHz

82
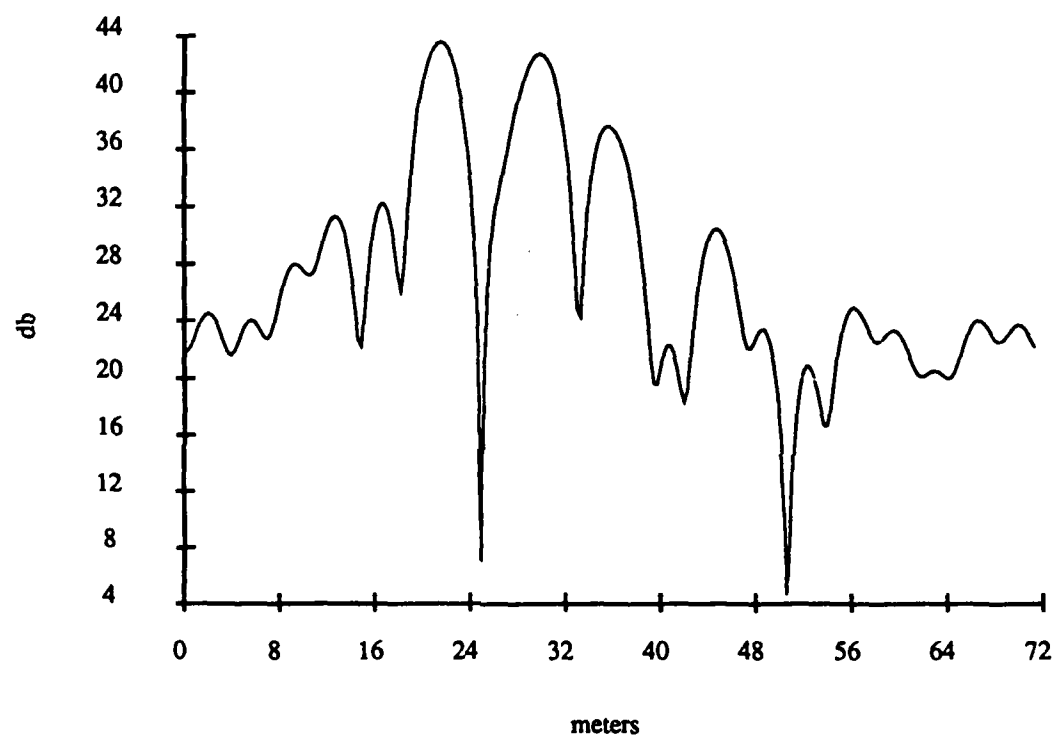
Figure A.51: FT of the Boeing 707 at Horizontal Polarization, 100° aspect angle, 20 frequency samples used, 40–80 MHz

83
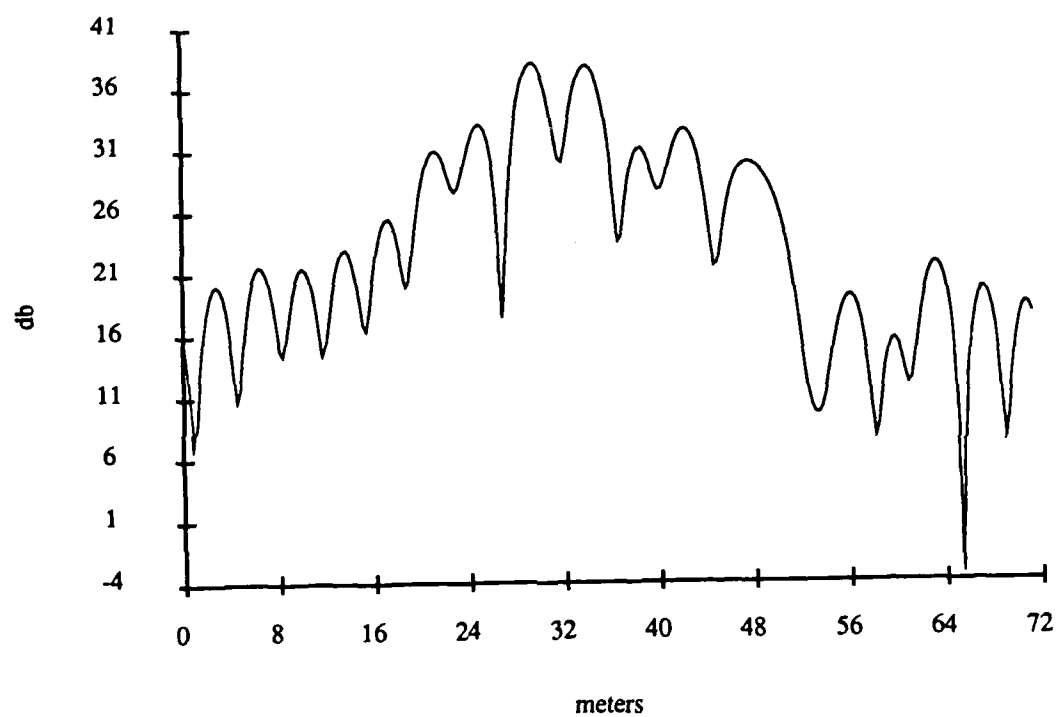
Figure A.52: FT of the Boeing 707 at Horizontal Polarization, 110° aspect angle, 20 frequency samples used, 40–80 MHz
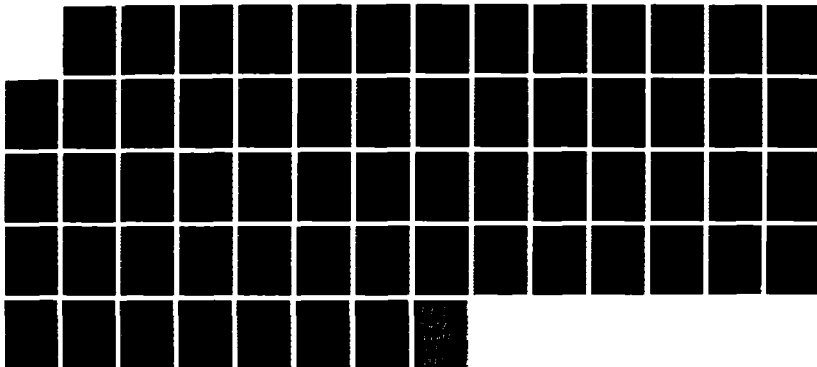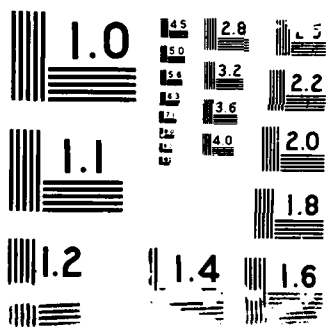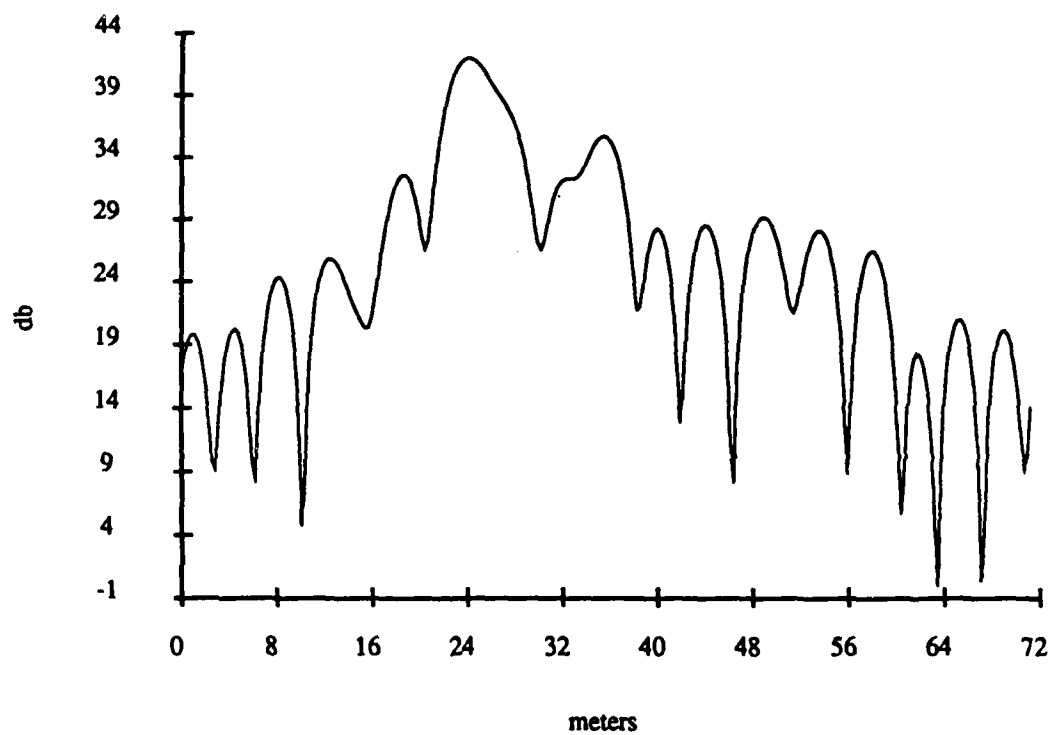
Figure A.53: FT of the Boeing 707 at Horizontal Polarization, 120° aspect angle, 20 frequency samples used, 40–80 MHz
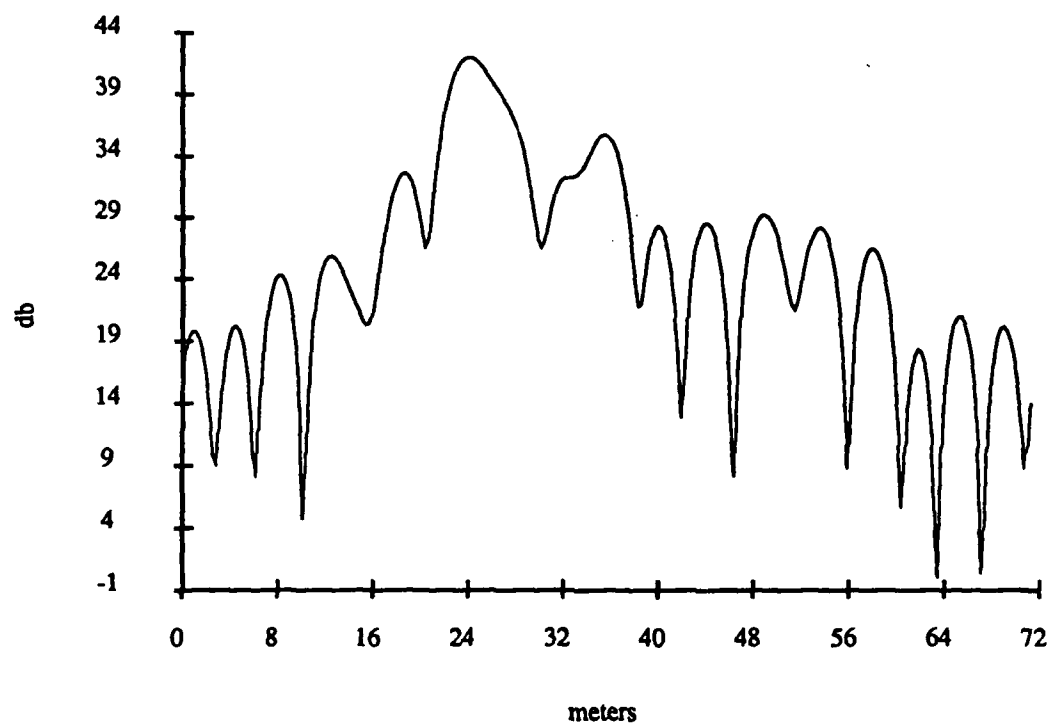
Figure A.54: FT of the Boeing 707 at Horizontal Polarization, 130° aspect angle, 20 frequency samples used, 40–80 MHz
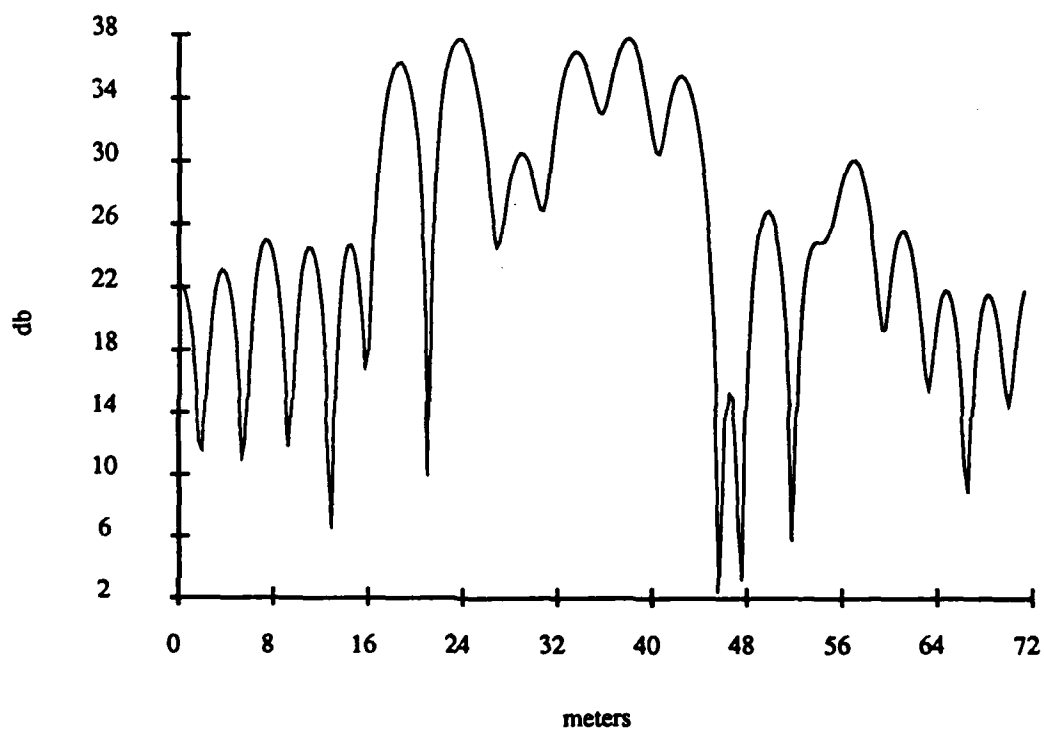
Figure A.55: FT of the Boeing 707 at Horizontal Polarization, 140° aspect angle, 20 frequency samples used, 40–80 MHz
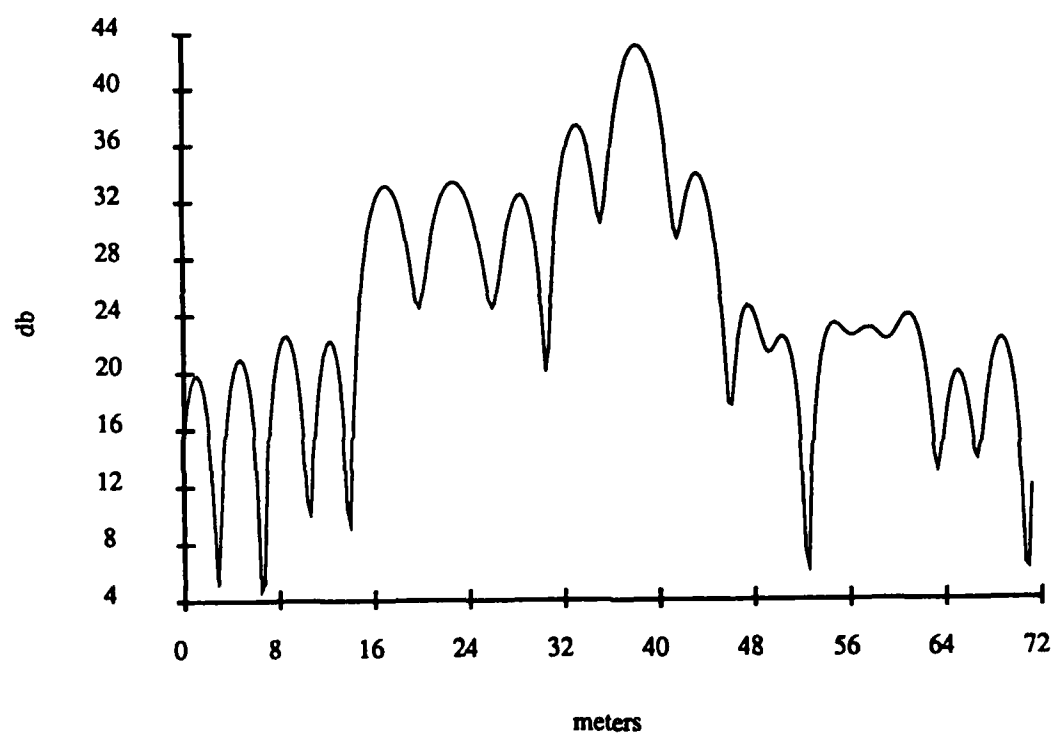
Figure A.56: FT of the Boeing 707 at Horizontal Polarization, 150° aspect angle, 20 frequency samples used, 40–80 MHz
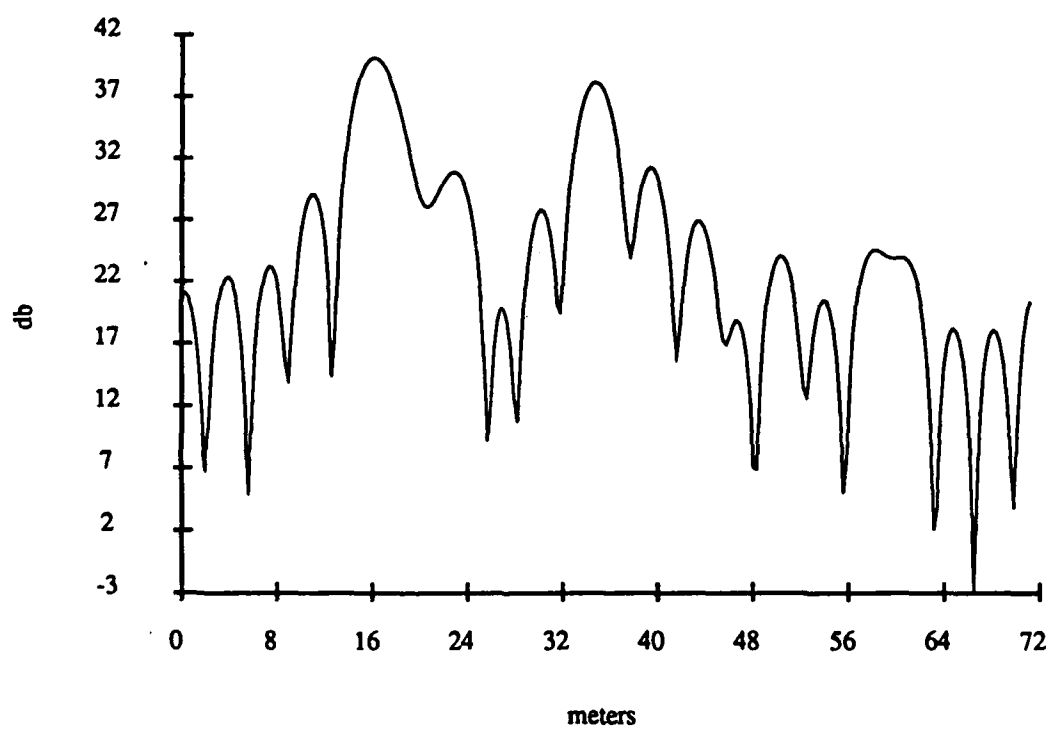
Figure A.57: FT of the Boeing 707 at Horizontal Polarization, 160° aspect angle, 20 frequency samples used, 40–80 MHz
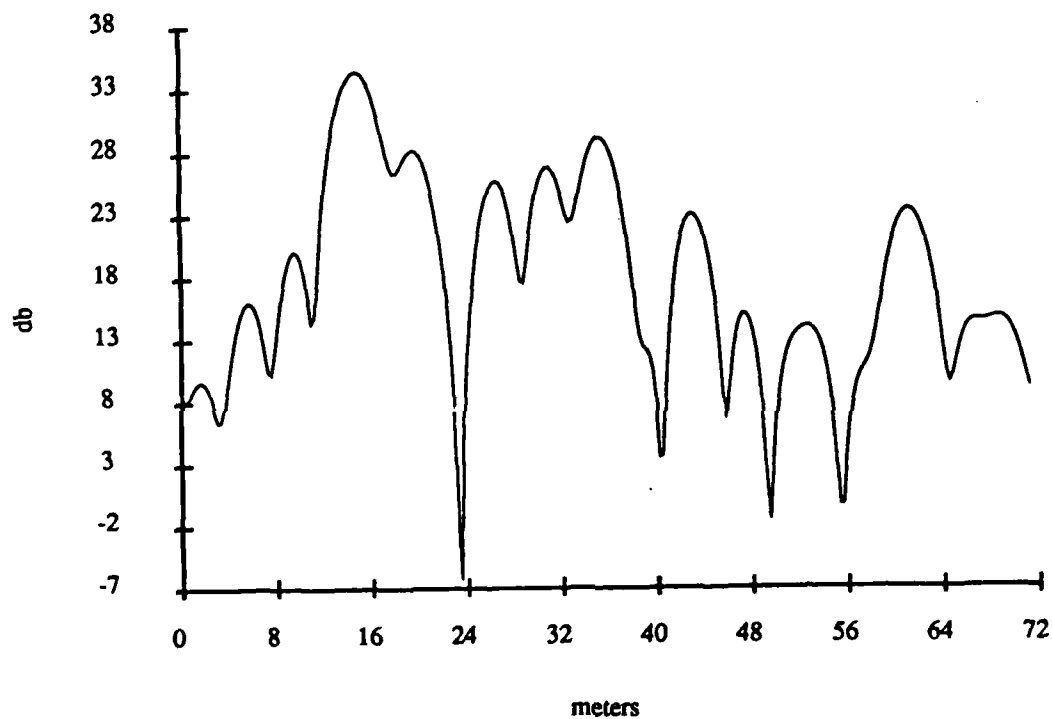
Figure A.58: FT of the Boeing 707 at Horizontal Polarization, 170° aspect angle, 20 frequency samples used, 40–80 MHz

90
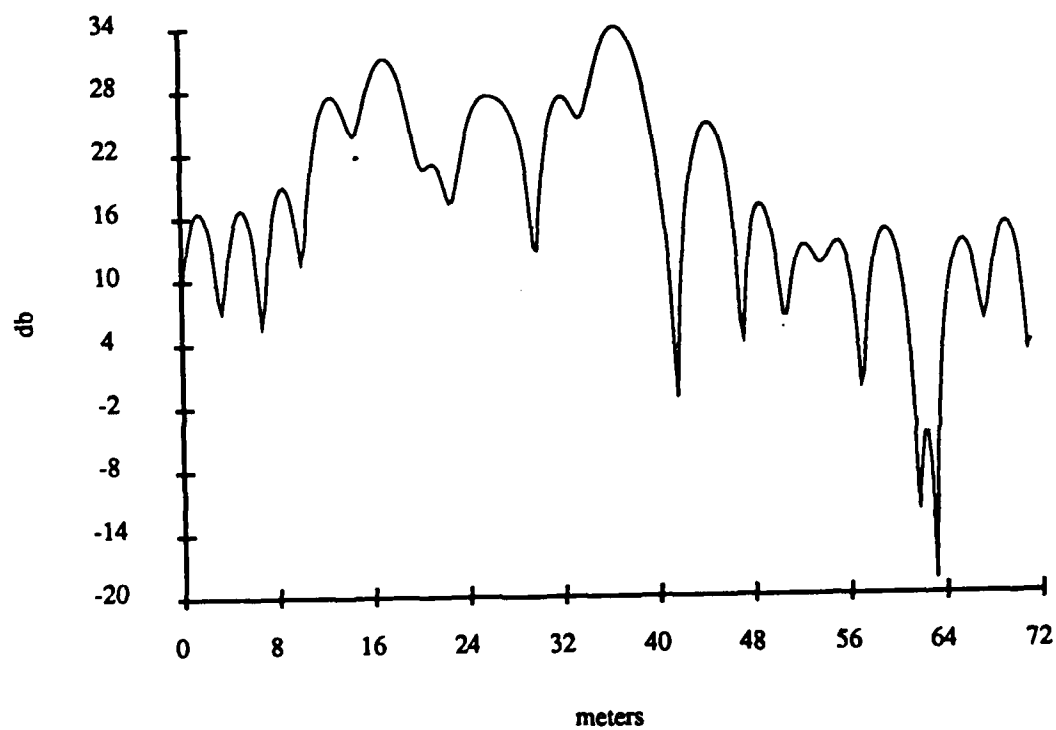
Figure A.59: FT of the Boeing 707 at Horizontal Polarization, 180° aspect angle, 20 frequency samples used, 40–80 MHz

Figure A.60: ARMA Response of the Concorde at Horizontal Polarization, 0° aspect angle, 20 frequency samples used, 40–80 MHz, 9th order model

Figure A.61: ARMA Response of the Concorde at Horizontal Polarization, 10° aspect angle, 20 frequency samples used, 40–80 MHz, 9th order model
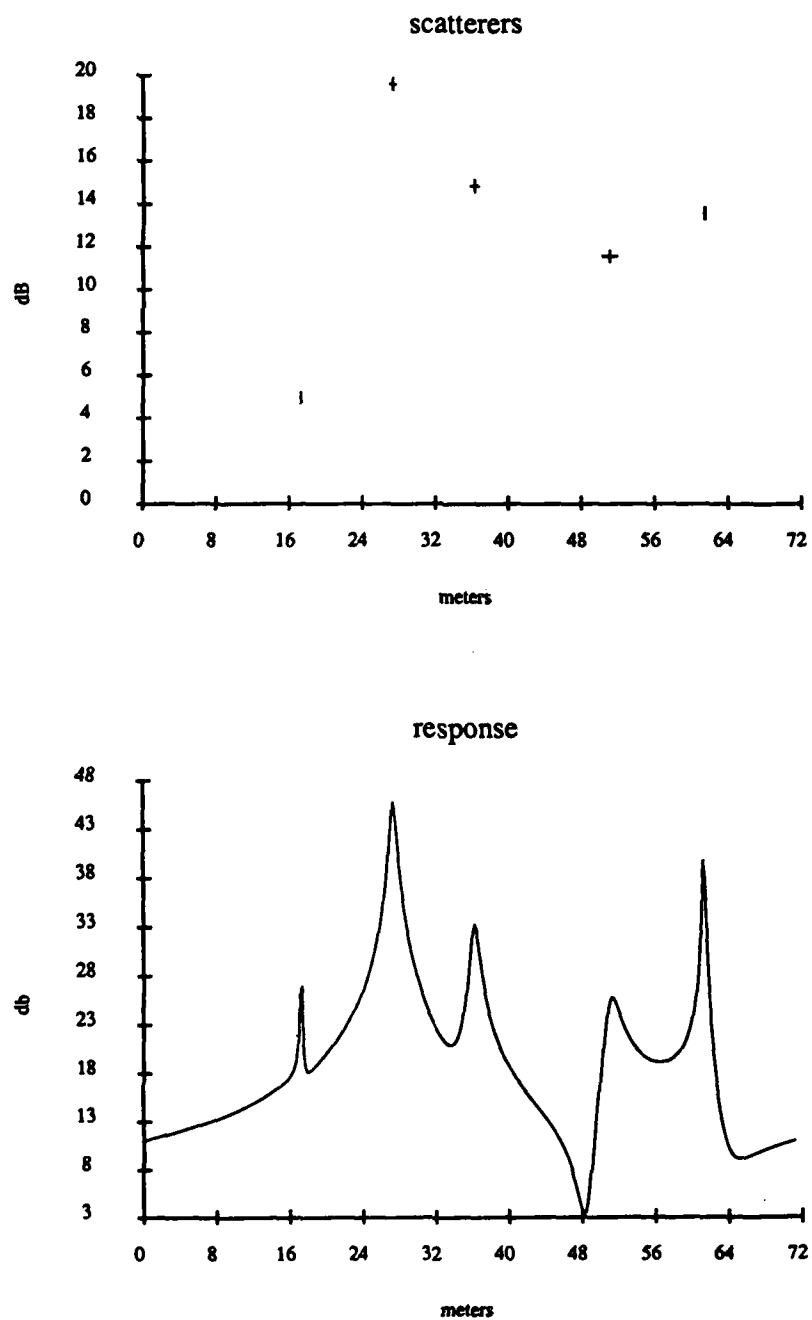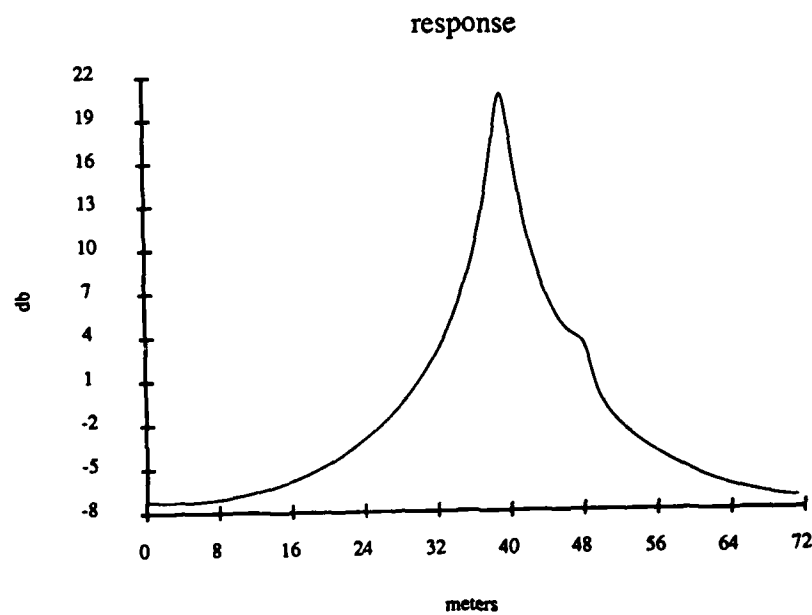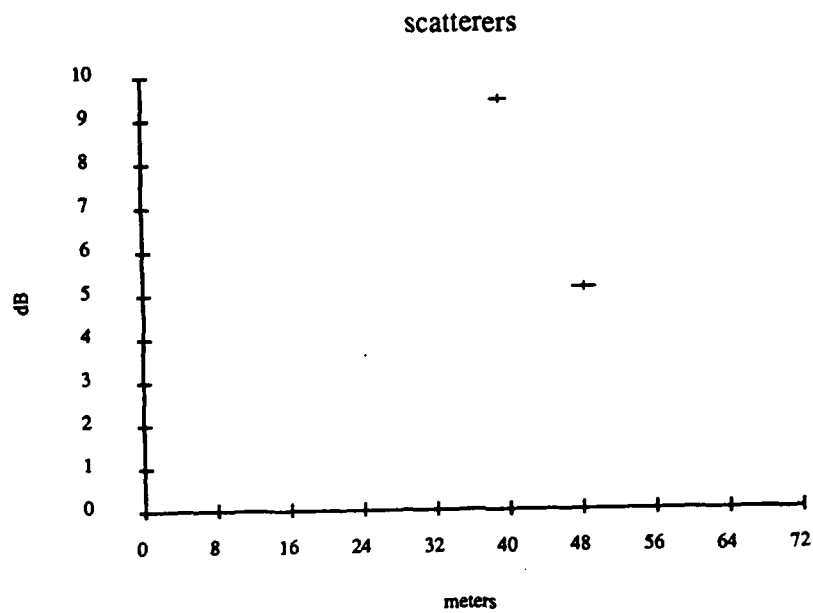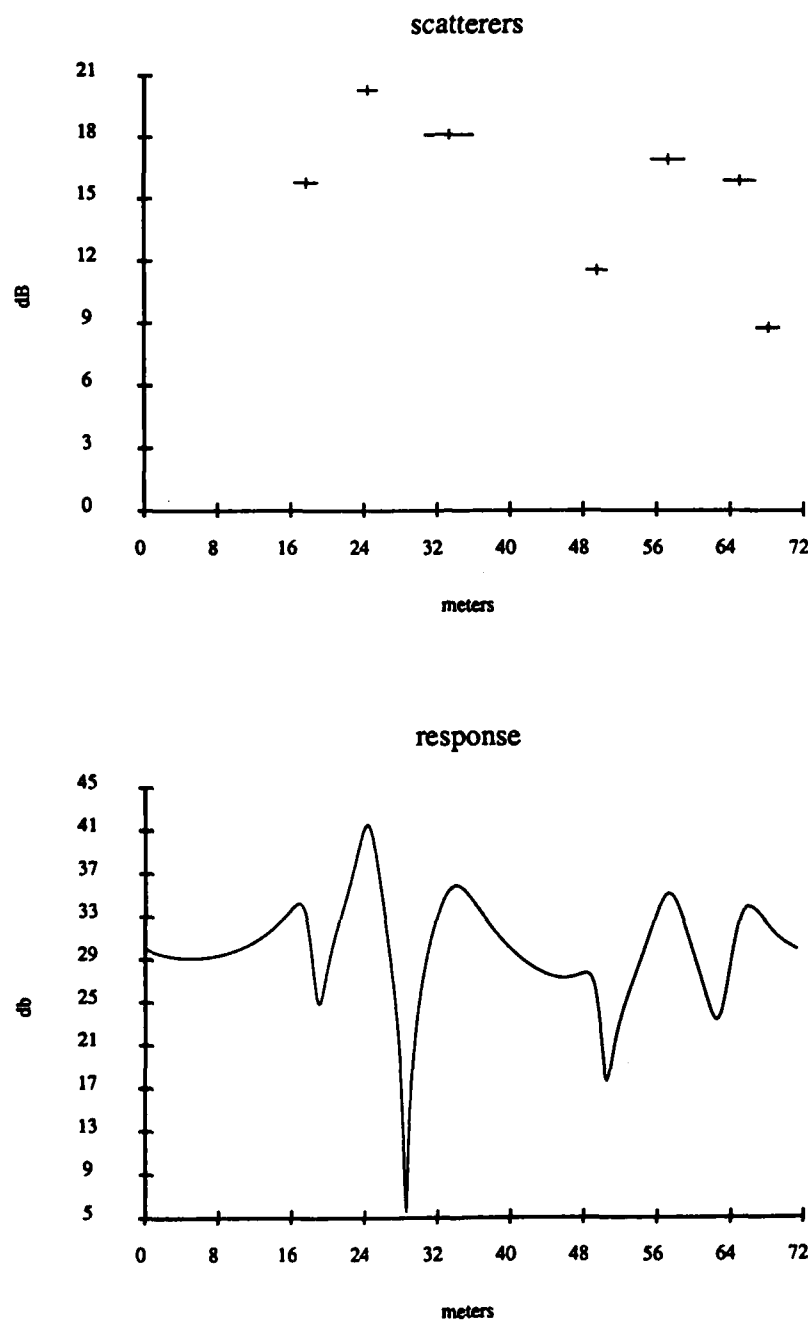
93

Figure A.62: ARMA Response of the Concorde at Horizontal Polarization, 20°
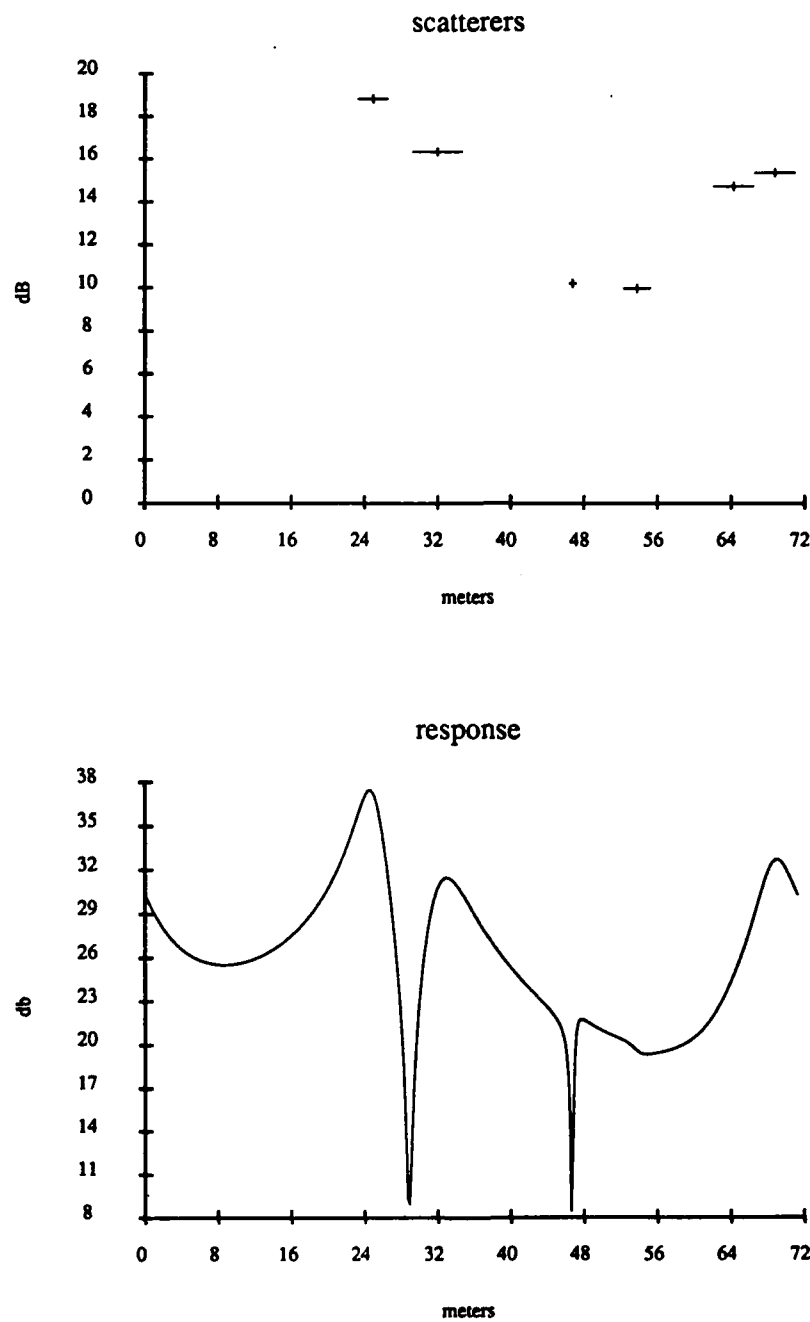aspect angle, 20 frequency samples used, 40–80 MHz, 9th order model

scatterers

response

Figure A.63: ARMA Response of the Concorde at Horizontal Polarization, 30°
aspect angle, 20 frequency samples used, 40–80 MHz, 9th order model

95

scatterers
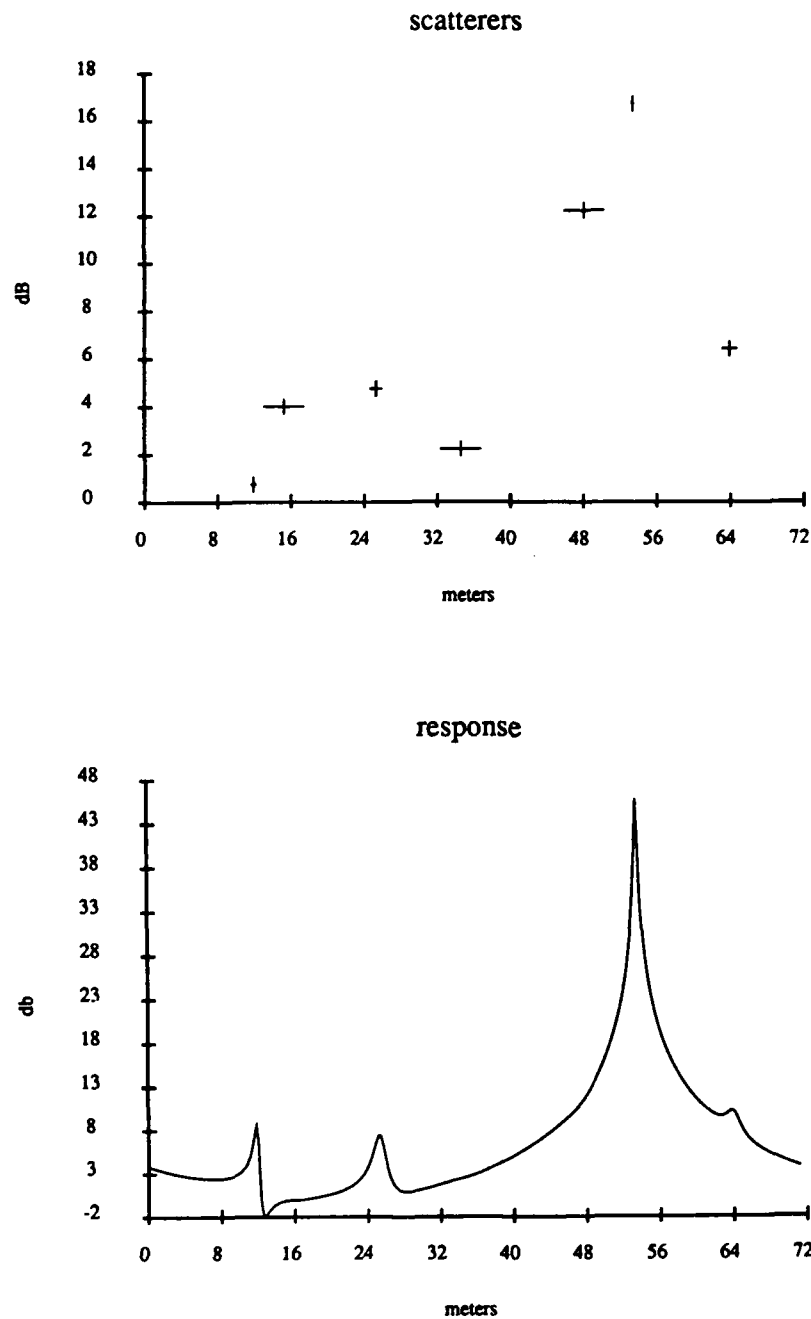
response

Figure A.64: ARMA Response of the Concorde at Horizontal Polarization, 40°
aspect angle, 20 frequency samples used, 40–80 MHz, 9th order model

96
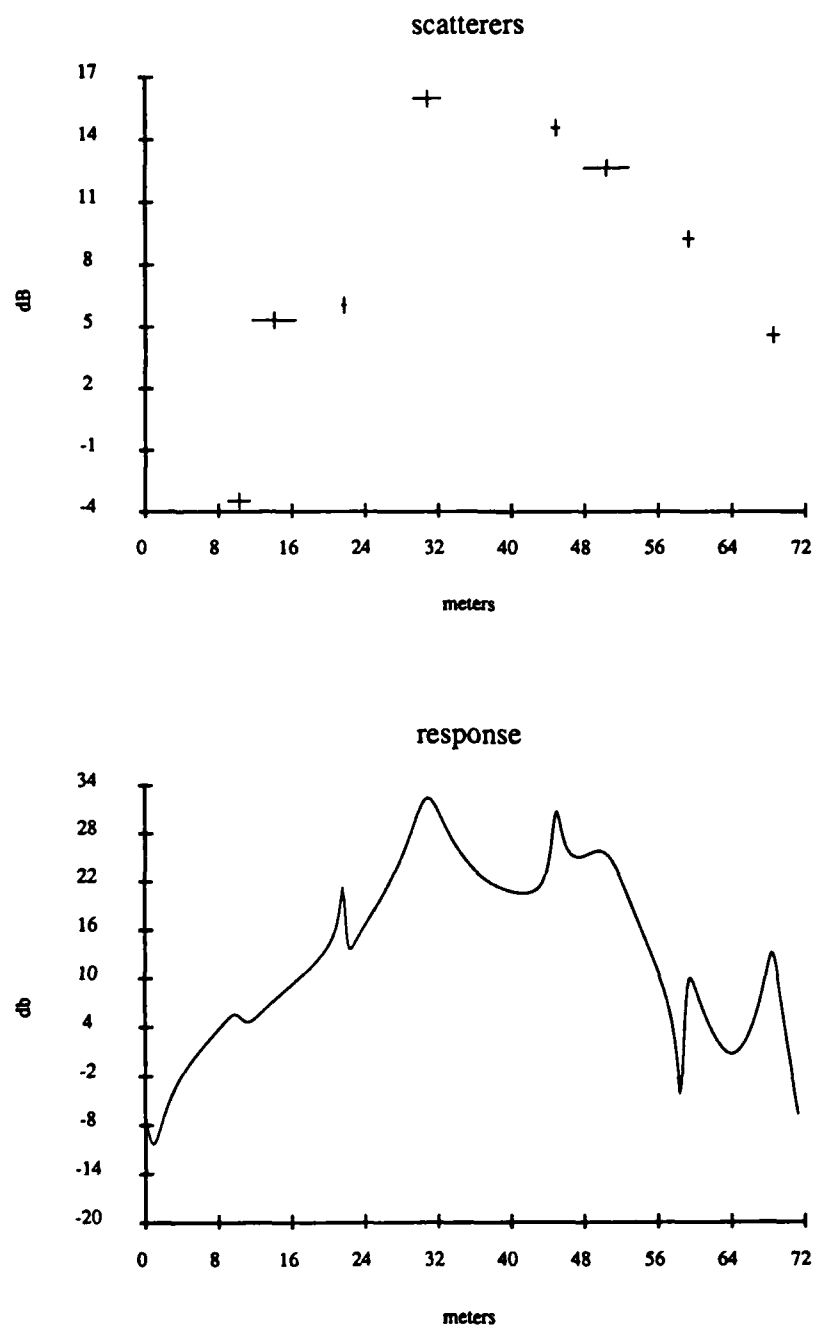
Figure A.65: ARMA Response of the Concorde at Horizontal Polarization, 50° aspect angle, 20 frequency samples used, 40–80 MHz, 9th order model
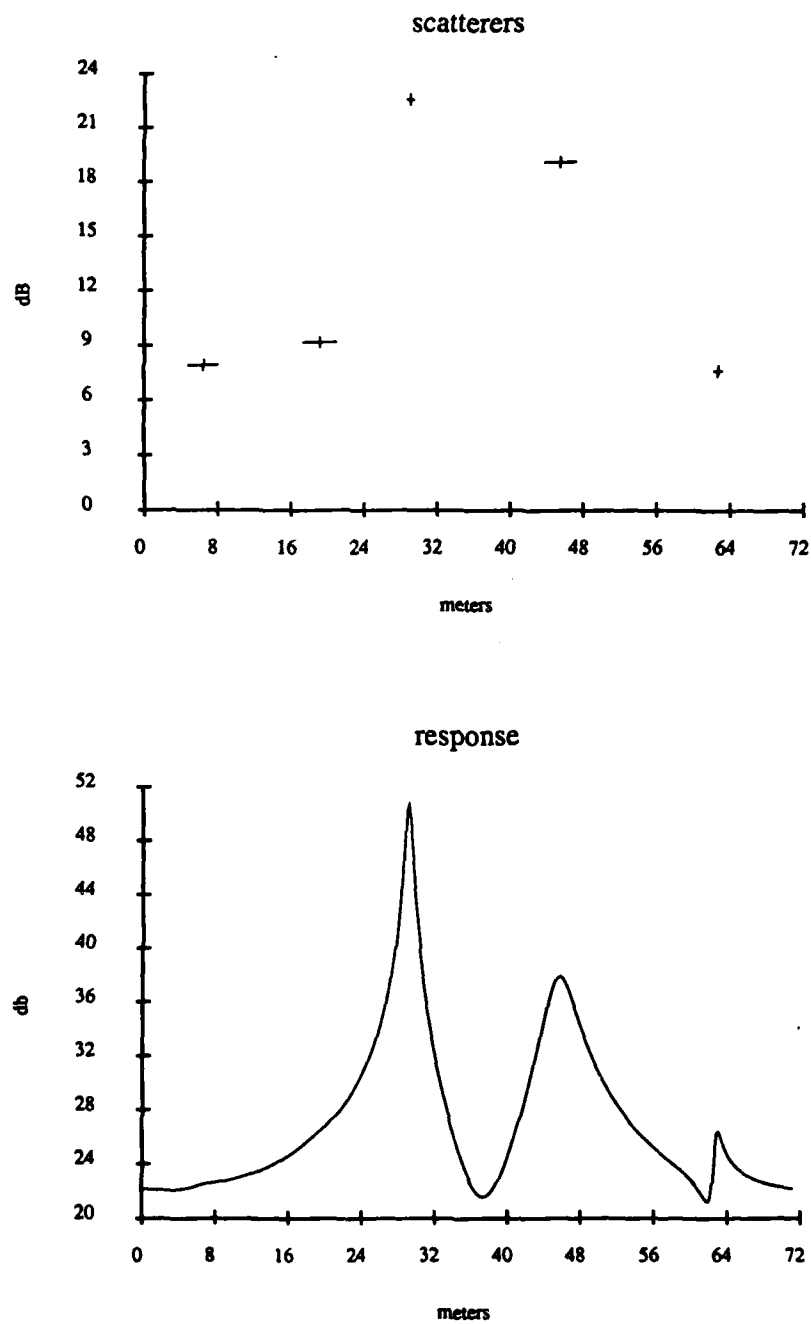
Figure A.66: ARMA Response of the Concorde at Horizontal Polarization, 60° aspect angle, 20 frequency samples used, 40–80 MHz, 9th order model
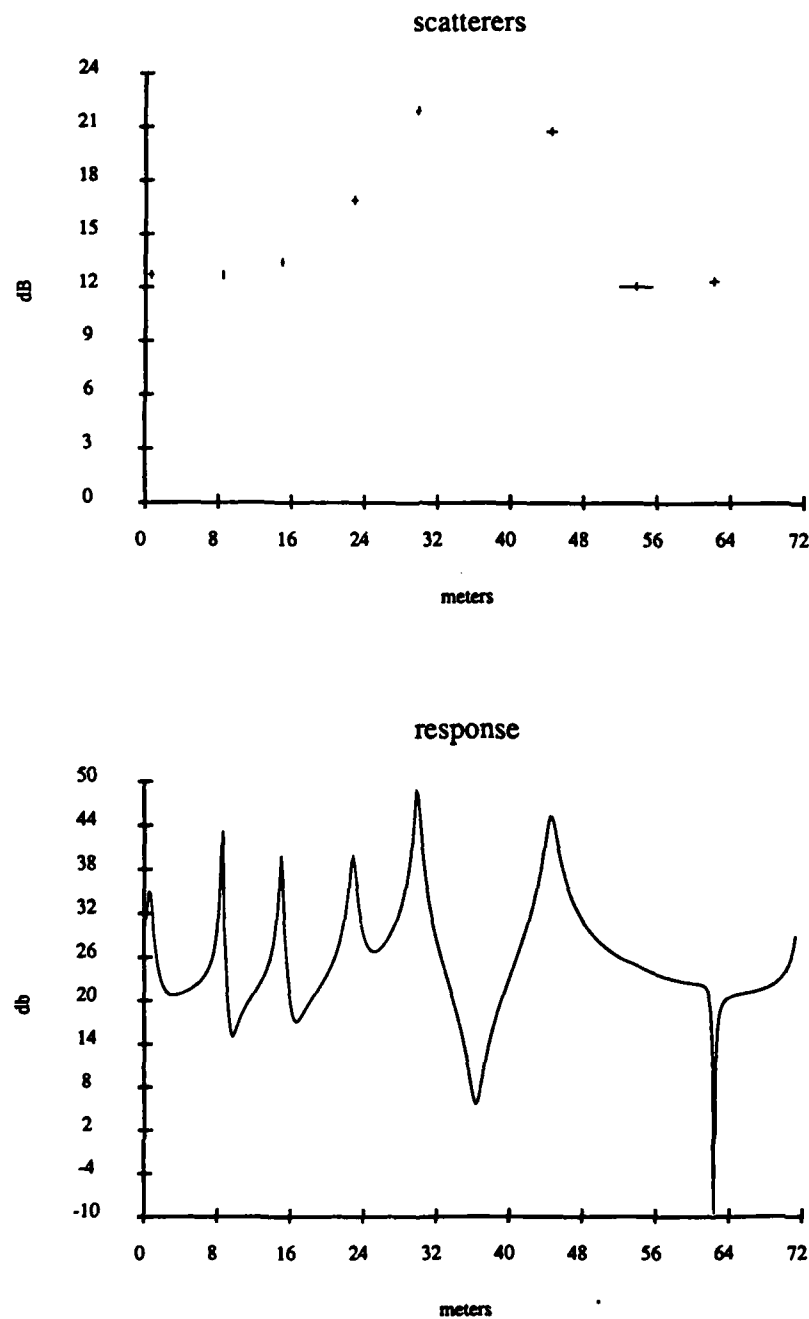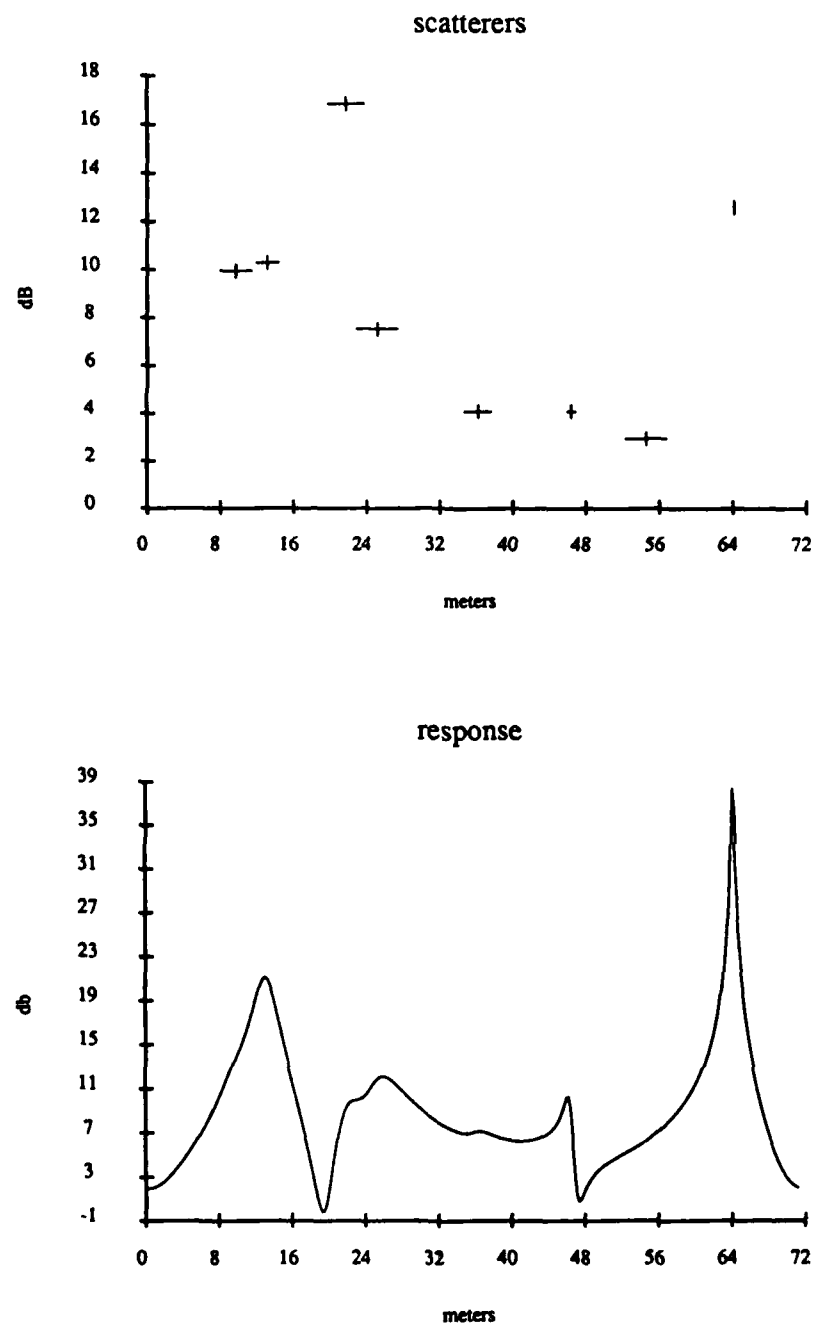
Figure A.67: ARMA Response of the Concorde at Horizontal Polarization, 70° aspect angle, 20 frequency samples used, 40–80 MHz, 9th order model
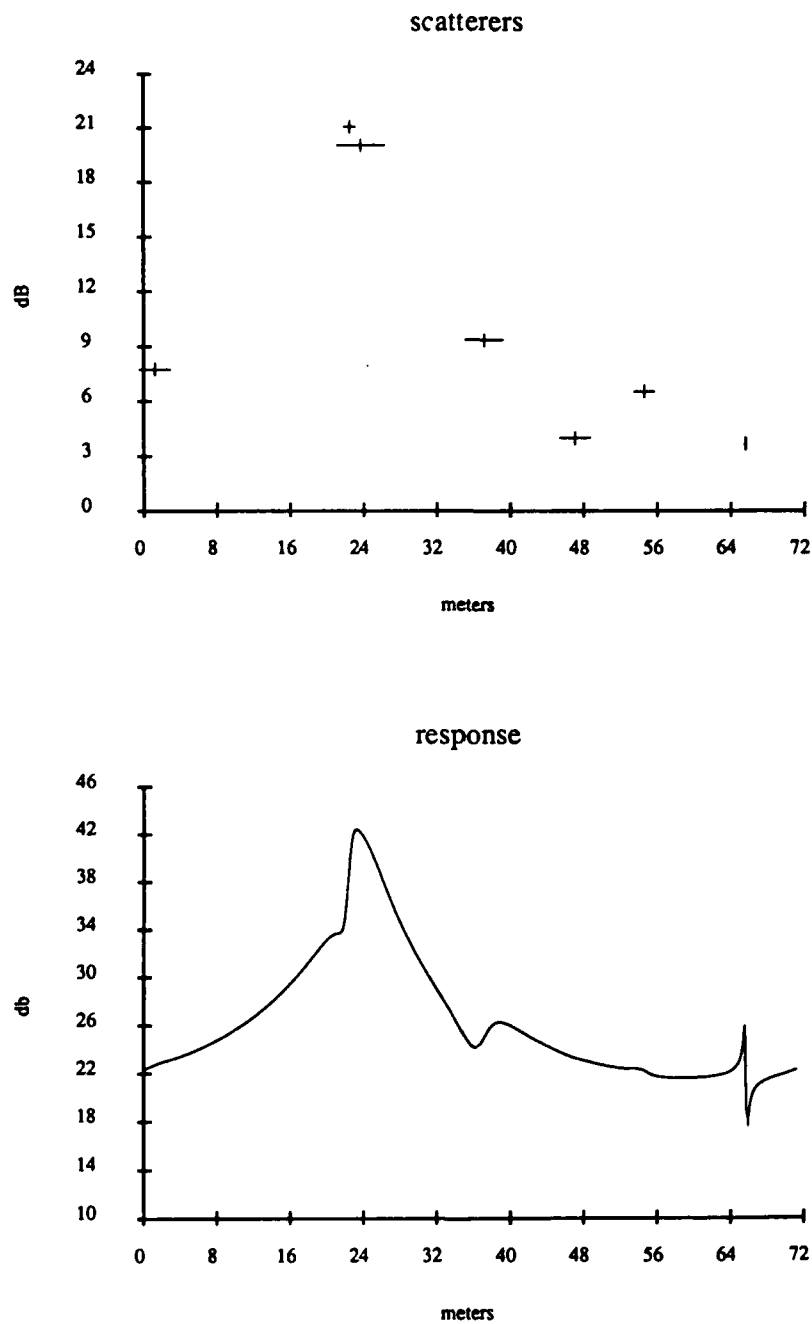
scatterers
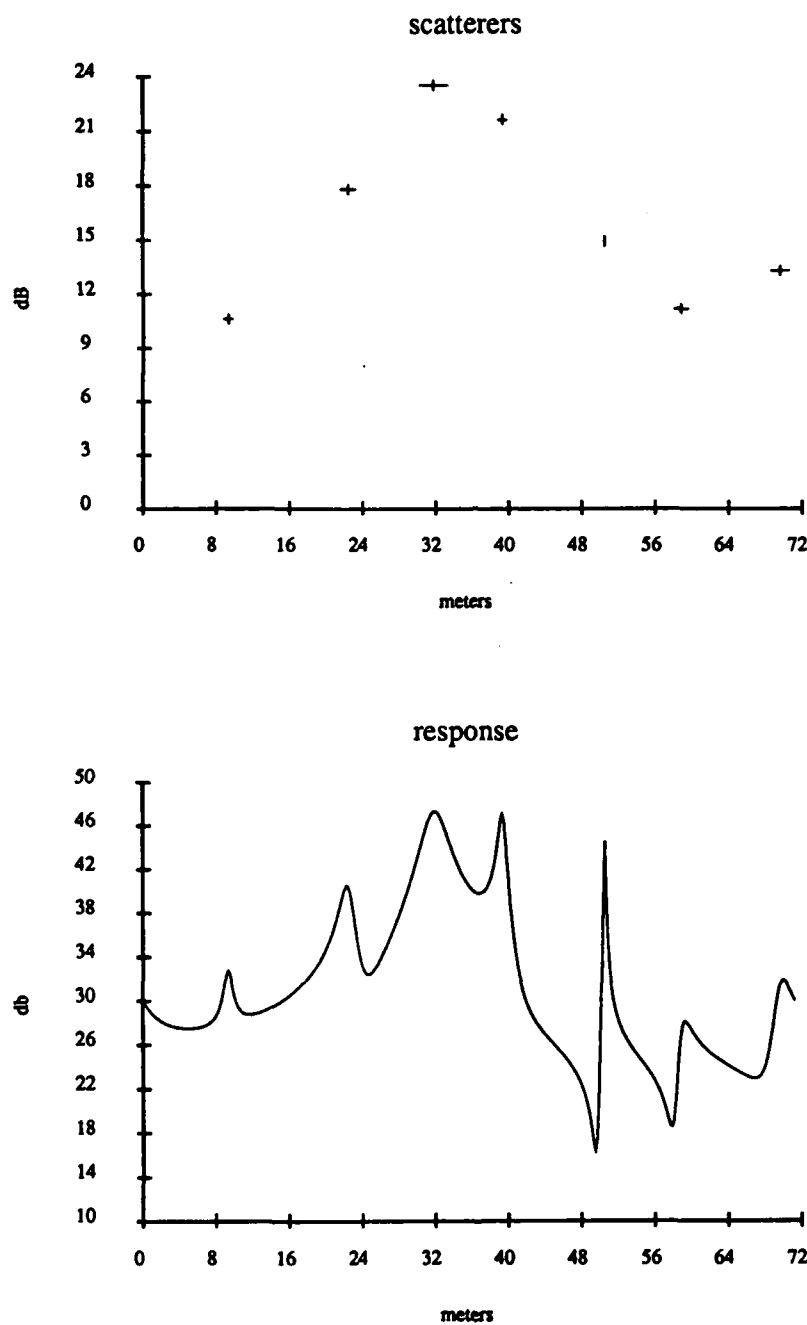
response

Figure A.68: ARMA Response of the Concorde at Horizontal Polarization, 80° aspect angle, 20 frequency samples used, 40–80 MHz, 9th order model

## scatterers
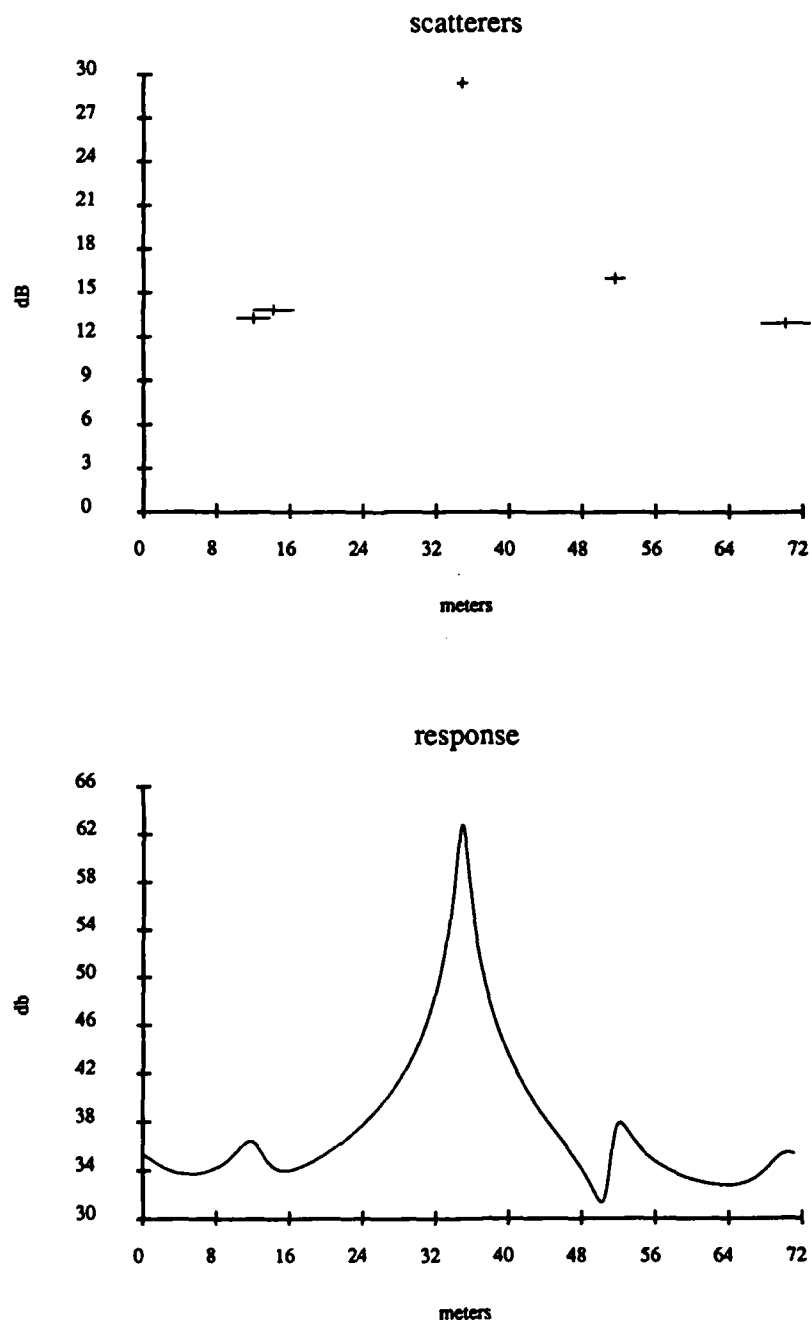
response

Figure A.69: ARMA Response of the Concorde at Horizontal Polarization, 90° aspect angle, 20 frequency samples used, 40–80 MHz, 9th order model

101
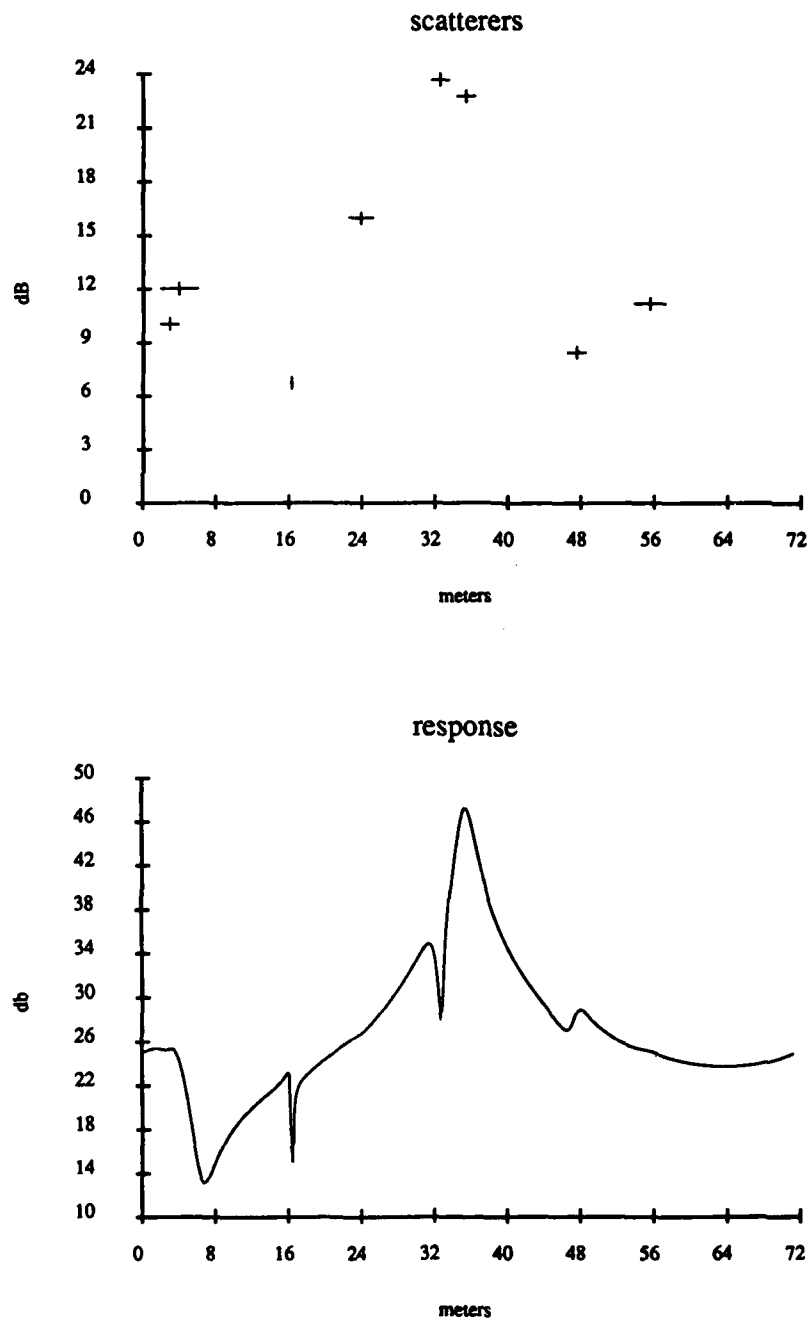
Figure A.70: ARMA Response of the Concorde at Horizontal Polarization, 100° aspect angle, 20 frequency samples used, 40–80 MHz, 9th order model
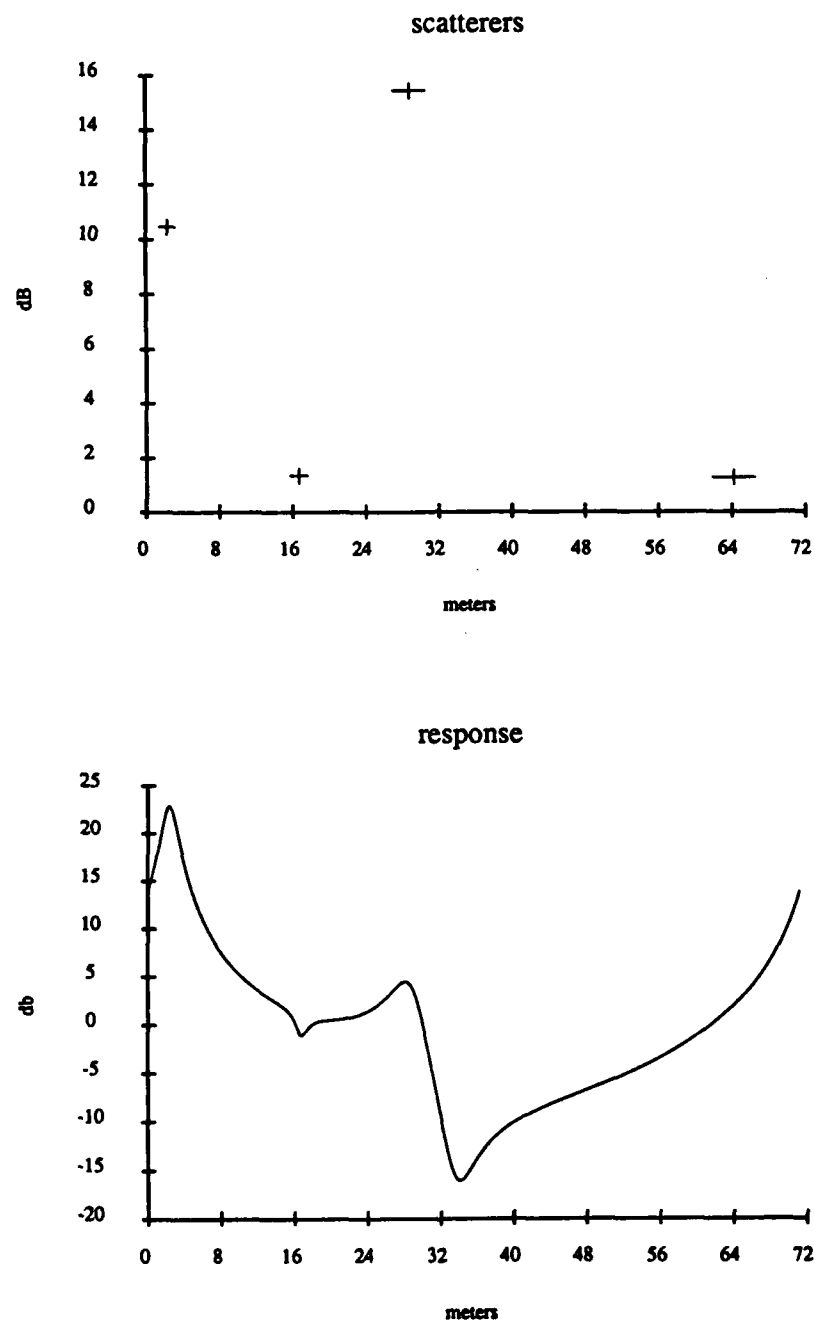
Figure A.71: ARMA Response of the Concorde at Horizontal Polarization, 110° aspect angle, 20 frequency samples used, 40–80 MHz, 9th order model

scatterers
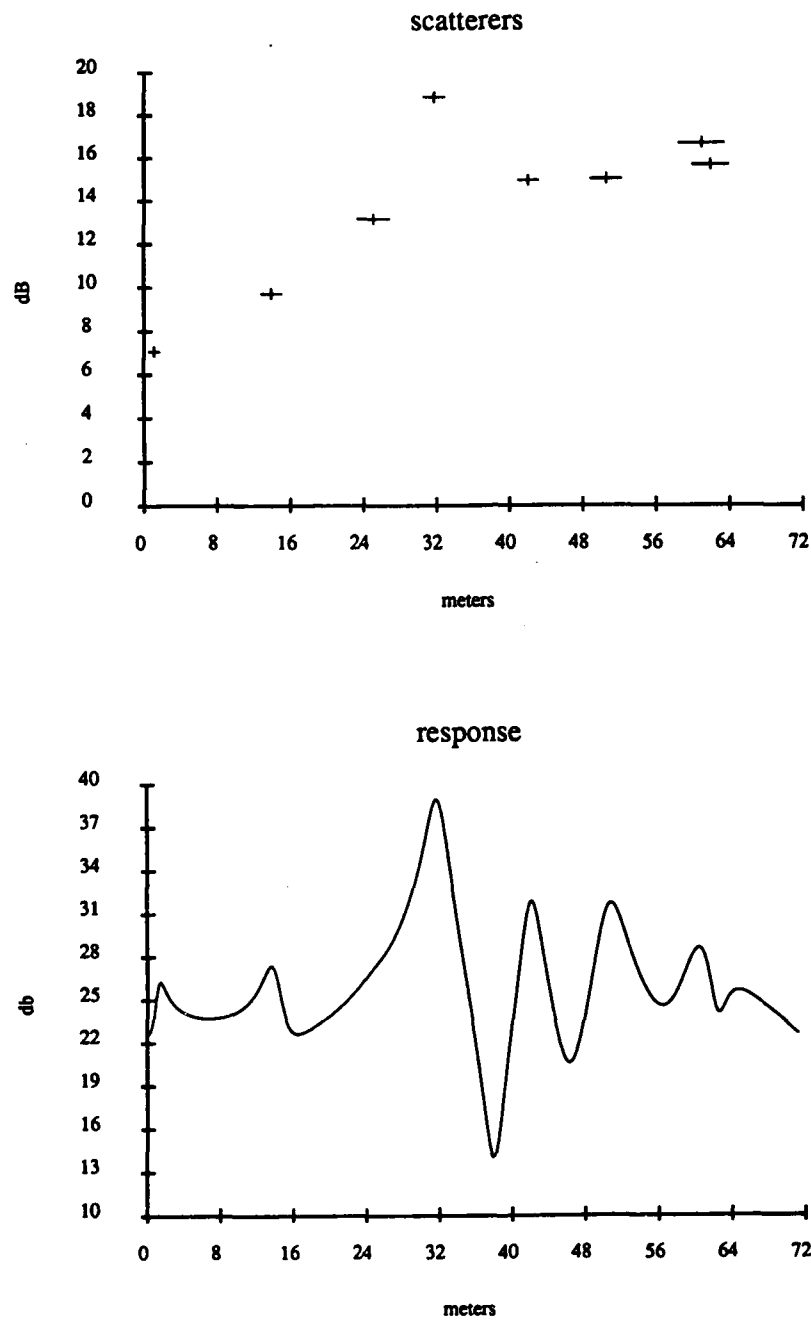
response

Figure A.72: ARMA Response of the Concorde at Horizontal Polarization, 120° aspect angle, 20 frequency samples used, 40–80 MHz, 9th order model

104

Figure A.73: ARMA Response of the Concorde at Horizontal Polarization, 130°
aspect angle, 20 frequency samples used, 40–80 MHz, 9th order model

105

scatterers

response

Figure A.74: ARMA Response of the Concorde at Horizontal Polarization, 140°
aspect angle, 20 frequency samples used, 40–80 MHz, 9th order model

106

scatterers

response

Figure A.75: ARMA Response of the Concorde at Horizontal Polarization, 150° aspect angle, 20 frequency samples used, 40–80 MHz, 9th order model

scatterers

response

Figure A.76: ARMA Response of the Concorde at Horizontal Polarization, 160° aspect angle, 20 frequency samples used, 40–80 MHz, 9th order model

108

scatterers

response

Figure A.77: ARMA Response of the Concorde at Horizontal Polarization, 170° aspect angle, 20 frequency samples used, 40–80 MHz, 9th order model

109

Figure A.78: ARMA Response of the Concorde at Horizontal Polarization, 180° aspect angle, 20 frequency samples used, 40–80 MHz, 9th order model

110
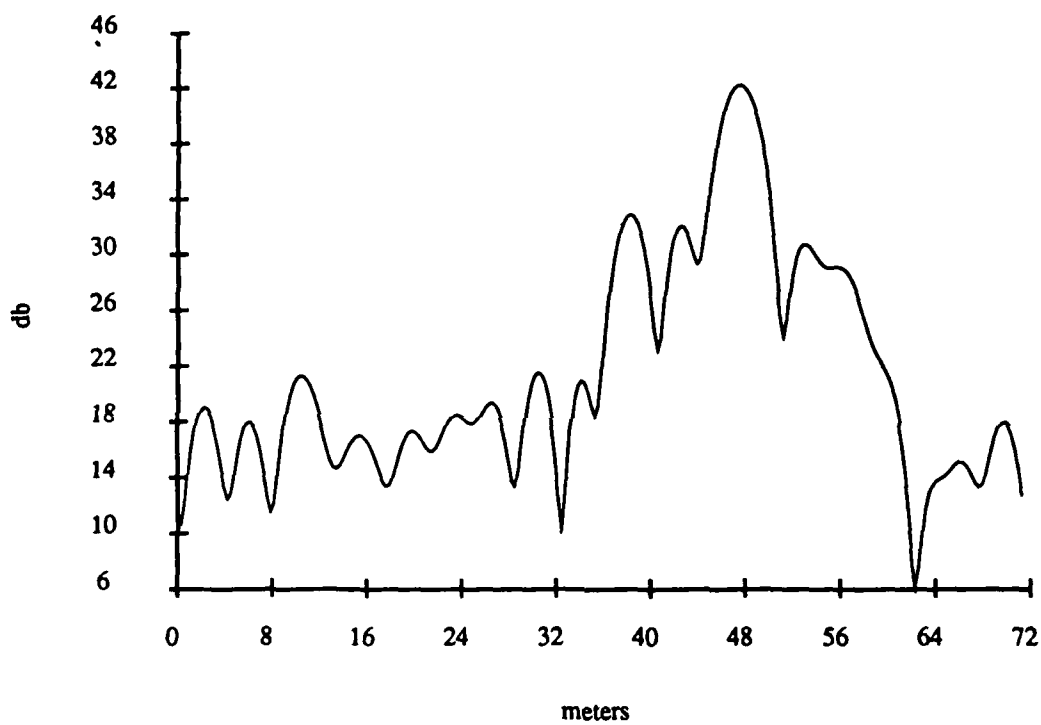
Figure A.79: FT of the Concorde at Horizontal Polarization, 0° aspect angle, 20 frequency samples used, 40–80 MHz
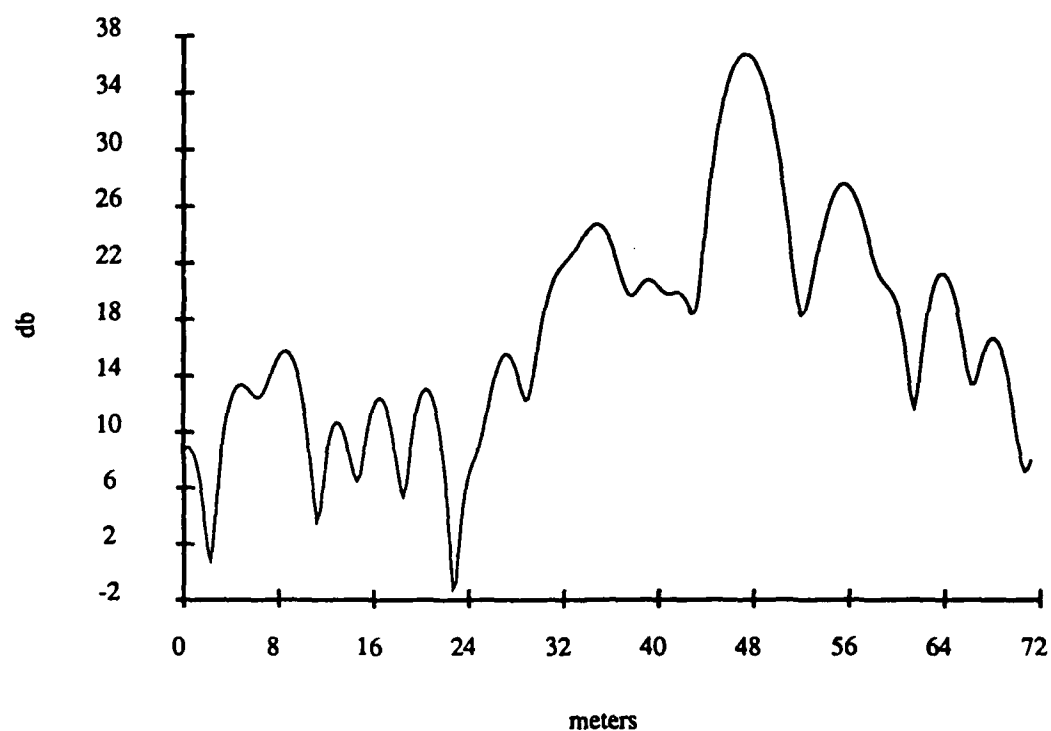
Figure A.80: FT of the Concorde at Horizontal Polarization, 10° aspect angle, 20 frequency samples used, 40–80 MHz
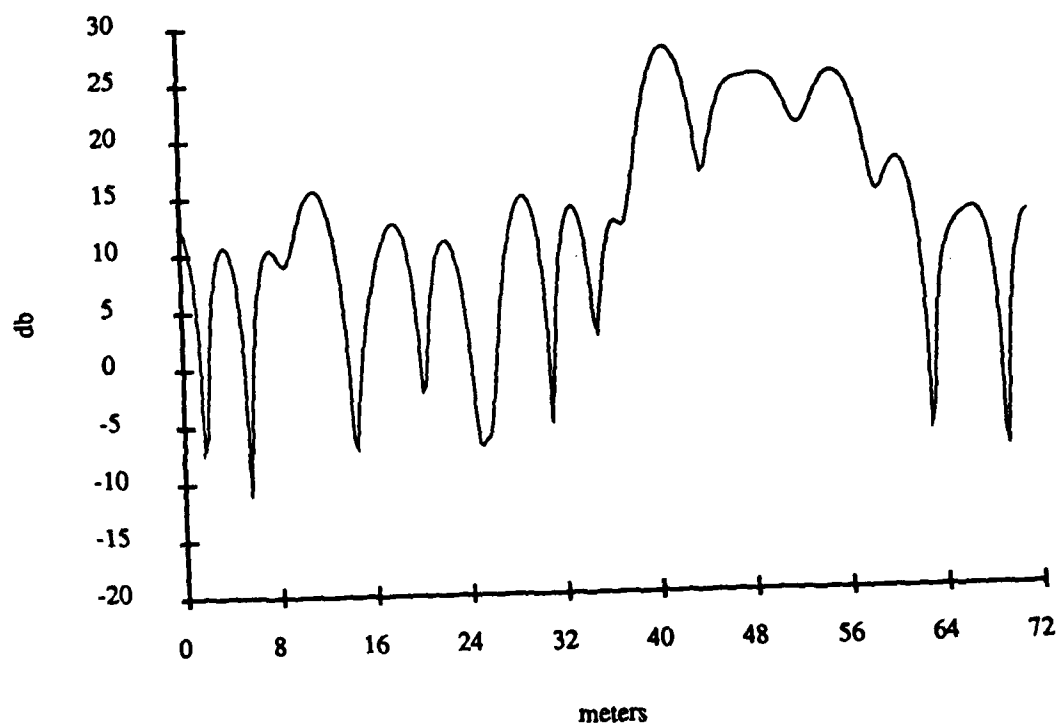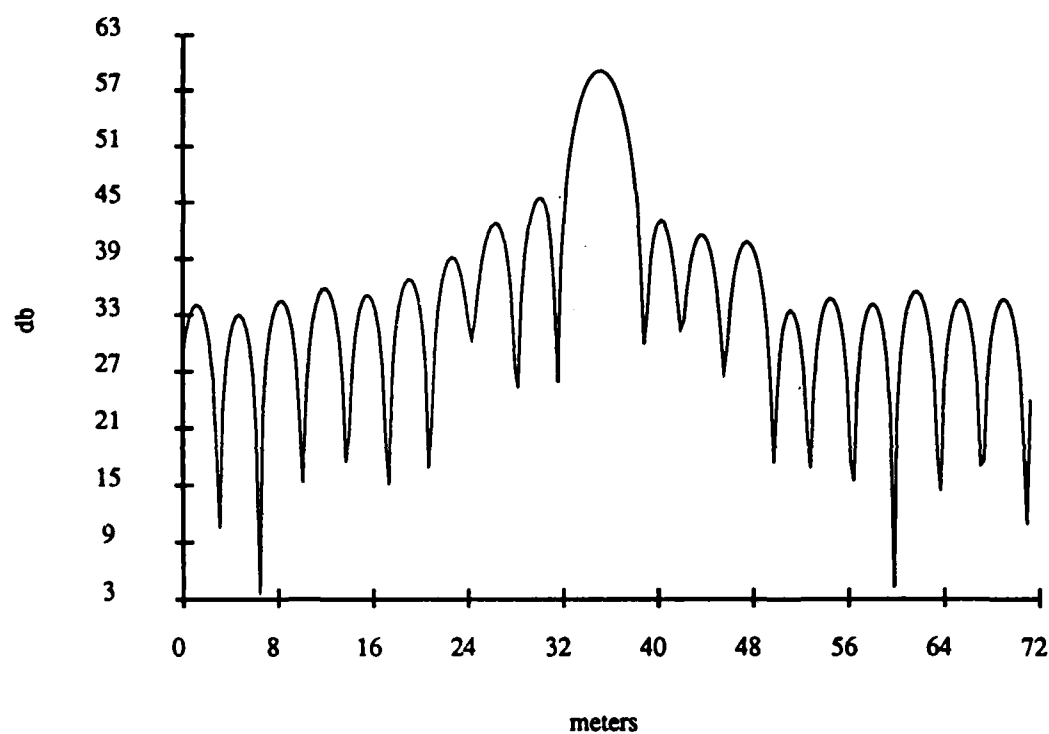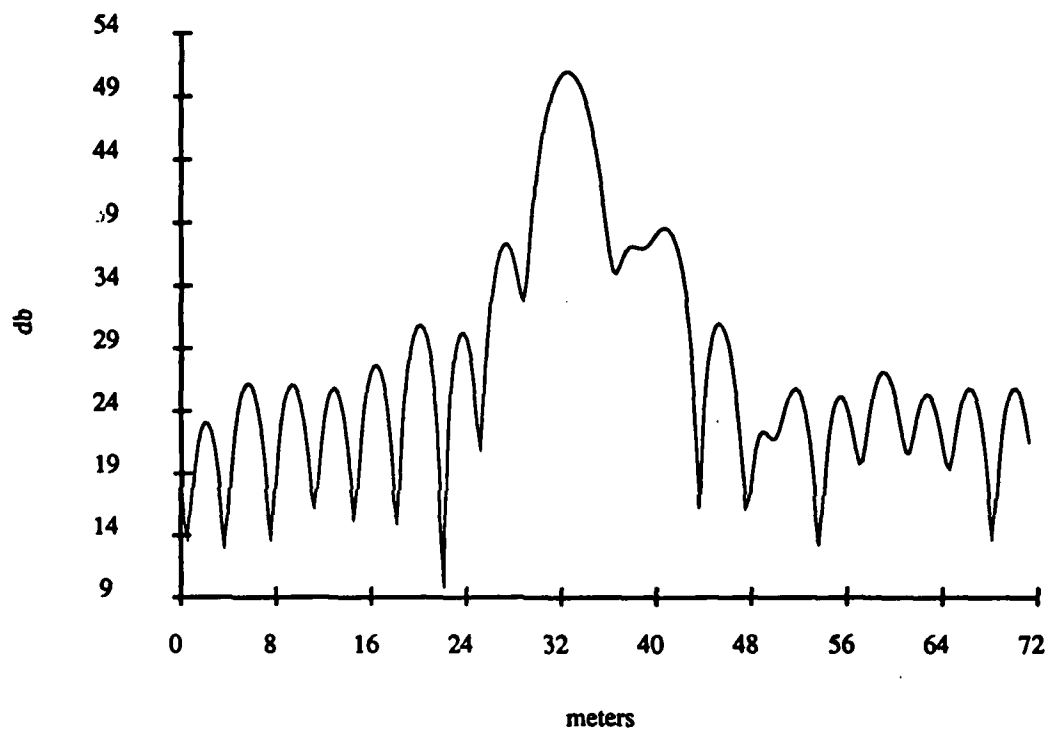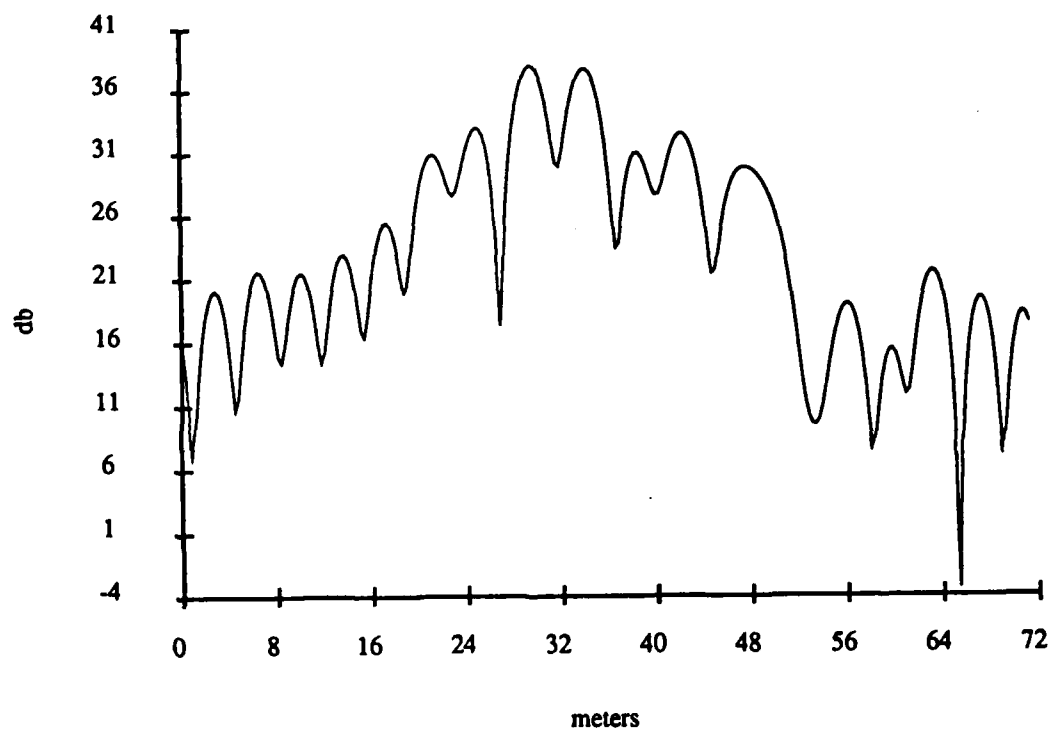
Figure A.81: FT of the Concorde at Horizontal Polarization, 20° aspect angle, 20 frequency samples used, 40–80 MHz

113
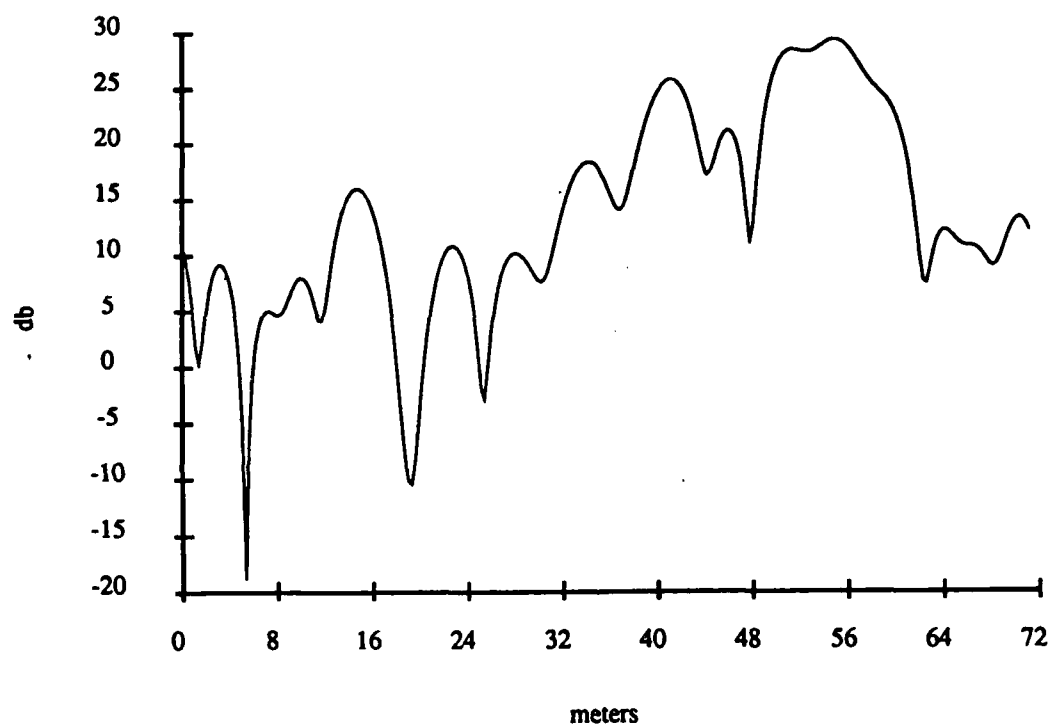
Figure A.82: FT of the Concorde at Horizontal Polarization, 30° aspect angle, 20 frequency samples used, 40–80 MHz
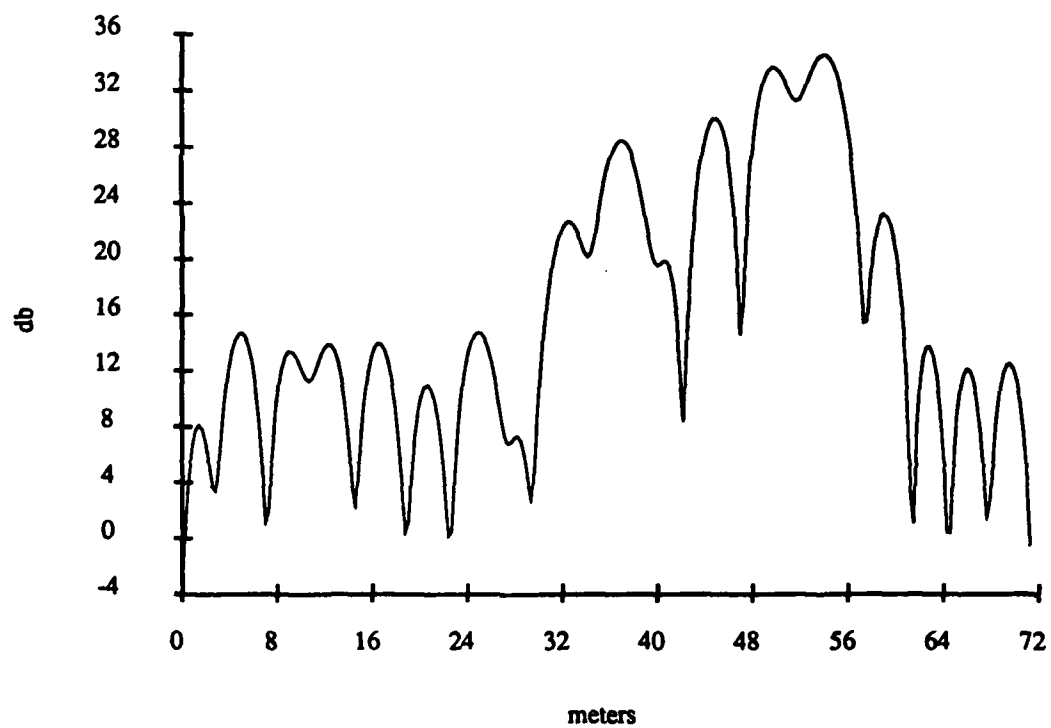
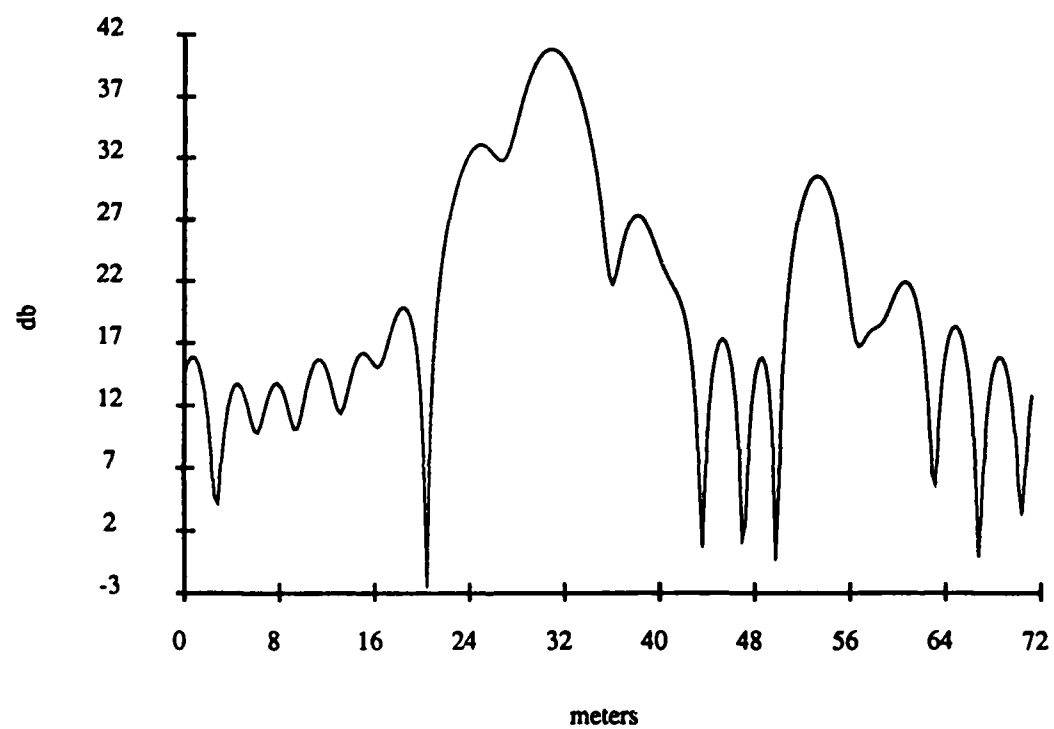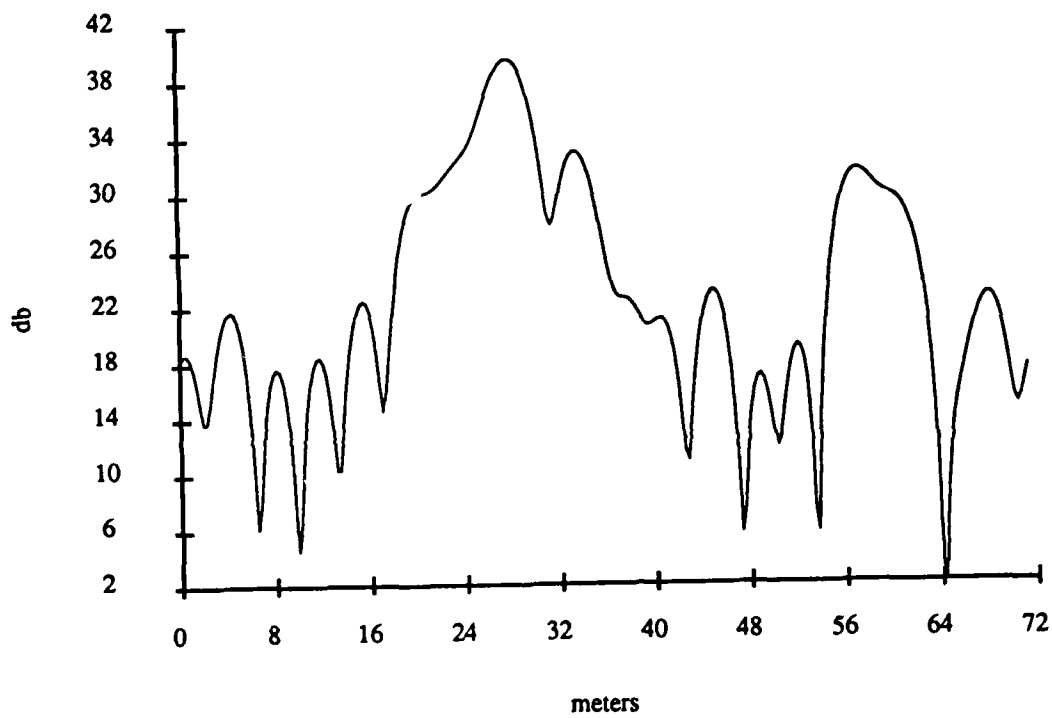Figure A.83: FT of the Concorde at Horizontal Polarization, 40° aspect angle, 20 frequency samples used, 40–80 MHz

115
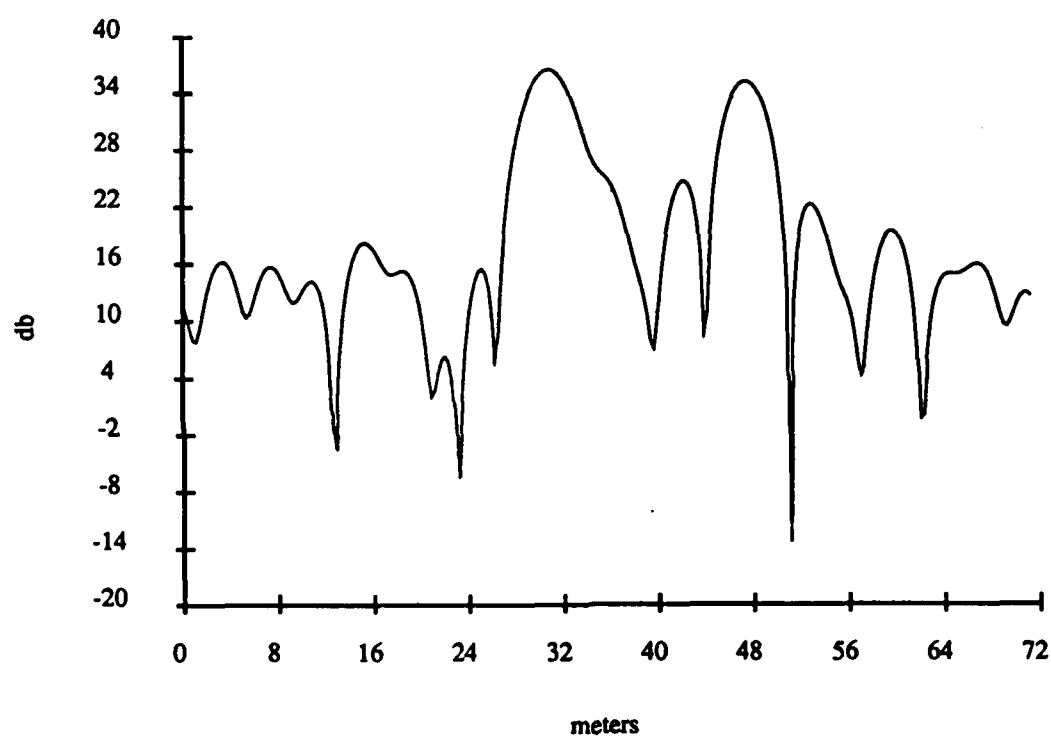
Figure A.84: FT of the Concorde at Horizontal Polarization, 50° aspect angle, 20 frequency samples used, 40–80 MHz
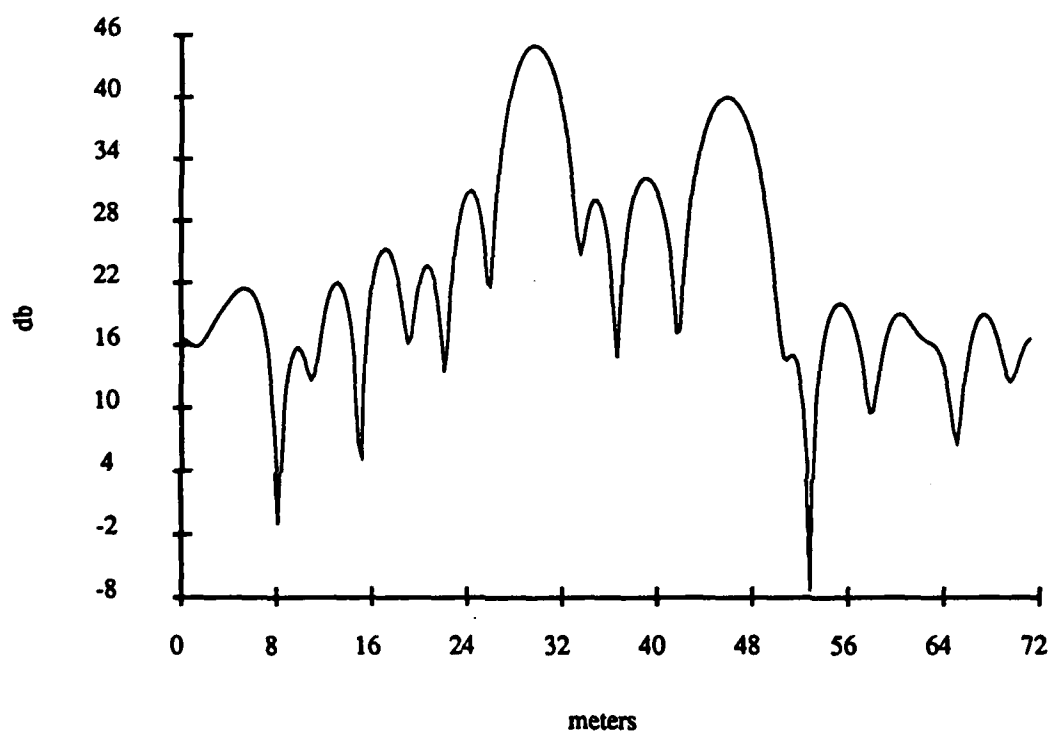
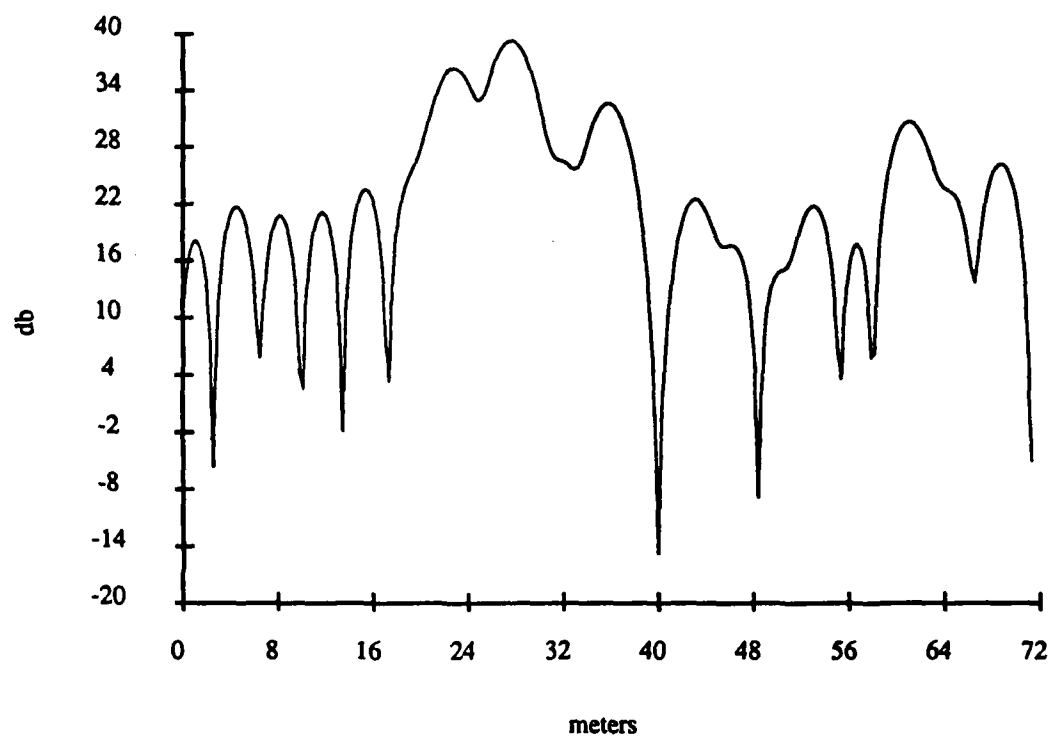Figure A.85: FT of the Concorde at Horizontal Polarization, 60° aspect angle, 20 frequency samples used, 40–80 MHz
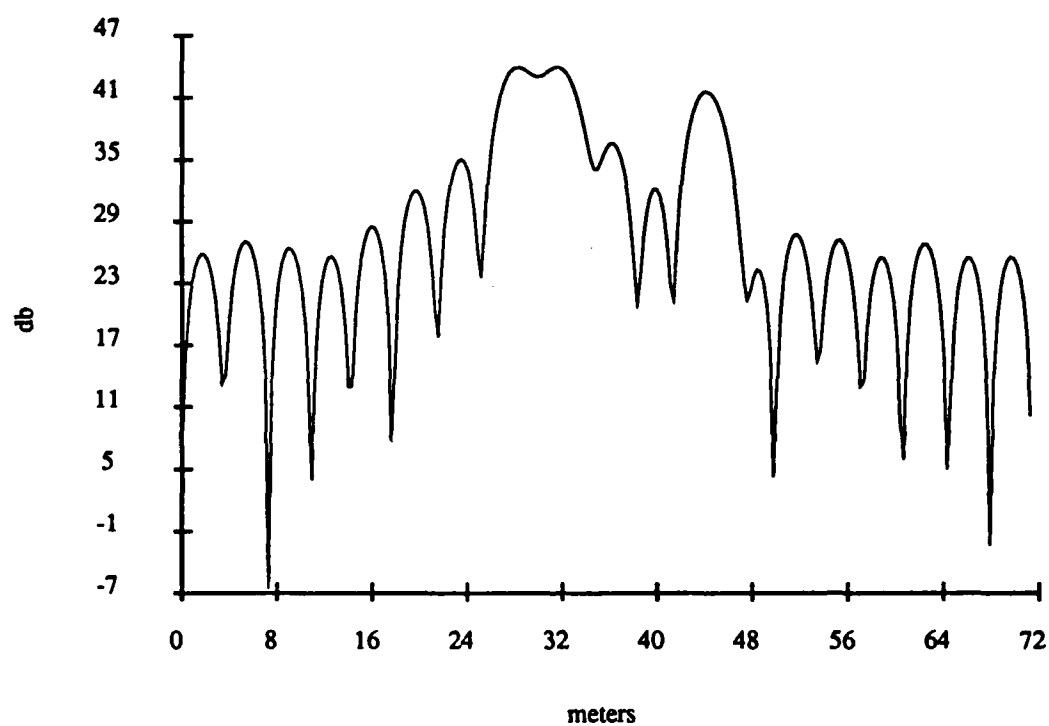
Figure A.86: FT of the Concorde at Horizontal Polarization, 70° aspect angle, 20 frequency samples used, 40–80 MHz

118
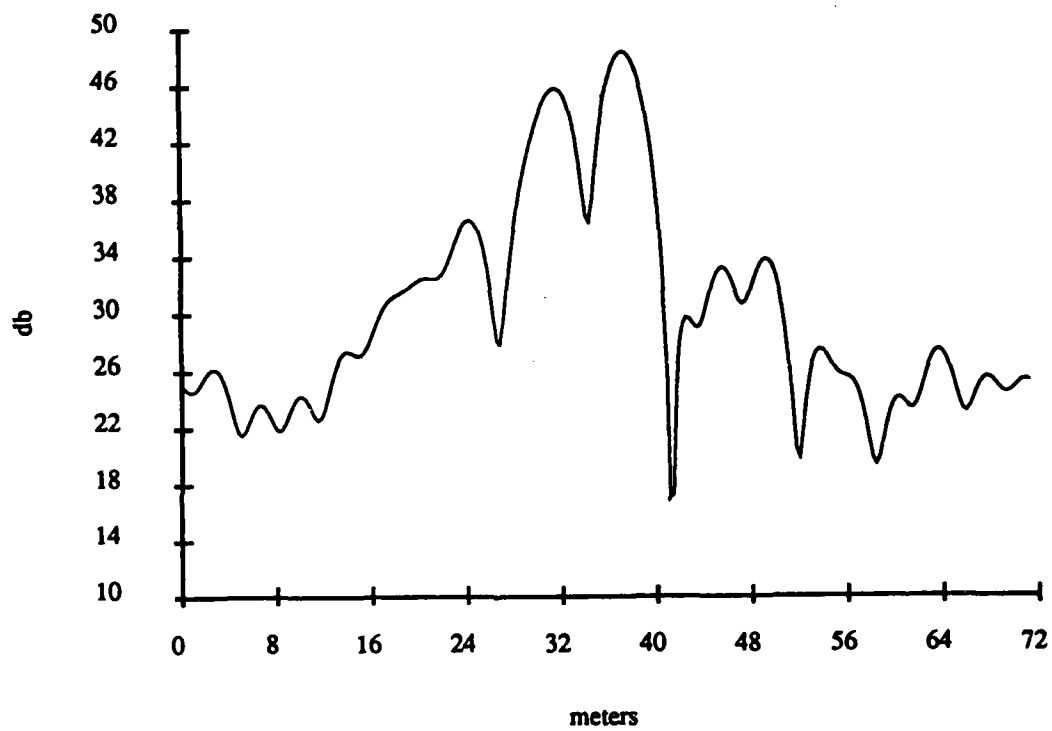
Figure A.87: FT of the Concorde at Horizontal Polarization, 80° aspect angle, 20 frequency samples used, 40–80 MHz

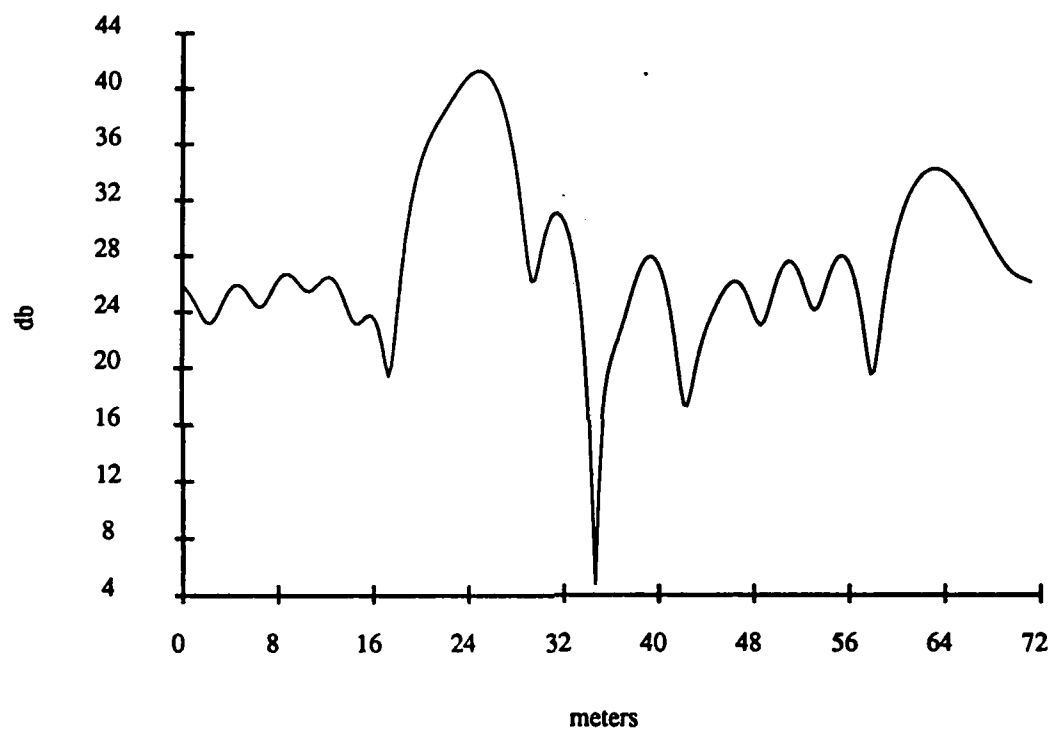Figure A.88: FT of the Concorde at Horizontal Polarization, 90° aspect angle, 20 frequency samples used, 40–80 MHz
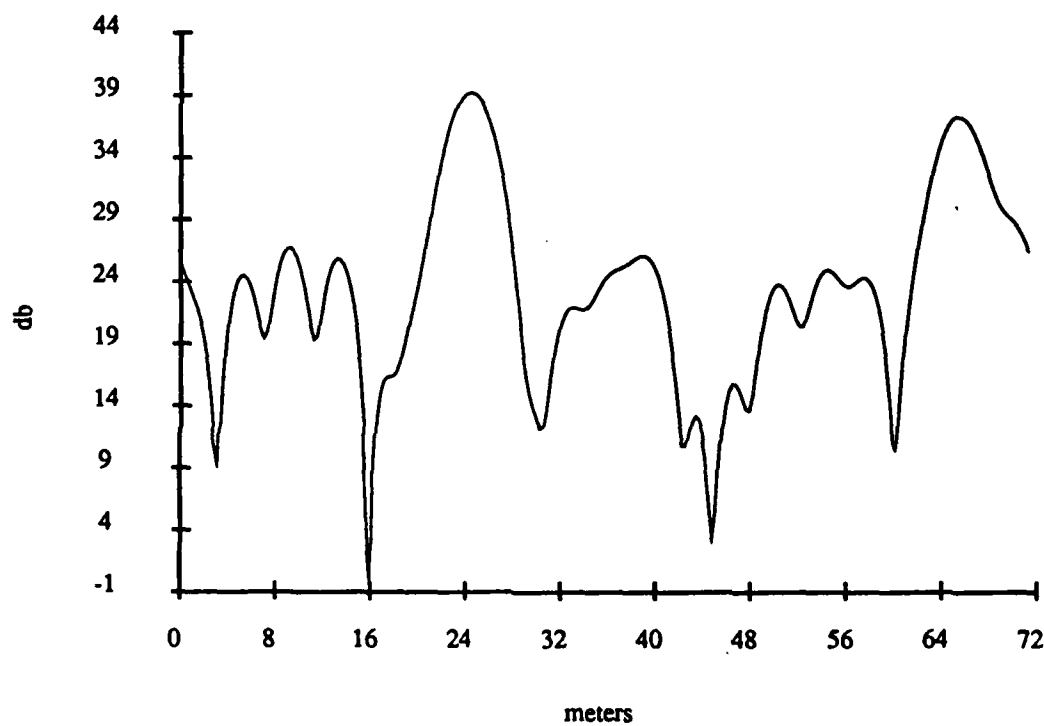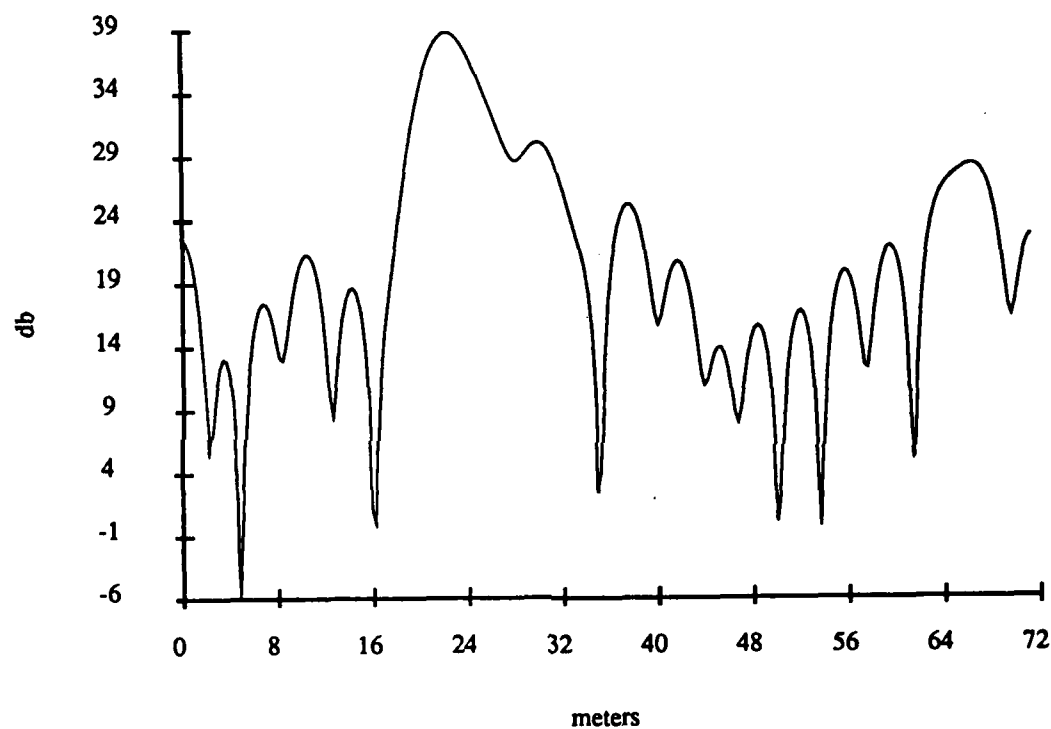
120

Figure A.89: FT of the Concorde at Horizontal Polarization, 100° aspect angle, 20 frequency samples used, 40–80 MHz

Figure A.90: FT of the Concorde at Horizontal Polarization, 110° aspect angle, 20 frequency samples used, 40–80 MHz
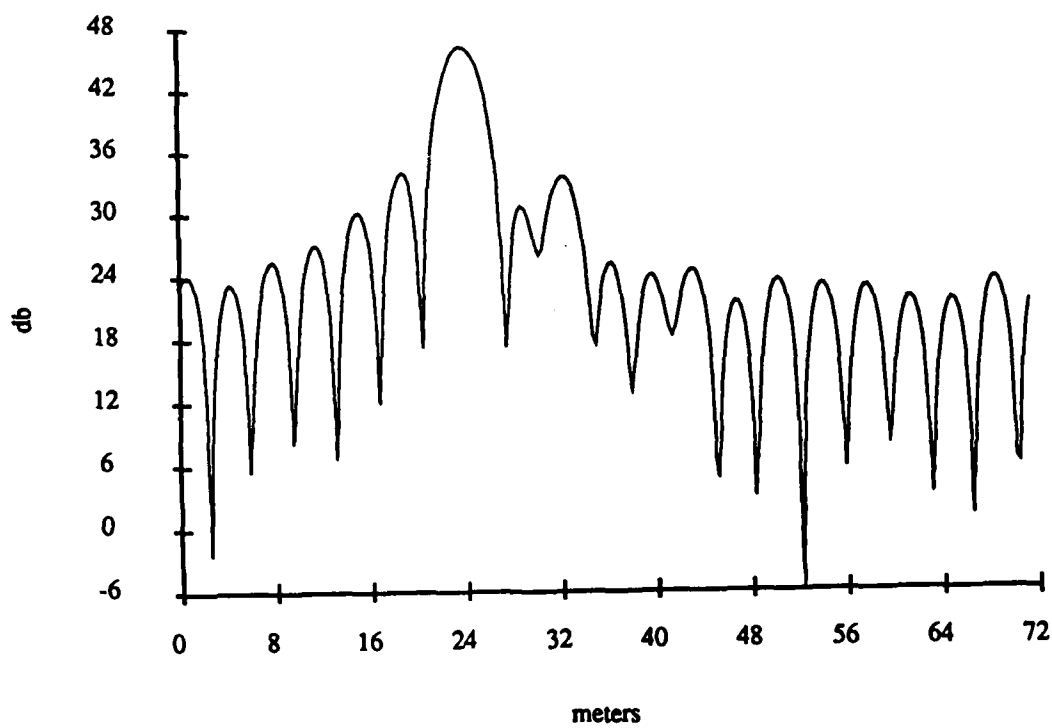
Figure A.91: FT of the Concorde at Horizontal Polarization, 120° aspect angle, 20 frequency samples used, 40–80 MHz

123

Figure A.92: FT of the Concorde at Horizontal Polarization, 130° aspect angle, 20 frequency samples used, 40–80 MHz

Figure A.93: FT of the Concorde at Horizontal Polarization, 140° aspect angle, 20 frequency samples used, 40–80 MHz
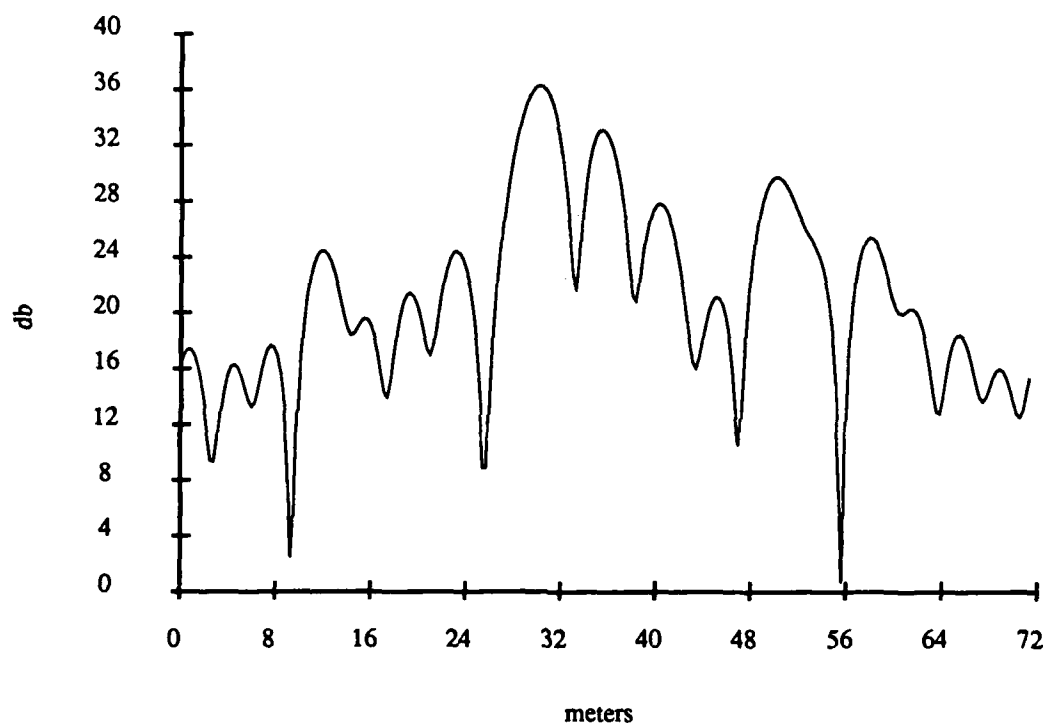
Figure A.94: FT of the Concorde at Horizontal Polarization, 150° aspect angle, 20 frequency samples used, 40–80 MHz

126

Figure A.95: FT of the Concorde at Horizontal Polarization, 160° aspect angle, 20 frequency samples used, 40–80 MHz
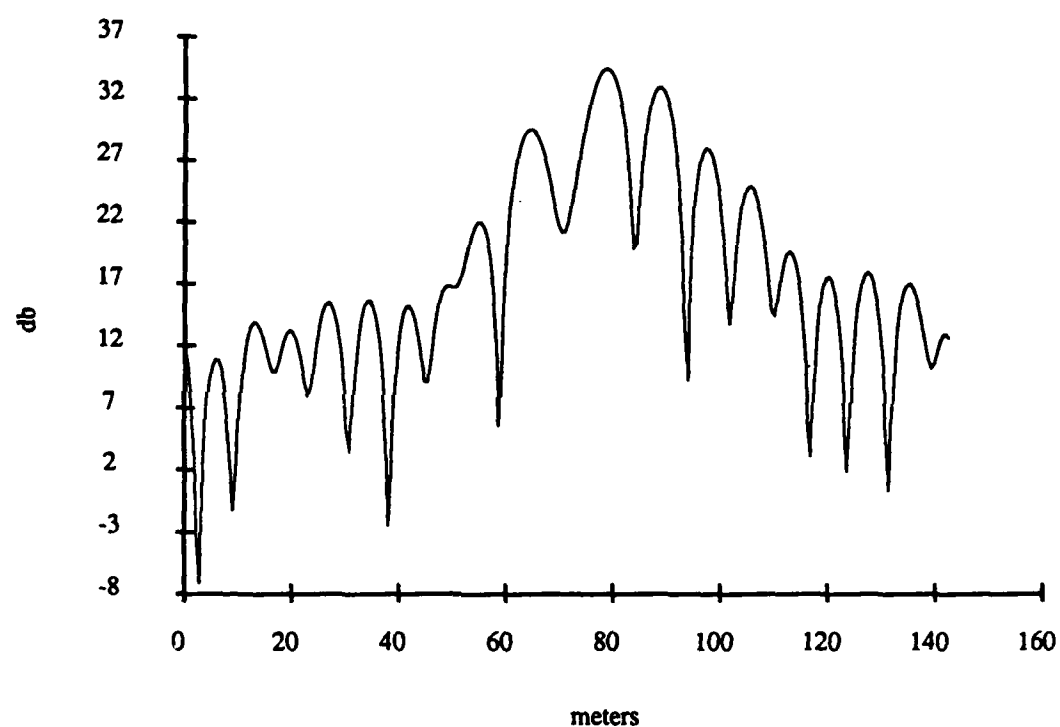
127

Figure A.96: FT of the Concorde at Horizontal Polarization, 170° aspect angle, 20 frequency samples used, 40–80 MHz

Figure A.97: FT of the Concorde at Horizontal Polarization, 180° aspect angle, 20 frequency samples used, 40–80 MHz

Figure A.98: FT of the Boeing 707 at Horizontal Polarization, 10° aspect angle, 20 frequency samples used, 40–80 MHz
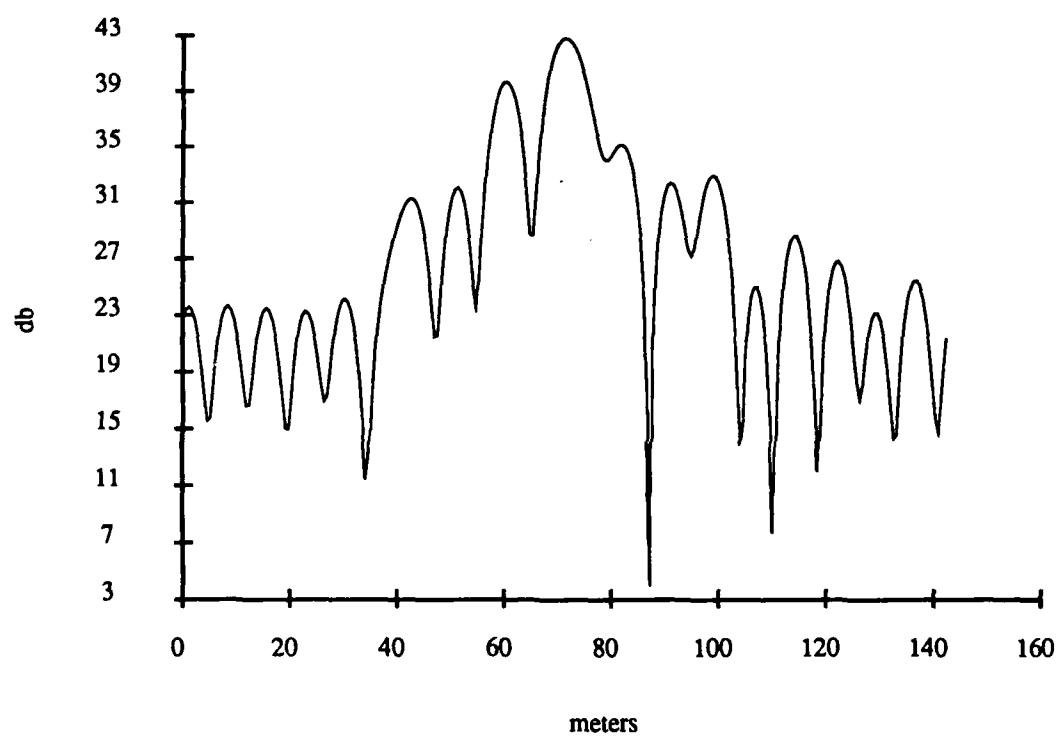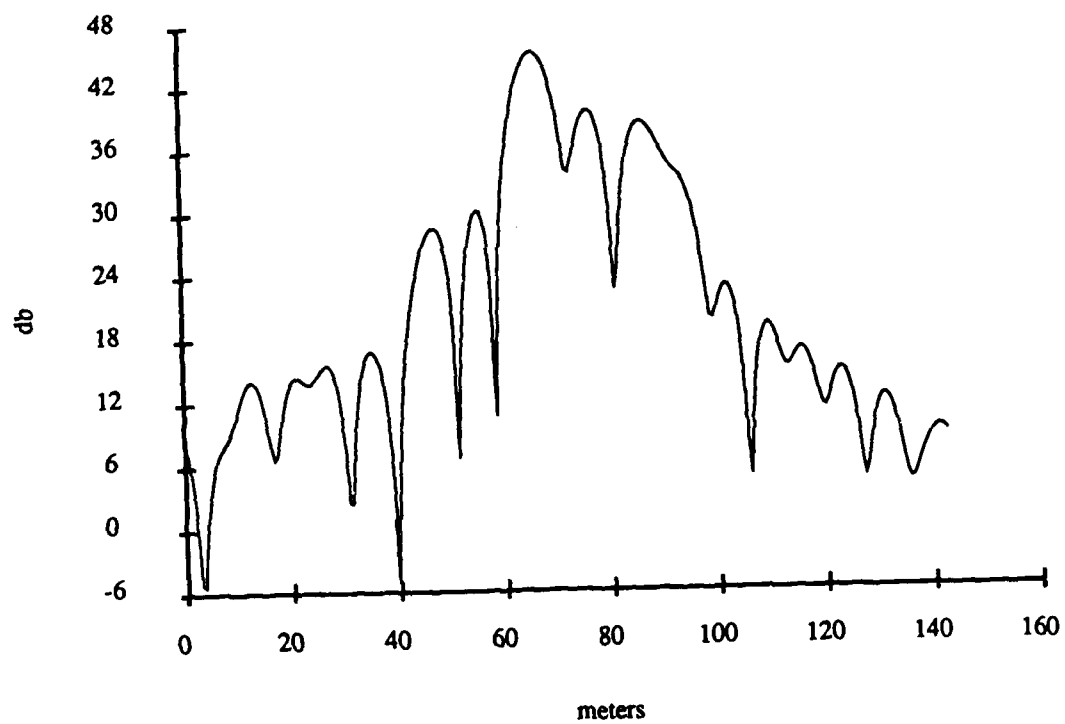
Figure A.99: FT of the Boeing 727 at Horizontal Polarization, 10° aspect angle, 20 frequency samples used, 40–80 MHz

Figure A.100: FT of the Boeing 747 at Horizontal Polarization, 10° aspect angle, 20 frequency samples used, 40–80 MHz

132

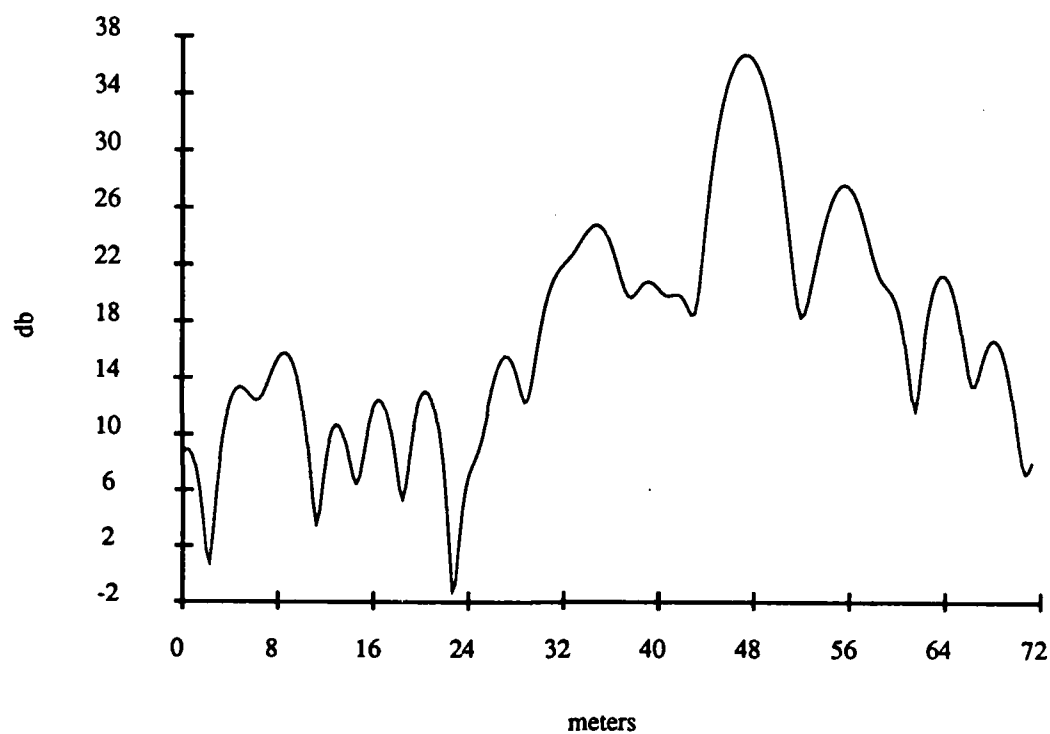Figure A.101: FT of the DC 10 at Horizontal Polarization, 10° aspect angle, 20 frequency samples used, 40–80 MHz

133

Figure A.102: FT of the Concorde at Horizontal Polarization, 10° aspect angle, 20 frequency samples used, 40–80 MHz
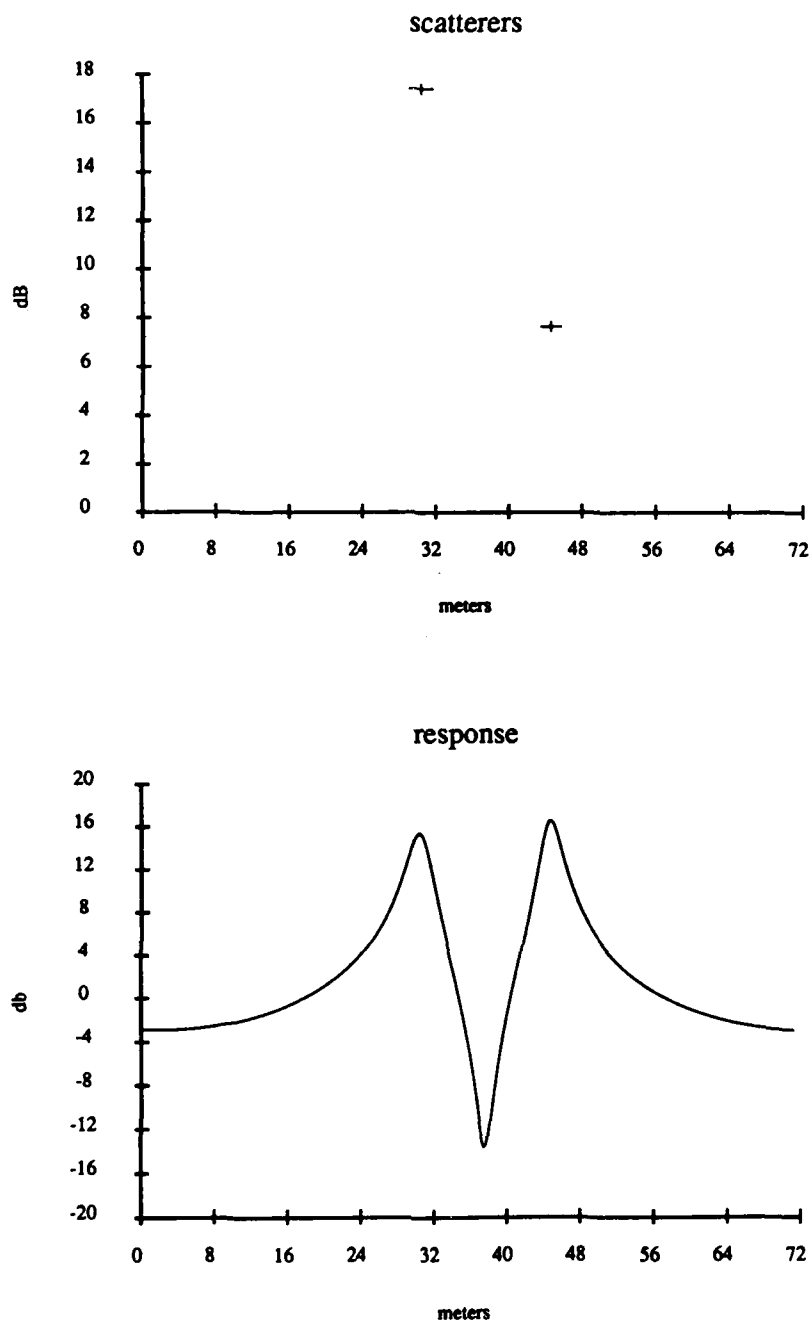
134

scatterers

response

Figure A.103: ARMA Response of the Boeing 707 at Horizontal Polarization, 10°
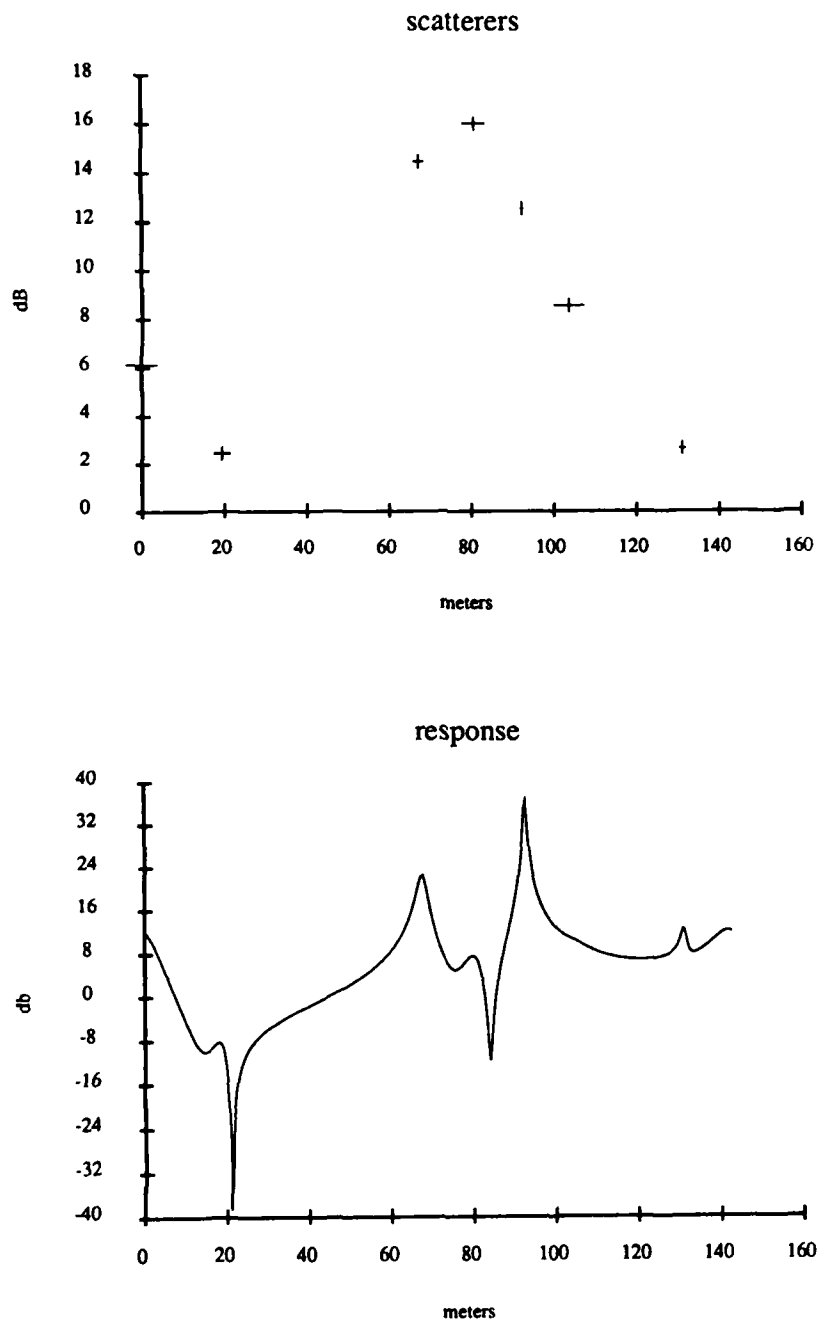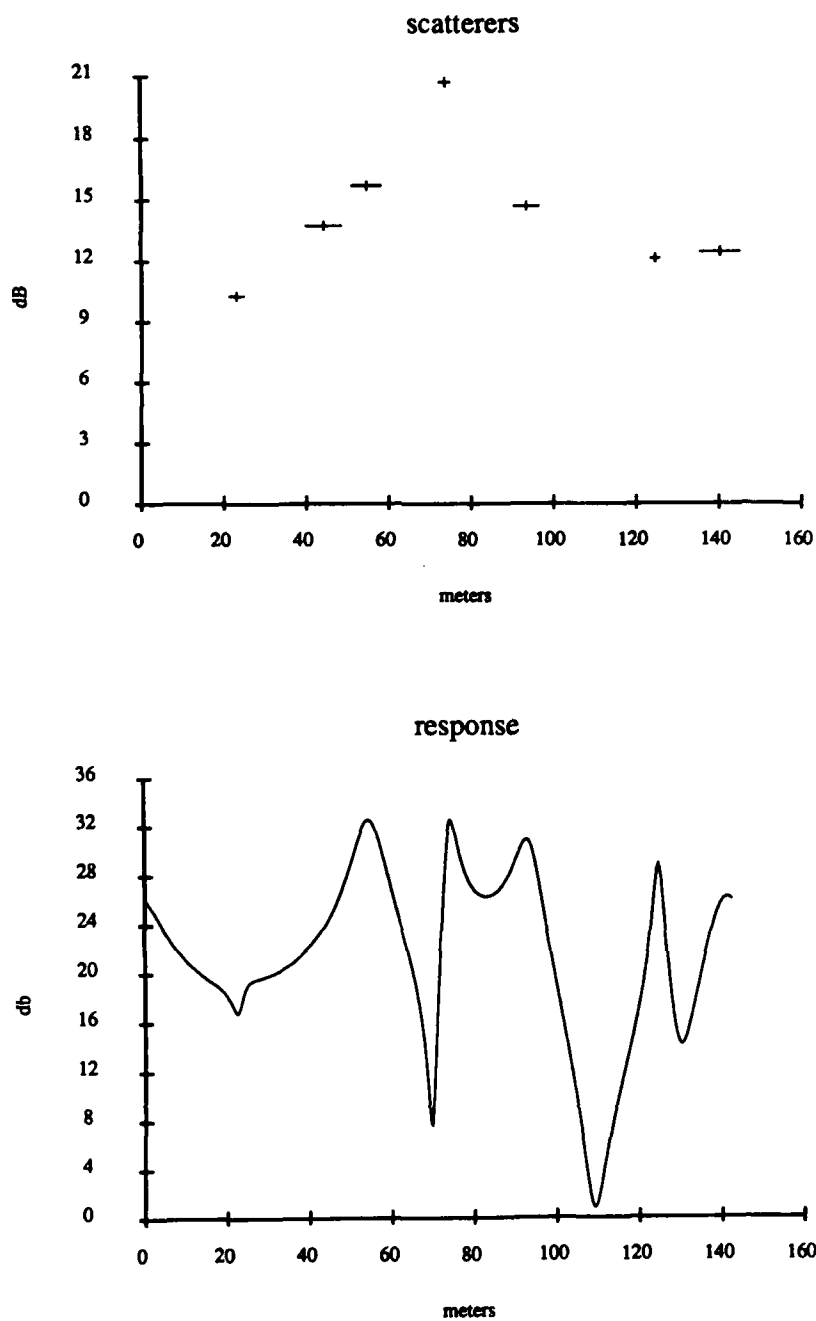aspect angle, 20 frequency samples used, 40–80 MHz, 9th order model

135

Figure A.104: ARMA Response of the Boeing 727 at Horizontal Polarization, 10°
aspect angle, 20 frequency samples used, 40–80 MHz, 9th order model

136

scatterers

response

Figure A.105: ARMA Response of the Boeing 747 at Horizontal Polarization, 10° aspect angle, 20 frequency samples used, 40–80 MHz, 9th order model
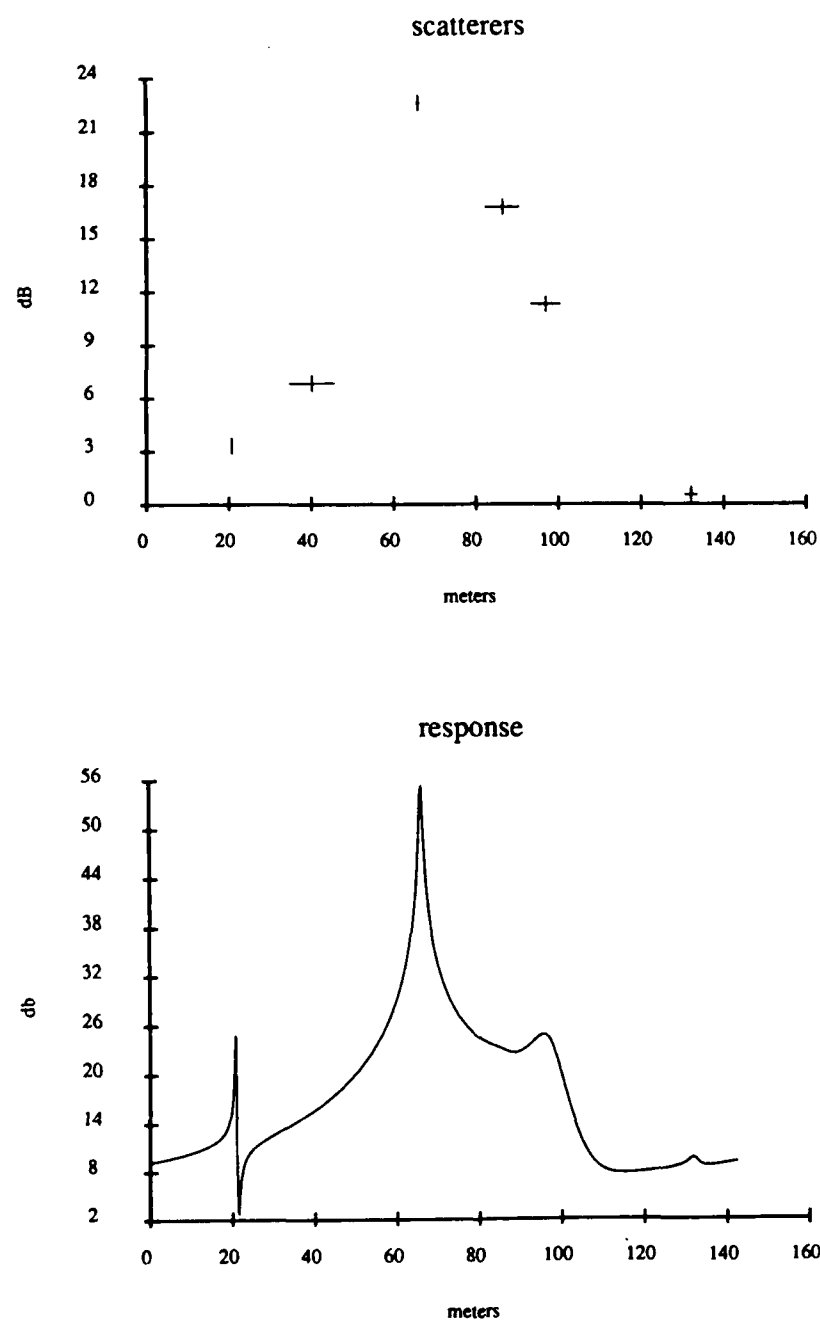
Figure A.106: ARMA Response of the DC10 at Horizontal Polarization, 10° aspect angle, 20 frequency samples used, 40–80 MHz, 9th order model

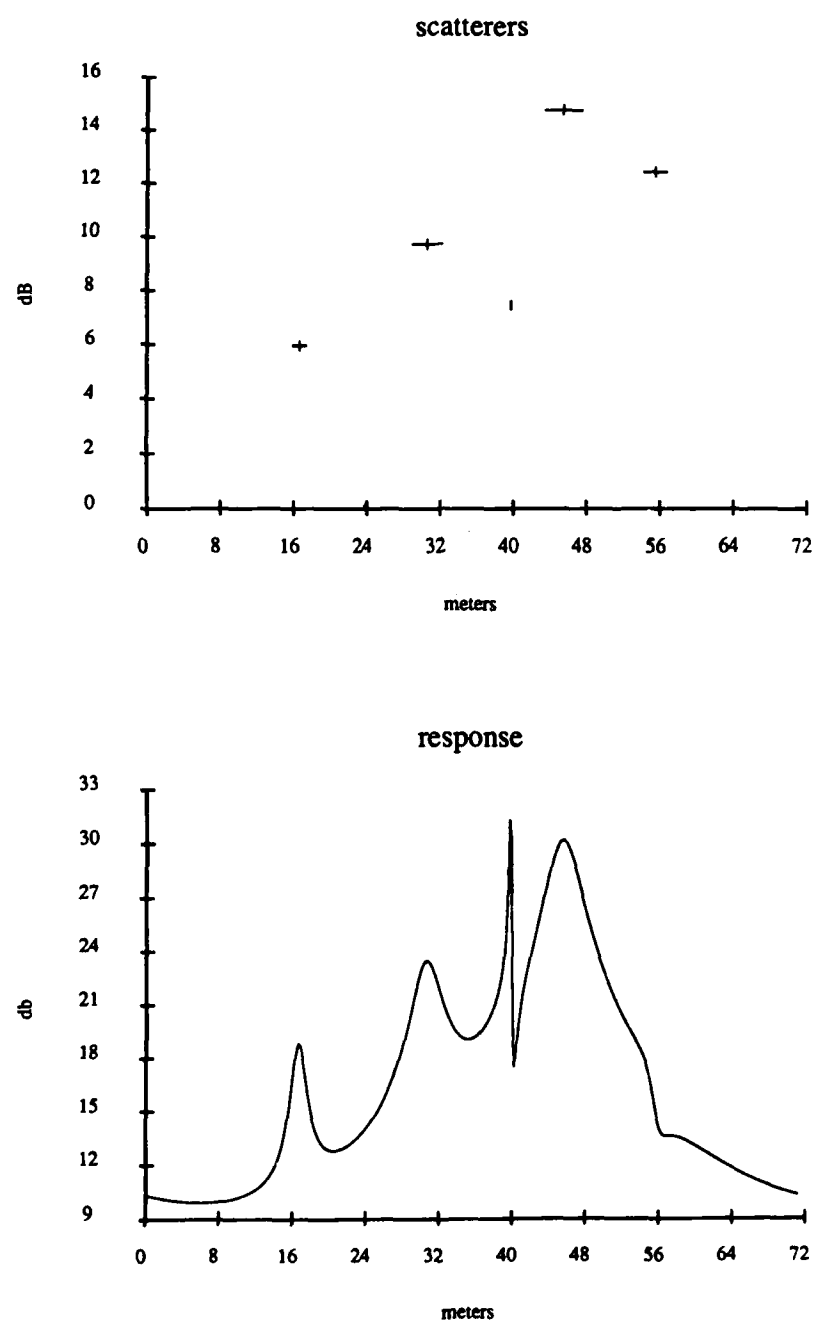138

scatterers

response

Figure A.107: ARMA Response of the Concorde at Horizontal Polarization, 10°
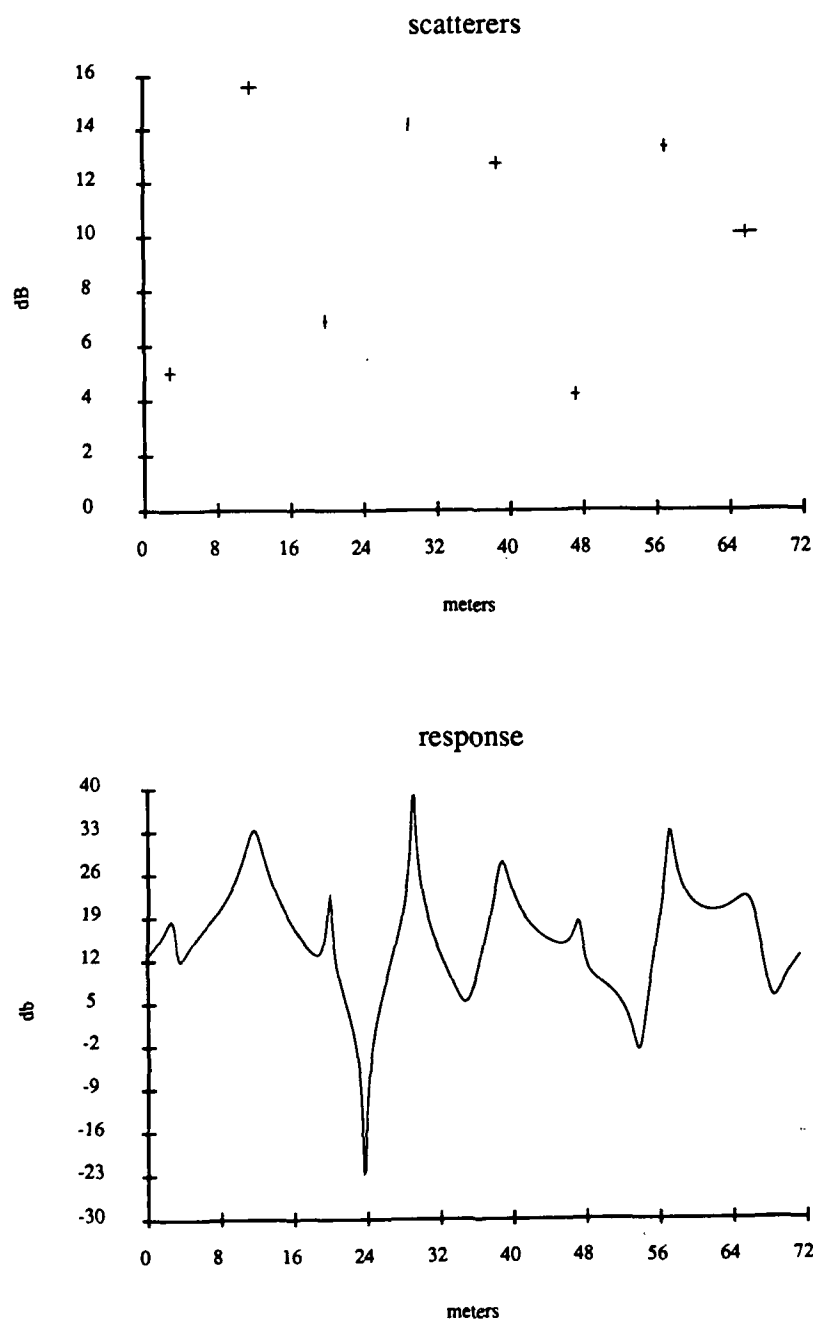aspect angle, 20 frequency samples used, 40–80 MHz, 9th order model

Figure A.108: ARMA Response of the Boeing 707 at Vertical Polarization, 10°
aspect angle, 20 frequency samples used, 40–80 MHz, 9th order model
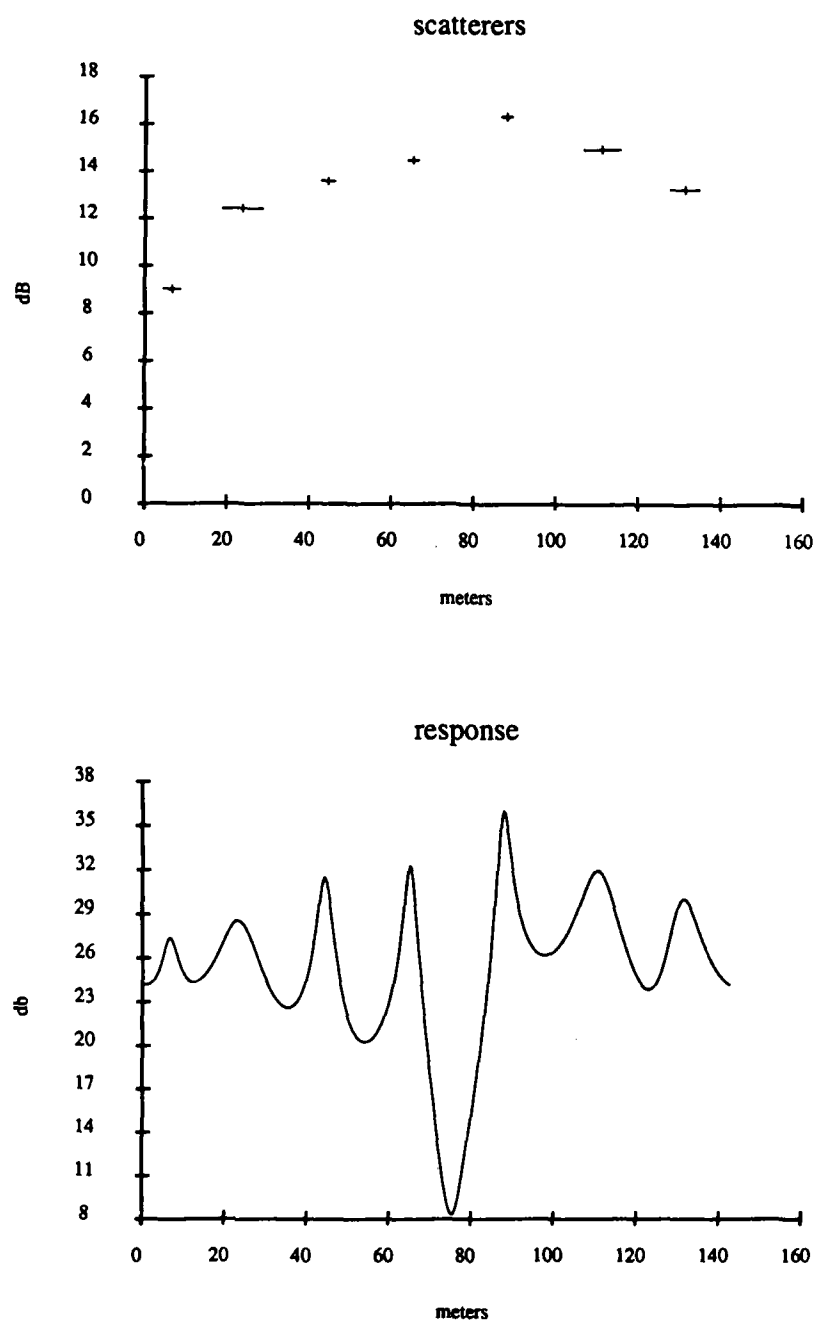
140

scatterers

response

Figure A.109: ARMA Response of the Boeing 727 at Vertical Polarization, 10°
aspect angle, 20 frequency samples used, 40–80 MHz, 9th order model
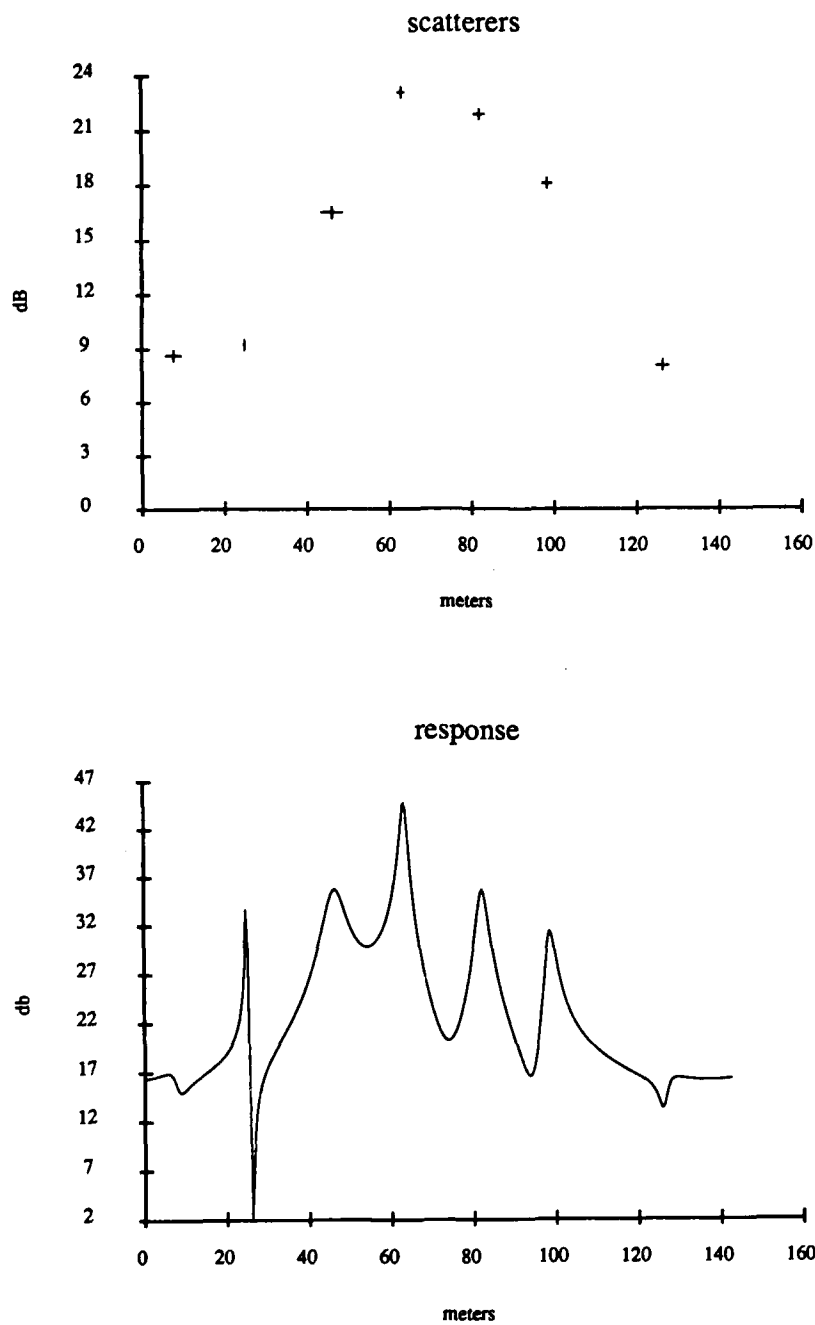
scatterers

response

Figure A.110: ARMA Response of the DC10 at Vertical Polarization, 10° aspect angle, 20 frequency samples used, 40–80 MHz, 9th order model
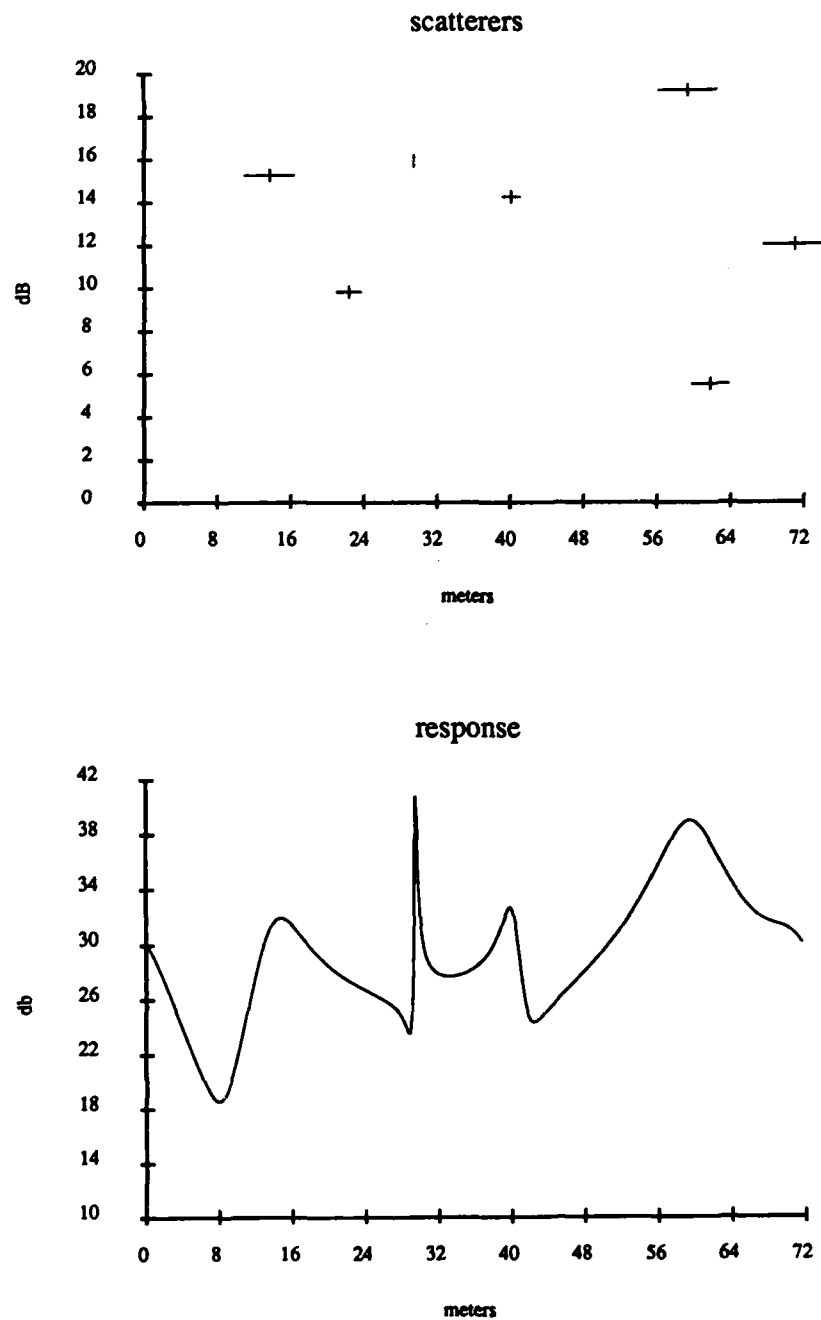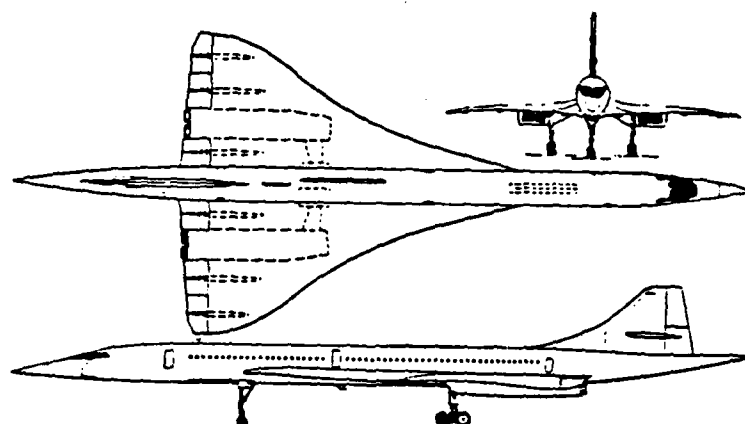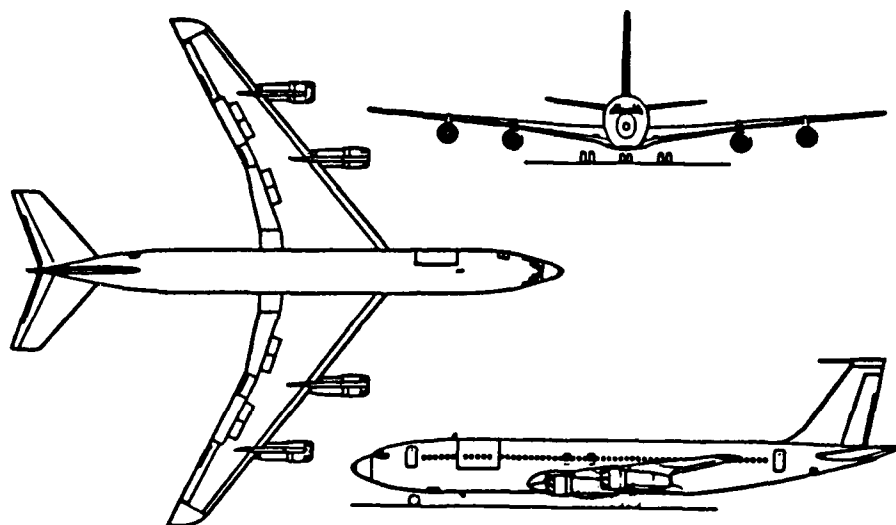
scatterers

response

Figure A.111: ARMA Response of the Concorde at Vertical Polarization, 10° aspect angle, 20 frequency samples used, 40–80 MHz , 9th order model

External Dimensions:

Length overall   202 ft 3.6 in (61.66m)
Height overall   40 ft 0.0 in (12.19m)
Wing span   83 ft 10.0 in (25.56m)

Figure A.112: The Concorde

External Dimensions:

Length overall	152 ft 11.0 in (46.61m)
Height overall	42 ft 5.0 in (12.93m)
Wing span	145 ft 9.0 in (44.42m)

Figure A.113: The Boeing 707

145

END

DATE

FILMED

8-88

DTIC